GDAŃSK UNIVERSITY OF TECHNOLOGY
FACULTY OF ELECTRONICS, TELECOMMUNICATIONS AND INFORMATICS

The author of the PhD dissertation: **Piotr Kurgan**
Scientific discipline: **electronics**

DOCTORAL DISSERTATION

Title of PhD dissertation: **Expedited EM-Driven Design of Miniaturized Microwave Hybrid Couplers Using Surrogate-Based Optimization**

Title of PhD dissertation (in Polish): **Szybkie projektowanie zminiaturyzowanych mikrofalowych sprzęgaczy hybrydowych przy użyciu optymalizacji numerycznej, modeli zastępczych i symulacji elektromagnetycznych**

Supervisor   *signature*
Dr. Sławomir Kozieł, PhD

Gdańsk, 2017

To my beloved wife Joanna

GDAŃSK UNIVERSITY OF TECHNOLOGY
FACULTY OF ELECTRONICS, TELECOMMUNICATIONS AND INFORMATICS

STATEMENT

The author of the PhD dissertation: **Piotr Kurgan**

I, the undersigned, agree/~~do not agree~~* that my PhD dissertation entitled:
Expedited EM-Driven Design of Miniaturized Microwave Hybrid Couplers Using Surrogate-Based Optimization
may be used for scientific or didactic purposes.[1]

Gdańsk,..... .....
signature of the PhD candidate

Aware of criminal liability for violations of the Act of 4th February 1994 on Copyright and Related Rights (Journal of Laws 2006, No. 90, item 631) and disciplinary actions set out in the Law on Higher Education (Journal of Laws 2012, item 572 with later amendments),[2] as well as civil liability, I declare, that the submitted PhD dissertation is my own work.

I declare, that the submitted PhD dissertation is my own work performed under and in cooperation with the supervision of Sławomir Kozieł.

This submitted PhD dissertation has never before been the basis of an official procedure associated with the awarding of a PhD degree.

All the information contained in the above thesis which is derived from written and electronic sources is documented in a list of relevant literature in accordance with art. 34 of the Copyright and Related Rights Act.

I confirm that this PhD dissertation is identical to the attached electronic version.

Gdańsk,..... .....
signature of the PhD candidate

I, the undersigned, agree/~~do not agree~~* to include an electronic version of the above PhD dissertation in the open, institutional, digital repository of Gdańsk University of Technology, Pomeranian Digital Library, and for it to be submitted to the processes of verification and protection against misappropriation of authorship.

Gdańsk,..... .....
signature of the PhD candidate

*) strikethrough where appropriate.

[1] Decree of Rector of Gdansk University of Technology No. 34/2009 of 9th November 2009, TUG archive instruction addendum No. 8.

[2] Act of 27th July 2005, Law on Higher Education: Chapter 7, Criminal responsibility of PhD students, Article 226.

GDAŃSK UNIVERSITY OF TECHNOLOGY
FACULTY OF ELECTRONICS, TELECOMMUNICATIONS AND INFORMATICS

DESCRIPTION OF DOCTORAL DISSERTATION

The Author of the PhD dissertation: Piotr Kurgan

Title of PhD dissertation: Expedited EM-Driven Design of Miniaturized Microwave Hybrid Couplers Using Surrogate-Based Optimization

Title of PhD dissertation in Polish: Szybkie projektowanie zminiaturyzowanych mikrofalowych sprzęgaczy hybrydowych przy użyciu optymalizacji numerycznej, modeli zastępczych i symulacji elektromagnetycznych

Language of PhD dissertation: English

Supervision: Sławomir Kozieł

Date of doctoral defense:……

Keywords of PhD dissertation in Polish: dekompozycja, komputerowo wspomagane projektowanie, komórki kompaktowe, miniaturyzacja, modele aproksymacyjne, modele wielopoziomowe, obwody zastępcze, odwzorowanie przestrzeni, optymalizacja, optymalizacja wielokryterialna, praca szerokopasmowa, sprzęgacze hybrydowe, sprzęgacze gałęziowe, sprzęgacze pierścieniowe, sprzęgacze zminiaturyzowane, strojenie, metody optymalizacji pośredniej, symulacje elektromagnetyczne, symulacyjne metody projektowania, wydajność obliczeniowa.

Keywords of PhD dissertation in English: branch-line couplers, compact cells, compact couplers, computational efficiency, computer-aided design, data-driven models, decomposition, EM simulations, equivalent circuits, fine-tuning, hybrid couplers, miniaturization, multi-objective optimization, optimization, rat-race couplers, response surface approximation, simulation-driven design, space mapping, surrogate-based optimization, wideband operation, variable-fidelity models.

Summary of PhD dissertation in Polish: Miniaturyzacja mikrofalowych sprzęgaczy hybrydowych ma duże znaczenie dla współczesnej komunikacji bezprzewodowej. Projektowanie struktur kompaktowych przy wykorzystaniu standardowych metod symulacyjnych stanowi niezwykle trudny problem badawczy ze względu na ogólny brak wydajnych obliczeniowo i dokładnych modeli komputerowych. Niewielka dokładność dostępnych modeli obwodowych wynika z pomijania efektów sprzężeń pasożytniczych, istotnych z punktu widzenia poprawnego określania parametrów elektrycznych struktur o zwartej konstrukcji. Z kolei symulacje elektromagnetyczne mogą zapewniać odpowiednią dokładność, lecz są bardzo kosztowne numerycznie. Zawarte w rozprawie metody projektowania zminiaturyzowanych sprzęgaczy hybrydowych stanowią rozwiązanie tak postawionego problemu badawczego. Opracowane metody bazują na koncepcji optymalizacji pośredniej i wykorzystują szereg technik pozwalających na zbudowanie dokładnych i wydajnych obliczeniowo modeli zastępczych. Do technik tych należy zaliczyć dekompozycję, modelowanie obwodowe, elektromagnetyczne czy aproksymacyjne, oraz od-

wzorowanie przestrzeni. Zaprezentowane wyniki numeryczne poparte badaniami eksperymentalnymi wskazują na wysoką dokładność i wydajność obliczeniową omawianych metod (średnio 25-krotne przyspieszenie w porównaniu z optymalizacją bezpośrednią modeli elektromagnetycznych), przy czym uzyskane rozwiązania układowe cechuje bardzo duża skala miniaturyzacji (pomiędzy 82% a 94%) przy zadanych parametrach pracy. Zgodnie z najlepszą wiedzą autora, zawarte w rozprawie metody stanowią pierwsze w literaturze kompleksowe rozwiązanie problemu szybkiego i wydajnego projektowania zminiaturyzowanych mikrofalowych sprzęgaczy hybrydowych.

Summary of PhD dissertation in English: Miniaturization of microwave hybrid couplers is important for contemporary wireless communication engineering. Using standard computer-aided design methods for development of compact structures is extremely challenging due to a general lack of computationally efficient and accurate simulation models. Poor accuracy of available equivalent circuits results from neglecting parasitic cross-couplings that greatly affect the performance of miniaturized devices. On the other hand, electromagnetic (EM) simulations may be very accurate, but at the same time they are extremely CPU-heavy and time consuming. The methodologies included in this dissertation address the problem of reliable and computationally efficient design of miniaturized hybrid couplers. The proposed methods are based on a generic SBO scheme and employ a number of customized techniques for development of fast and accurate surrogates. These techniques include decomposition, equivalent circuits, EM modeling, response surface approximations, and space mapping. The presented numerical results, confirmed also experimentally, indicate a dramatic reduction in the computational cost of the discussed methods (on average, 25 times speedup in comparison to direct EM optimization). A suite of novel hybrid couplers obtained in this work demonstrate outstanding miniaturization ratios ranging between 82% and 94% with good transmission characteristics. To the best of author's knowledge, the developed methods are the only procedures so far in the literature that allow for obtaining high-performance EM-validated design solutions of miniaturized hybrid couplers at a low computational cost.

ACKNOWLEDGEMENTS

The author wishes to express his sincerest appreciation to Dr. Sławomir Kozieł for this supervision, expert guidance, encouragement and constant support throughout the course of this work.

The author would also like to thank Dr. Adrian Bekasiewicz for his motivation, advice, constructive discussions and continuous help.

The author offers deep gratitude to Prof. Stanisław Szczepański for his advice and support.

The author wishes to acknowledge Dr. Marek Kitliński for his mentoring and supervision during the first years of research.

The author would like to thank Sonnet Software, Inc., Syracuse, NY, as well as Computer Simulation Technology AG, Darmstadt, Germany, for making ***em***™ and CST Microwave Studio available, respectively.

The author also acknowledges the financial support provided by National Science Center of Poland (grant numbers 4699/B/T02/2011/40 and 2014/15/B/ST7/04683) and by the Icelandic Centre for Research (RANNIS) (grant number 163299051 and 130450051).

LIST OF SYMBOLS AND ACRONYMS

SYMBOLS

$\boldsymbol{R}_f$ – fine model

$\boldsymbol{R}_c$ – coarse model

$\boldsymbol{R}_s$ – surrogate model

$\boldsymbol{x}$ – vector of designable parameters

x – element of vector $\boldsymbol{x}$

$\boldsymbol{x}^*$ – optimized parameter vector

$\boldsymbol{x}^{(0)}$ – initial parameter vector

U – merit function

$U(\boldsymbol{R})$ – objective function

$\boldsymbol{p}$ – vector of auxiliary SM parameters

$\boldsymbol{l}$ – lower bounds vector

$\boldsymbol{u}$ – upper bounds vector

$\prec$ – relation of Pareto dominance

X_p – Pareto-optimal set

A – circuit area

dS – power split

β – penalty coefficient

$\boldsymbol{q}$ – input SM shift vector

B, c – input SM parameters

f_0 – operating frequency

$\boldsymbol{\omega}$ – vector of frequencies

ACRONYMS

SBO – surrogate-based optimization

SM – space mapping

ISM – implicit space mapping

OSM – output space mapping

NSM – nested space mapping

SSM – sequential space mapping

EM – electromagnetic

BW – bandwidth

MO – multi-objective

RSA – response surface approximation

PE – parameter extraction

BLC – branch-line coupler

RRC – rat-race coupler

CONTENTS

1 INTRODUCTION

1.1 State of the Knowledge

1.1.1 General Overview

Nowadays, size reduction is an important prerequisite for the development of modern microwave circuits and components. This topic has gained much attention in recent years due to the rapid expansion of commercial, industrial, and military markets aimed at low-cost, small-size, and high-performance microwave devices [1-4]. The diversity of their applications includes—but is not limited to—mobile communication, telemedicine, remote sensing, defense electronics, and portable measurement equipment [5-9]. Miniaturization has been a prevailing trend in the electronics industry for several decades now and a catalyst for persistent technological innovation worldwide [10]. Unfortunately, the Moore's Law that describes the tremendous integration capabilities of semiconductor devices [11] does not apply to many areas of microwave engineering. The reason is that a proper operation of a system, which heavily relies on wave phenomena, cannot be achieved when its distributed components are replaced by lumped elements [12]. This is pertinent to microwave structures that feature a modular architecture primarily based on uniform transmission lines (UTLs) whose longitudinal dimensions are comparable to the guided wavelength and require a certain (and fixed) relation with respect to it to ensure that the entire device works as defined by system specifications [13]. With the downshifting of operating frequency spectrum, e.g., as in case of Long Term Evolution or Radio Frequency Identification standards [14], handling large layouts of conventional microwave structures becomes increasingly challenging. For the above reasons, the development of efficient miniaturization schemes is one of important research directions with the potential of contributing to the progress in applied microwave technologies. This is a pressing issue for a variety of microwave components, but perhaps most notably for hybrid couplers, such as branch-lines or rat-races. These are constructed from multiple quarter-wavelength UTLs in such a way that a considerable substrate area inside the structure is left unoccupied [15]. Thus, in this work we almost exclusively consider hybrid couplers as subjects of the miniaturization process.

The excessive size of standard microwave components can be mitigated to some extent by exploiting a slow-wave phenomenon to construct transmission lines with an increased electrical length to physical length ratio [16]. To date, four main size reduction methods have been suggested in the scientific literature to capitalize on this concept: (i) application of lumped or lumped-distributed elements instead of UTLs [17-19], (ii) utilization of high-permittivity dielectric substrates [13], [20], [21], (iii) exploitation of artificially engineered materials with recur-

rent patterns etched in the ground plane metallization [22-24] or periodic inclusions/cavities located in the dielectric substrate [25-27] and (iv) spatially separated storage of electric and magnetic energy by means of short (typically smaller than half-quarter wavelength) transmission line sections of low and high characteristic impedances, respectively [28-35]. The last method is often alternatively described as an implementation of intentional disturbances in the signal line metallization layer of transmission lines [36]. The first technique offers substantial miniaturization capabilities (even a threefold length diminution in comparison to conventional lines [15], [37], but also suffers from common unavailability of suitable lumped elements with high quality factors, narrowband operation, and hindered assembly of lumped capacitors in microstrip technology, requiring the use of via-holes [15], [38]. The second technique permits a linear reduction of physical dimensions of the circuit, proportional to the square root of the relative dielectric permittivity [39], but—at the same time—it poses serious obstacles, such as high material cost, difficulty in realizing high-impedance UTLs, and high sensitivity to small variations in physical dimensions [13]. The third approach creates a viable chance of shortening ordinary transmission lines (roughly up to one third of their initial length) [40], however, due to the half-wavelength period of material perturbation placement, the artificially engineered transmission medium itself is hard to be confined to a small area [21], [23]. None of the above methods is suitable for low-budget miniaturization, mostly due to the increased complexity of the fabrication process or the cost of the materials themselves. On the other hand, the fourth technique is fully compatible with a standard printed circuit board fabrication process and is free from limitations inherent to the other methods. It is probably for this reason that the discussed size reduction concept has gained so far the most recognition in microwave community, resulting in numerous examples of miniaturized structures composed of slow-wave transmission lines with singular or quasi-periodic perforations located in the signal line metallization [28], [30], [34], [41-45]. Despite the prevalence of this topic in the leading literature, little research has been reported to date on reliable design of compact microwave components. The present work focuses exclusively on circuit miniaturization based on transmission lines with disturbed signal line metallization, and aims at providing relevant methodological tools to address pressing design-related issues covered in the following paragraphs.

Practical application of the selected size reduction technique allows for the construction of structures with compact, yet intricate layouts comprising arrangements of high-impedance lines and low-impedance stubs. Several examples of microwave devices miniaturized this way are illustrated in Figure 1.1. A fundamental problem that arises from the geometric complexity of the discussed circuits and components is an unavoidable trade-off between the accuracy and the computational cost of standard modeling techniques used in the relevant design process [46]. High-fidelity electromagnetic (EM) simulations may be very accurate, but at the same time extremely CPU-expensive. A precise evaluation of compact microwave structures using full-wave EM models may vary from about half an hour to as much as dozens of hours per design [47]. In case of circuits that comprise a large number of miniaturized components—such as a Butler matrix of Figure 1.1(d)—an accurate EM analysis may exceed available computational resources of standard personal computers [48]. Furthermore, EM modeling is an effective tool for handling customized designs as well as accounting for the proximity of periphery elements, such as SMA connectors, housing fixtures, shields etc. that may alter system response [49]. However, its practical use in trial-and-error design procedures (e.g., parameter sweeps or optimization routines that involve multiple evaluations of a given EM model) is severely limited or even prohibitive [50]. On the other end of the spectrum are computationally cheap equivalent circuit models of rather limited accuracy. From the perspective of design reliability, simplified theoretical models of compact structures, neglecting numerous parasitic effects that affect the operation of the circuit, can merely be used to obtain a crude estimate of the desired solution [46]. For this reason, a consequent EM-driven fine-tuning (preferably realized as an optimization task) is indispensable to meet the predefined performance requirements. At the same time, such a precise design closure faces the same challenges as outlined above, which makes its use impractical in many real-world design problems.

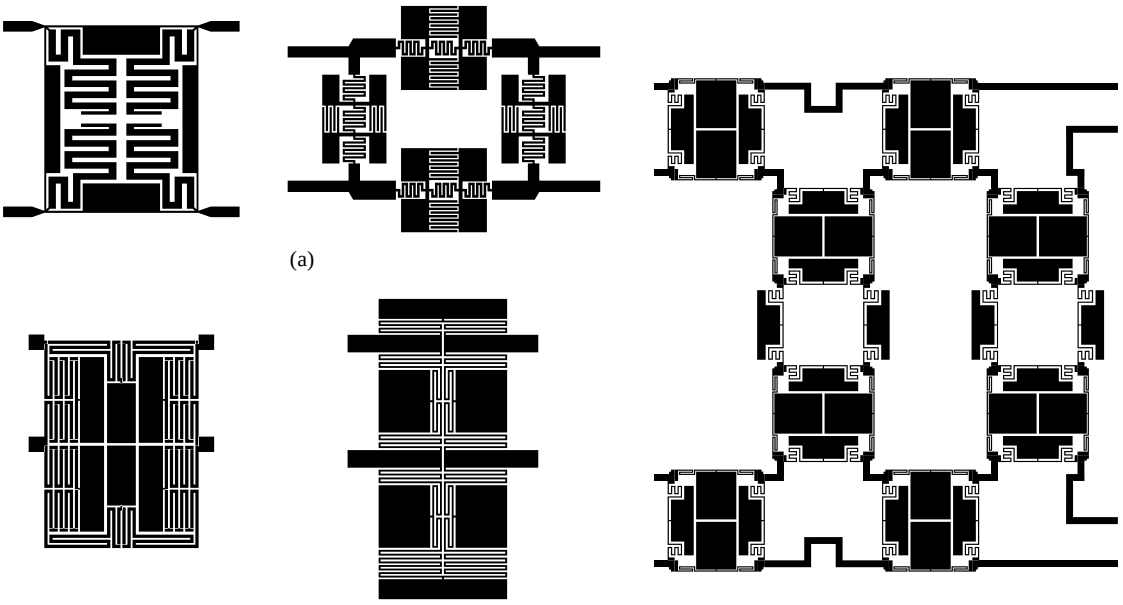

Figure 1.1: Examples of miniaturized hybrid couplers and an antenna feeding network: (a) branch-line couplers of [51] and [52]; (b) rat-race couplers reported in [53] and [54]; (c) 4 × 4 Butler matrix proposed in [48] as an application of a compact branch-line coupler. The presented structures are described by a large number of parameters ranging between 8 and 25.

In addition to the discussed shortcomings, miniaturized microwave circuits and components are parameterized by many variables (often a dozen or more, cf. Figure 1.1), which have to be simultaneously adjusted in the search for a design solution that satisfies system specifications. In this context, obtaining acceptable designs by manual, experienced-based parameter tuning procedures is extremely laborious or may be even futile due to (i) complex and ambiguous interrelation between design variables [55], (ii) counter-intuitive parameter setups of target design solutions [46], and (iii) excessively large parameter ranges assuring that the goal design is located within the prescribed lower and upper bounds [56]. On the other hand, satisfactory (or even optimal) designs may be found without a constant human supervision, by means of numerical optimization algorithms [57]. Unfortunately, this approach is computationally expensive, especially in case of high dimensionality of the corresponding design problem, and—as mentioned before—when high-fidelity EM simulation models are exclusively used for evaluating system performance.

Difficulties related to the excessive CPU cost of EM-driven optimization can be partially alleviated by resorting to the concept of surrogate-based optimization (SBO) [57-59]. In principle, SBO benefits from exploiting a much cheaper (yet well-aligned) representation of an expensive high-fidelity model, utilized in the design process as a prediction tool, which—upon iterative refinement—produces ever more accurate approximations of the high-fidelity model optimum [60]. In such a scheme, the high-fidelity model is evaluated only for the purpose of design verification and surrogate model refinement [60]. Probably the most recognized SBO technique is microwave engineering is space mapping (SM) [61]. Unfortunately, a straightforward application of an SM algorithm (or similar ones [62]) to design of miniaturized microwave structures may encounter several serious obstacles. First, a general lack of a fairly accurate low-fidelity models (e.g., equivalent circuits) that account for the cross-coupling effects between closely packed building blocks of the structure under consideration may lead to convergence problems [63], [64]. Second, the use of a multi-element equivalent circuit model with a large number of independent variables contributes to the numerical complexity of optimization as well as extraction of auxiliary parameters with issues such as poor generalization [65] or non-uniqueness [66], respectively. Third, SM-like algorithms require the high-fidelity model of the miniaturized structure to be evaluated from the very first iteration, which is a major contributor to the elevat-

ed cost of the entire design process [46]. Other potentially useful SBO techniques are also available, including a design strategy that employs multiple coarse-discretization EM models of variable fidelity [67] or global data-driven models [68]. In the former approach, the selection of adequate variable-fidelity models is not straightforward and requires elaborated preliminary studies on model trade-offs between accuracy and computational cost [69]. On the other hand, the latter technique is still reserved for design problems with only a few independent variables as the CPU cost of acquiring training data samples for ensuring a usable model accuracy grows exponentially with the dimensionality of the design space [70]. To the best of author's knowledge, the application of SBO techniques to design of miniaturized microwave structures has not been tested and reported prior to author's research, leaving the aforementioned issues unresolved.

1.1.2 Main Design Concepts of Miniaturized Microwave Hybrid Couplers

Miniaturization of microwave hybrid couplers has been the focus of continuous research for more than a decade now [71-73]. The prevailing approach to hybrid coupler size reduction is based on the decomposition of a conventional circuit, followed by replacement of its building blocks (i.e., UTLs) with slow-wave transmission lines (more precisely, combinations of high-impedance strips and low-impedance stubs of different quantity and complexity) that are intended to mimic electrical parameters of their conventional counterparts, while offering advantageous physical properties, such as an increased electrical length to physical length ratio [74]. The slow-wave transmission lines (also referred to as CMRCs, i.e., compact microstrip resonant cells or, in short, compact cells) presented in the literature exhibit a diversity of geometries, ranging from simple T-shaped or π-shaped topologies [75] up to sophisticated layouts devised arbitrarily by the designer [76]. A common feature of prior works on circuit miniaturization is that the final size reduction ratio is merely a byproduct of adjusting geometry parameters of the slow-wave transmission line to satisfy certain electrical performance requirements [43], [72], [77-80]. Thus, this practice should be altered to ensure that the novel circuit realizations reach the limits of miniaturization without compromising performance requirements imposed on the system.

Another essential characteristic of the previous miniaturization-related research is that the design problem of compact hybrid couplers is almost entirely narrowed down to the problem of finding a convenient replacement for UTLs that constitute the original circuit. For a number of publications presenting small-size structures with low to moderate miniaturization ratios [81-83], this strategy introduces only a minor misalignment between the desired circuit performance, most probably attributed to T-junction phase shifts [84]. In case of highly compressed layouts with adjacent slow-wave transmission lines closely fit to each other, the end result typically exhibits a major degradation of device performance [75], [80]. The reason for this conjunction is the lack of reliable design closure procedures, which are imperative for addressing the effects of strong cross-couplings between the adjacent compact cells that assemble a densely arranged microwave structure. However, employing high-fidelity EM models to an exhaustive enumeration or local optimization routines to compensate for strong parasitic phenomena within a miniaturized circuit is almost just as CPU expensive as executing the respective procedures from an initial design.

The largest body of works on finding abbreviated substitutes for original coupler building blocks utilizes the transmission line theory and simple compact cell topologies (mainly based on stepped-impedance line sections and T- or π-networks) to supply the designers with closed-form expressions of key electrical parameters pertaining to the most elementary cell components [53], [85], [86]. This is usually done in one of two ways, either by choosing a lumped-element equivalent circuit of a conventional transmission line and subsequently using short line sections or stubs to approximate constitutive elements of the lumped-element model, or by deriving a chain matrix of the composite compact cell and comparing it to the ABCD matrix of the reference UTL. Furthermore, the even- and odd-mode analysis is often used to derive explicit design formulas for the synthesis of compact cells [2], [40], [87]. It is noteworthy that the equivalence conditions for a conventional line and its T- or π-like counterparts are obtained only for a single

frequency (typically the operating frequency), in the vicinity of which they are merely approximated. Another obstacle is related to the translation of an electrically-described circuit to its corresponding EM model. This group of techniques is suitable only for basic compact cell topologies and is otherwise useless, especially for design aiming at efficient miniaturization of hybrid couplers.

Slow-wave structures with complex geometries (e.g., [36], [45], [88]) that cannot be conveniently analyzed by means of the transmission line theory, are realized as parameterized EM models and handled either by repetitive parameter sweeps guided by engineering experience (which most commonly provide inferior design solutions) or local optimization algorithms. It should be reiterated that these conventional EM-driven design approaches are extremely laborious and time-consuming and cannot guarantee the desired circuit performance once the individual compact cell design solutions are merged together in a complete miniaturized structure.

Apart from the EM-simulation-related challenges discussed in the previous paragraphs, approaching the compact coupler design problem from the perspective of numerical optimization generates some additional methodological issues. First, the proper formulation of the design task should involve several objectives related to size, bandwidth, phase response, power division, as well as isolation and matching levels of the coupler under development [3]. Considering multiple design goals (often conflicting) at the same time, without the predetermined knowledge of possible outcomes or priorities defined in advance, requires multi-objective optimization [56]. Such a process aims at identifying a so-called Pareto front that represents the best possible trade-offs between conflicting objectives [89]. The most popular solution approach to this problem are population-based metaheuristics (e.g., genetic algorithms [90] or particle swarm optimizers [91]) that are capable of generating the entire Pareto front is a single algorithm run by evaluating large populations of candidate solutions (also referred to as agents or individuals). Unfortunately, performing numerous objective function evaluations (typically ranging from thousands to tens of thousands [91]) can be realized in a reasonable timeframe only when lumped-element models or data-driven models are employed for system performance evaluation. As already mentioned, these are not generally available for miniaturized hybrid couplers. On the other hand, translating the multi-objective design problem into a single-objective one limits the amount of information about the system that can be obtained (including information about available trade-off designs), but is more beneficial in terms of computational expenditure. A standard strategy for single-objective optimization involves focusing on the primary goal and controlling the remaining goals through explicit constraints [92]. Other problem definitions exploit implicit constraints (e.g., a penalty function approach [93]) or aggregation of multiple goals using a weighted sum approach [94]. Formulating the design problem in the former manner allows for establishing certain objective thresholds, whose violation triggers contribution of the respective penalty terms to the objective function. The latter way leads to a solution that is a compromise between the user-defined weighted (typically intuitively) objectives. Unfortunately, numerical optimization has been a niche approach to designing miniaturized hybrid couplers so far, as indicated by the number of research articles on this topic. On the other hand, conventional optimization routines with basic functionalities such as weighted sum or minimax objective function formulations are available in commercial EM software [95], [96].

1.1.3 Summary

The state of the knowledge presented in the preceding subsections indicates that current paradigms for designing miniaturized hybrid couplers have to be redefined to provide higher miniaturization rates and to ensure improved reliability, automation, and—most importantly—computational efficiency. The list below highlights the core problems that need to be addressed:

1. Currently available methods for design of miniaturized hybrid couplers fail to include size minimization as an explicit design objective. Size reduction ratios reported as a result of using these methods are just a byproduct of finding a suitable set of geometry pa-

rameters of a slow-wave transmission line, for which certain performance specifications are met.

2. State-of-the-art techniques simplify the design problem of miniaturized hybrid couplers to the design task of slow-wave transmission lines that mimic electrical parameters of original coupler building blocks. In doing so, they neglect cross-coupling effects that occur in a miniaturized coupler assembled from the designed compact components. As a direct consequence, a severe deterioration of system performance can be observed, especially for densely packed structures.
3. Vast majority of techniques dedicated to design of miniaturized hybrid couplers are based on the transmission line theory and involve equivalent circuit models. The latter cannot account for all internal EM couplings that affect the operation of a compact cell at hand, which leads to poor reliability of the discussed techniques. In addition to the above, this approach is limited exclusively to simple compact cell topologies that do not allow for high miniaturization rates.
4. The use of full-wave EM simulations—although necessary to precisely evaluate the performance of miniaturized hybrid couplers—is severely limited for routine simulation-driven design procedures due to a high computational cost and time consumption.
5. Development of accurate data-driven models for multi-dimensional and wide-ranged design spaces of miniaturized hybrid couplers is too CPU intensive to be used in practice.
6. Conventional optimization techniques are largely unsuitable for handling reliable simulation-driven design of miniaturized hybrid couplers due to a large number of high-fidelity EM model evaluations involved in the process. Also, weighting factors or minimal/maximal levels pertaining to performance goals in standard objective function formulations available in commercial EM software are hard to be precisely determined without the knowledge of possible outcomes or extensive preliminary studies.
7. General-purpose SBO techniques offer poor reliability and computational efficiency when applied to complex design problems of miniaturized hybrid couplers. The fundamental problem lies in obtaining a fast low-fidelity model of a compact coupler that is also well-aligned with its high-fidelity EM model.

1.2 Goals and Theses of the Work

This work aims at addressing the design problems summarized in Section 1.1.3 by developing methodologies tailored for design of miniaturized hybrid couplers with emphasis on computational efficiency and improved reliability (both compared to the relevant state-of-the-art design techniques). The complementary goals to be accomplished in the present dissertation are as follows:

1. Adaptation of general-purpose SBO techniques to design of miniaturized hybrid couplers.
2. Development of a customized SBO technique with built-in procedures for the construction of miniaturized hybrid coupler models that combine the advantages of equivalent circuits and EM simulations.
3. Development of a surrogate-assisted design closure technique for miniaturized hybrid couplers.
4. Adaptation of a single-objective SBO technique for explicit size reduction of hybrid couplers.
5. Development of a multi-objective SBO technique for an expedite identification of design objective trade-offs for miniaturized hybrid couplers.

The aforementioned goals have been accomplished by positively verifying the following theses:

1. SBO methods can be successfully used for computationally-efficient design of miniaturized hybrid couplers.
2. Low-cost design optimization of miniaturized hybrid couplers can be realized with the accuracy of EM-simulation models.

3. It is possible to develop SBO techniques that allow for explicit coupler size reduction, while ensuring a required circuit operation.

1.3 Scope of the Work

In general, the present thesis is concerned with the design problem of miniaturized microwave circuits and components. The state of the knowledge presented in Section 1.1 is therefore limited to the description of the fundamental design challenges as well as the state-of-the-art design concepts relevant to the miniaturization of microwave structures.

Although valid for a wide range of microwave circuits that feature a modular architecture (as demonstrated, e.g., in [97-100]), the majority of findings presented in this work have been specifically tailored for hybrid couplers. These are important microwave components, extensively utilized in antenna feeding networks [48] or balanced-type circuits (e.g., mixers [101] or amplifiers [102]) as devices offering an equal power division between the output ports with a certain phase shift. Conventional hybrid couplers, owing to their circuit topology primarily based on quarter-wavelength transmission lines, consume large real estate areas, which makes them probably the most represented microwave components in the scientific literature on miniaturization.

The main contribution of this work is related to new design methodologies for hybrid couplers with compact cells utilized as their fundamental building blocks. The assumption made here is that parameterized layouts of compact cells are given at the start of the design process. However, to make the content of this dissertation more intelligible, a brief introduction to compact cells is provided in Section 2.

An introduction to numerical optimization as the main methodological tool utilized in this work is given in Section 3. This includes an outline of both direct optimization techniques as well SBO ones that find application in the further part of this dissertation. An exhaustive description of all SBO techniques reported to this date in the scientific literature has been omitted. An interested reader is referred to [60], [103] for in-depth treatment of SBO techniques in contemporary engineering.

The considerations provided in this work are limited to hybrid couplers that do not require via-holes or bonding wires in planar implementations, which includes branch-line and rat-race couplers and excludes structures such as Lange or tandem couplers [15]. This has been done to lower the cost and complexity of experimental verification. Also, we exclusively use microstrip technology for circuit implementation throughout the work. Not only does it offer cheap and convenient fabrication, but it is also well characterized in leading computer-aided design (CAD) software [104].

Numerical case studies illustrated in this work cover a lower part of the microwave spectrum. For the sake of convenience, most devices under consideration are designated for a 1-GHz operating frequency.

1.4 Contributions

This thesis describes several original design methodologies that contribute to the state of the art of microwave coupler miniaturization in terms of extended applicability, improved reliability and—most importantly—computational efficiency. This study is based on a consistent series of six peer-reviewed articles that are a part of author's research on miniaturized microwave circuits and components, counting 37 Web of Science (WoS) entries by May 2017.

A list of publications included in this thesis (according to the order of appearance) is presented below. These have been arranged to be in line with the consecutive goals enumerated in Section 1.2.

1. A. Bekasiewicz, P. Kurgan, and M. Kitlinski, "New approach to a fast and accurate design of microwave circuits with complex topologies," *IET Microwaves, Antennas & Propagation*, vol. 6, no. 14, pp. 1616–1622, Nov. 2012.

2. S. Koziel, A. Bekasiewicz, and P. Kurgan, "Rapid EM-driven design of compact RF circuits by means of nested space mapping," *IEEE Microwave and Wireless Components Letters*, vol. 24, no. 6, pp. 364–366, Jun. 2014.
3. P. Kurgan and S. Koziel, "Fast surrogate-assisted simulation-driven optimization of compact microwave hybrid couplers," *Engineering Optimization*, vol. 48, no. 7, pp. 1109–1120, Nov. 2015.
4. P. Kurgan and S. Koziel, "Design of high-performance hybrid branch-line couplers for wideband and space-limited applications," *IET Microwaves, Antennas & Propagation*, vol. 10, no. 12, pp. 1339–1344, Sept. 2016.
5. S. Koziel, A. Bekasiewicz, and P. Kurgan, "Rapid design and size reduction of microwave couplers using variable-fidelity EM-driven optimization," *International Journal of RF and Microwave Computer-Aided Engineering*, vol. 26, no. 1, pp. 27–35, Aug. 2015.
6. P. Kurgan and S. Koziel, "Surrogate-assisted multi-objective optimization of compact microwave couplers," *Journal of Electromagnetic Waves and Applications*, vol. 30, no. 15, pp. 2067–2075, Sept. 2016.

The original developments presented in this thesis correspond to the publications itemized above. The list of author's individual contributions is the following:

Ad 1. Conceptual development of a simulation-driven design framework for modular microwave circuits, based on sequential reconstruction and optimization of circuit components. Computational efficiency of this approach results from using a truncated vector of optimization variables (updated after each iteration) with the remaining vector elements fixed. This generic concept enables accounting for cross-coupling effects between adjacent circuit components, which is one of the fundamental obstacles pertinent to decomposition-based miniaturization methods.

Ad 2. (i) Conceptual development and implementation of a generic compact cell surrogate model with improved accuracy for nested space mapping (NSM) algorithm. The improved accuracy of a component-level model is attributed to a combination of several space mapping techniques adapted by the author. (ii) Conceptual development and implementation of a fast coarse model of a complete miniaturized circuit using an ABCD matrix representation.

Ad 3. Conceptual development of EM-driven techniques for low-cost determination of a near-optimized solution to miniaturized hybrid coupler design problem. This involves (i) sequential optimization of detached compact cells (with upper bound update scheme) and (ii) concurrent optimization of detached compact cells with the emphasis on a framework for determining geometric dependence of optimization variables (to ensure physical consistency of the coupler layout). (iii) Conceptual development and implementation of a fast coarse model of a complete coupler for the purpose of a surrogate-assisted fine-tuning procedure. The model involves using ABCD matrix representation and local response surface approximations set up in the vicinity of compact cell optimized solutions.

Ad 4. (i) Development of an optimization scheme for obtaining a family of wideband coupler reference solutions with a 3-dB power split and maximized bandwidth using iteratively adjusted electrical parameters of the model. (ii) Conceptual development and implementation of a technique for determination of a repetition factor of a recurrent slow-wave structure for specified design requirements. (iii) Conceptual development and implementation of a cascaded response surface approximation model of a recurrent slow-wave structure for the purpose of fast SBO of a wideband hybrid coupler.

Ad 5. (i) Development and implementation of techniques for setting up a family of simplified EM models for multi-fidelity coupler design. (ii) Development of a new single-objective design problem formulation for miniaturized hybrid couplers that aims at explicit size reduction with sufficient performance indicators ensured with a penalty function approach.

Ad 6. (i) Development and implementation of a surrogate model for rapid multi-objective coupler design optimization. The surrogate model involves implicit and frequency

space mapping applied to an underlying equivalent circuit model of the miniaturized coupler for improved accuracy. (ii) Adaptation of a point-by-point multi-objective optimization scheme. (iii) Defining objectives for explicit coupler size reduction and bandwidth maximization (other performance goals are ensured through penalty function objective formulation).

The specific journal metric data for the above-listed publications as well as author's percentage contribution to these works have been shown in Table 1.1.

1.5 Dissertation Outline

This dissertation is organized as follows. Chapter 2 presents a short introduction to compact cells, focusing on currently prevailing engineering approaches to cell selection and development. Basic modeling strategies of compact cells are included. Chapter 3 is an exposition of numerical optimization methods (both direct and surrogate-based ones) considered in the context of simulation-driven design of microwave circuits. A list of relevant references to the descriptive part of this thesis is provided after Chapter 3. This is followed by a body of publications that include original methodological developments of this work, numerical case studies, experimental verifications, and benchmarking with state-of-the-art structures or methods. Chapters 4 and 5 present methods for rapid design of compact microwave circuits using equivalent circuits and space mapping technology. Application examples for the proposed methods include both multi-section matching transformers and hybrid couplers. Supplementary data on numerical validation of the method presented in Chapter 5 are collected in Appendix A. Chapter 6 contains an original methodology for expedited EM-driven design optimization of miniaturized hybrid couplers based on EM models, response surface approximations and space mapping technology. An extension to the last method is provided in Chapter 7 that aims at design of miniaturized hybrid couplers with wideband operation. Methods of Chapters 4 through 7 introduce different means allowing for compensation of deteriorating EM cross-coupling effects that occur in miniaturized layouts. Chapters 8 and 9 present original formulations of the relevant design problem that enable an explicit miniaturization of hybrid couplers, with single-objective approach given in Chapter 8 and a multi-objective one presented in Chapter 9. Chapter 10 concludes the dissertation and discusses directions for the future work.

TABLE 1.1: JOURNAL METRIC DATA AND AUTHOR'S PERCENTAGE CONTRIBUTIONS

Ref.	Abbreviated Journal Title	Year of Publication	Journal Impact Factor	Contribution
1	IET Microw. Ant. Propag.	2012	0.836	50%
2	IEEE Microw. Wireless Comp. Lett.	2014	1.703	33%
3	Eng. Opt.	2015	1.380	50%
4	IET Microw. Ant. Propag.	2016	0.817	50%
5	J. RF Microw. Comp. Aided Eng.	2015	0.524	33%
6	J. Electromag. Waves Appl.	2016	0.772	50%

2 Development and Modeling of Compact Cells

In this chapter, a short introduction to compact cells is presented. Compact cells are utilized in the further part of this dissertation as the key components of microwave hybrid couplers that enable their size reduction. It is to be noted that—in the design methods proposed in this work—specific parameterized compact cell realizations are assumed to be given. The aim of this chapter is therefore to give the reader a basic insight into the transmission properties of compact cells as well as to outline the prevalent engineering approaches to the their development. In addition, the main simulation models of compact cells are briefly discussed.

2.1 Theoretical Model of Slow-Wave Transmission Lines

The use of compact-cell-based slow-wave transmission lines as fundamental building blocks of miniaturized microwave components, including hybrid couplers (in highest numbers) [77], [79], [86], power dividers [35], [105], matching transformers [106], [107] or filters [108], [109], has begun at the turn of the twentieth century (e.g., [30]). Prior to these works, much effort has been directed towards theoretical analysis of recurrent slow-wave structures such as transmission lines with coil loadings [39]. Historically, slow-wave transmission lines as utilized today in research on miniaturization, descend from a long lineage of intertwined scientific findings in transmission line theory [110], circuit theory of periodic structures [39], early elements of microwave filter theory [111], and the theory of non-uniform transmission lines [112].

The fundamental properties of slow-wave structures can be determined using transmission line theory [113]. To this end, consider an incremental unit cell model shown in Figure 2.1. It is constituted by a per-unit-length series impedance Z' [Ω/m] composed of a per-unit-length inductance L'_{se} [H/m] in parallel with a times-unit-length capacitance C'_{se} [F·m], resonating at the ω_{se} [rad/s] angular frequency, and a per-unit-length shunt admittance Y' [S/m] comprising a times-unit-length inductance L'_{sh} [H·m] in series with a per-unit-length capacitance C'_{sh} [F/m], resonating at the ω_{sh} [rad/s] angular frequency. The equivalent circuit model proposed here is a combination of low-pass and high-pass configurations of a uniform transmission line (the former being valid for electrical lengths ranging from 0 to π and the latter one for electrical lengths between π and 2π [114]). The selection of this particular cell model is also justified by

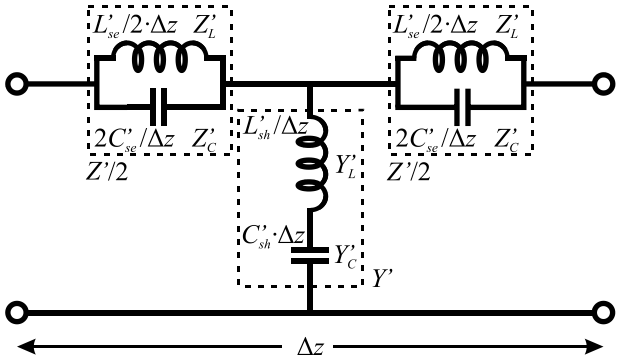

Figure 2.1: Incremental ($\Delta z \to 0$) model of a slow-wave transmission line. Primes denote per-unit-length or times-unit-length parameters. Z_L' and Z_C' represent impedances of series inductance and capacitance, whereas Y_L' and Y_C' are admittances of shunt inductance and capacitance, respectively.

a number of preliminary studies conducted by the author [36, 41, 44, 45, 76, 115], indicating that a variety of different compact cell realizations can be adequately described by the model under discussion. For comparison, an analogous theoretical analysis of slow-wave transmission lines is given in [116].

Note that the equivalent circuit model of Figure 2.1 is characterized by an infinitesimal length. This is an important assumption made in transmission line theory that enables (among others) derivation of the telegrapher's equations describing the behavior of a transmission medium [12], [117]. For discontinuous transmission lines (e.g., composite right/left-handed ones), however, this assumption (also referred to as a perfect-homogeneity condition [113]) does not hold in practice and thus it is reserved exclusively for theoretical speculations. This is evident considering that physical implementations of slow-wave transmission lines realize specified electrical lengths and are based on a finite number of unit cells. To address that, Caloz and Itoh formulate an effective-homogeneity condition ($\Delta z << \lambda_g$), whose satisfaction allows for obtaining physically-realizable slow-wave structures that mimic ideal UTLs in a restricted frequency range [113]. The model of Figure 2.1 is still applicable to such realistic problems, provided that $L_{se}=L'_{se}\Delta z$, $C_{se}=C'_{se}/\Delta z$, $L_{sh}=L'_{sh}/\Delta z$, and $C_{sh}=C'_{sh}\Delta z$. The rule of thumb is that the above requirement is met for the cell lengths smaller than one quarter of the guided wavelength [113]. In the limit case of $\Delta z = \lambda_g/4$, a compact cell can be equivalent to a UTL only at a single frequency, in the vicinity of which characteristics of the homogeneous line are merely approximated [53].

Explicit formulas for Z' and Y' are given by

$$Z' = \frac{j\omega L'_{se}}{1-\omega^2 L'_{se} C'_{se}} = \frac{j\omega L'_{se}}{1-\left(\frac{\omega}{\omega_{se}}\right)^2} \tag{2.1}$$

$$Y' = \frac{j\omega C'_{sh}}{1-\omega^2 L'_{sh} C'_{sh}} = \frac{j\omega C'_{sh}}{1-\left(\frac{\omega}{\omega_{sh}}\right)^2} \tag{2.2}$$

where ω_{se}, ω_{sh} are defined as:

$$\omega_{se} = \frac{1}{\sqrt{L'_{se} C'_{se}}} \tag{2.3}$$

$$\omega_{sh} = \frac{1}{\sqrt{L'_{sh} C'_{sh}}} \tag{2.4}$$

The asymptotic behavior of an ideal slow-wave transmission line can be inferred from the analysis of the unit cell model of Figure 2.1 in two limit cases: (i) $\omega \to 0$, and (ii) $\omega \to \infty$. In the first case, for the angular frequency approaching zero, it follows that $Z'_L \to 0$, $Z'_C \to \infty$,

$Y'_L \to \infty$, $Y'_C \to 0$, so that the compact cell operates as a series inductance and shunt capacitance circuit (a so-called right-handed structure), exhibiting low-pass filtering characteristics. In the second case, as ω approaches infinity, $Z'_L \to \infty$, $Z'_C \to 0$, $Y'_L \to 0$, $Y'_C \to \infty$, hence, the unit cell behaves as a series capacitance and shunt inductance circuit (a so-called left-handed structure), illustrating a high-pass filtering performance. At other frequencies, all lumped elements of the compact cell model contribute to its characteristics, however, at low frequencies right-handed elements (L'_{se}, C'_{sh}) dominate over the left-handed ones (L'_{sh}, C'_{se}) and at high frequencies these relations are inverted.

The detailed theoretical behavior of the considered class of slow-wave structures is obtained by deriving explicit formulas for the key transmission line parameters, that is, complex propagation constant γ and characteristic impedance Z_0. This is accomplished by substituting (2.1) and (2.2) into general expressions for γ and Z_0 [12]

$$\gamma = \alpha + j\beta = \pm\sqrt{Z'Y'} \tag{2.5}$$

$$Z_0 = \sqrt{\frac{Z'}{Y'}} \tag{2.6}$$

yielding

$$\gamma = s(\omega)\frac{j\omega\sqrt{L'_{se}C'_{sh}}}{\sqrt{\left[1-\left(\frac{\omega}{\omega_{se}}\right)^2\right]\cdot\left[1-\left(\frac{\omega}{\omega_{sh}}\right)^2\right]}} \tag{2.7}$$

$$Z_0 = \sqrt{\frac{L'_{se}}{C'_{sh}}}\sqrt{\frac{1-\left(\frac{\omega}{\omega_{sh}}\right)^2}{1-\left(\frac{\omega}{\omega_{se}}\right)^2}} \tag{2.8}$$

where $s(\omega)$ is a sign function that returns +1 for $\omega < \min(\omega_{se},\omega_{sh})$ and –1 for $\omega > \min(\omega_{se},\omega_{sh})$. An inspection of (2.7) reveals that, in general, the propagation constant is purely imaginary ($\gamma = j\beta$) when the denominator is positive, and purely real ($\gamma = \alpha$) when the denominator is negative. The first case occurs for two frequency ranges: (i) $\omega < \min(\omega_{se},\omega_{sh})$ and (ii) $\omega > \min(\omega_{se},\omega_{sh})$. These frequencies define passbands, in which EM waves propagate without attenuation ($\alpha = 0$). The second case determines a bandgap, in which EM wave propagation is prohibited ($\beta = 0$), and happens for ω ranging between $\min(\omega_{se},\omega_{sh})$ and $\max(\omega_{se},\omega_{sh})$. At the resonant frequencies ω_{se} and ω_{sh}, the propagation constant tends to $\pm\infty$, depending on the sign function $s(\omega)$. For the angular frequency limit cases, $\omega \to 0$ and $\omega \to \infty$, the propagation constant approaches zero.

A detailed attenuation and dispersion diagram for ideal slow-wave transmission lines is depicted in Figure 2.2. One can identify three different regions of operation: (i) the low (right-handed) passband, (ii) the bandgap, and (iii) the high (left-handed) passband. The low passband is located below the first resonant frequency and demonstrates a slow-wav behavior due to the denominator of (2.7) smaller than 1 and approaching 0 at the resonant frequency. It is worth noting that the propagation constant of the slow-wave TL increases in a linear fashion approximately up to the half of the first resonant frequency, above which a rapid change in the phase coefficient can be observed. In the bandgap region located between distinct resonant frequencies, the angular frequency of minimum attenuation is the root of the derivative of the complex propagation constant. The high passband that occurs above the second resonant frequency is a composition of sub-regions supporting a slow-wave and fast-wave propagation.

Figure 2.3 presents real and imaginary parts of the characteristic impedance of slow-wave transmission lines. Here, two different operation cases are considered: (i) $\omega_{se} < \omega_{sh}$ and (ii) $\omega_{se} > \omega_{sh}$.

This is due to the fact that, based on (2.8), the characteristic impedance has a zero at ω_{sh} and a pole at ω_{se}. Examining Figure 2.3 confirms the existence of three separate regions of interest. Regions I and III may support EM wave propagation, because the characteristic impedance is purely real and the absolute reflection coefficient ranges between 0 and 1. Conversely, the absolute reflection coefficient for the second region is equal to unity, which is due to purely imaginary characteristic impedance in the range currently discussed.

The theoretical model of compact cells proposed here offers an insight into the frequency phenomena that take place in compact-cell-based slow-wave transmission lines, which is valuable from the epistemic point of view. It can also be used as an approximate prediction tool for the operation of a given compact cell upon the variation of the values of its constitutive elements, leading to formulation of general design guidelines for compact cells [36], [76]. On the other hand, the accuracy of the model is poor (especially when Δz becomes comparable to λ_g).

For an exhaustive theoretical treatment of the slow-wave structures, an interested reader is referred to the literature (e.g., [40], [87] or [116]).

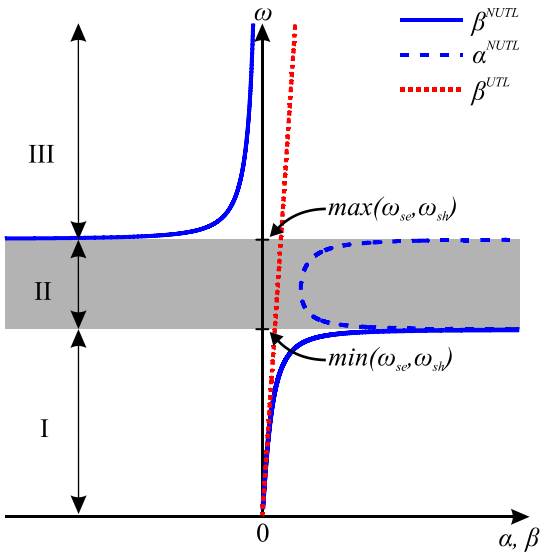

Figure 2.2: Attenuation/dispersion characteristics of ideal slow-wave lines in a general (unbalanced) case $\omega_{se} \neq \omega_{sh}$. Labels I, II, and III denote the low (right-handed) passband, bandgap, and high (left-handed) passband, respectively. The phase constant of a UTL has been included for comparison purposes. Here, superscript NUTL refers to geometrically non-uniform transmission lines.

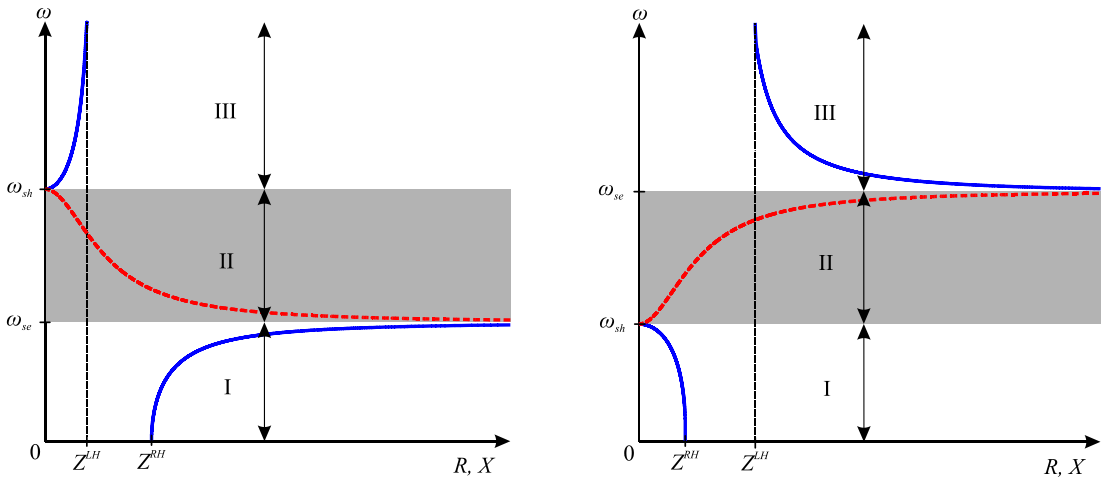

Figure 2.3: Characteristic impedance of slow-wave lines in a general (unbalanced) case $\omega_{se} \neq \omega_{sh}$ ($\omega_{se} < \omega_{sh}$ for inset on the left and $\omega_{se} > \omega_{sh}$ for the one on the right). Resistance R and reactance X are plotted with solid and dashed lines, respectively. Z^{RH} and Z^{LH} denote characteristic impedances of purely right-handed and purely left-handed transmission lines, respectively, $Z^{RH} = (L_{se}'/C_{sh}')^{0.5}$ and $Z^{LH} = (L_{sh}'/C_{se}')^{0.5}$.

2.2 Development of Compact Cells

Broadly speaking, slow-wave TLs are periodic structures with a compact cell inserted as a recurrent element. As already mentioned, their practical implementations follow the concept of spatially separated storage of magnetic and electric energy, which is typically realized by means of intricate combinations of short (with respect to the guided wavelength) high-impedance strips and low-impedance stubs [118]. From the perspective of transmission characteristics exhibited by slow-wave lines, only a restricted frequency range of the low passband region (cf. Figures 2.2, 2.3) is most commonly utilized for guided-wave applications. Filtering properties may also be used for harmonic rejection [119].

The selection of a suitable repetition factor of recurrent slow-wave transmission line in an important aspect pertaining to the development of compact-cell-based structures. In practice, it is established based on engineering insight with consideration of the target operational bandwidth [36]. The rule of thumb is that the repetition factor of one or two is used for narrowband applications [76]; in case of a wideband operation, the repetition factor above three is more preferable [84]. The reason is the location of the cut-off frequency, which is usually restrictively low for small values of the repetition factor, thus limiting the width of the usable passband [76].

As already stated, in a large number of articles on size reduction of microwave components, the dominant approach to the selection of a particular compact cell geometry is to choose (typically in an arbitrary manner) from a wide catalogue of previously reported cells (e.g. [76]). Depending on the specific application, such a compact cell undergoes adjustment of designable parameters (for devices operating in the vicinity of the central frequency) or is cascaded and then subjected to parameter tuning (for wideband applications). A large collection of example compact cells is shown in Figure 2.4.

An alternative approach is to devise a new compact cell geometry. Most commonly, this follows the concept based on using semi-lumped elements to approximate a lumped representation of a UTL section [53]. Conceptual illustration of this method is shown in Figure 2.5. More information on manual development of a compact cell or its selection from available library can be found in [76].

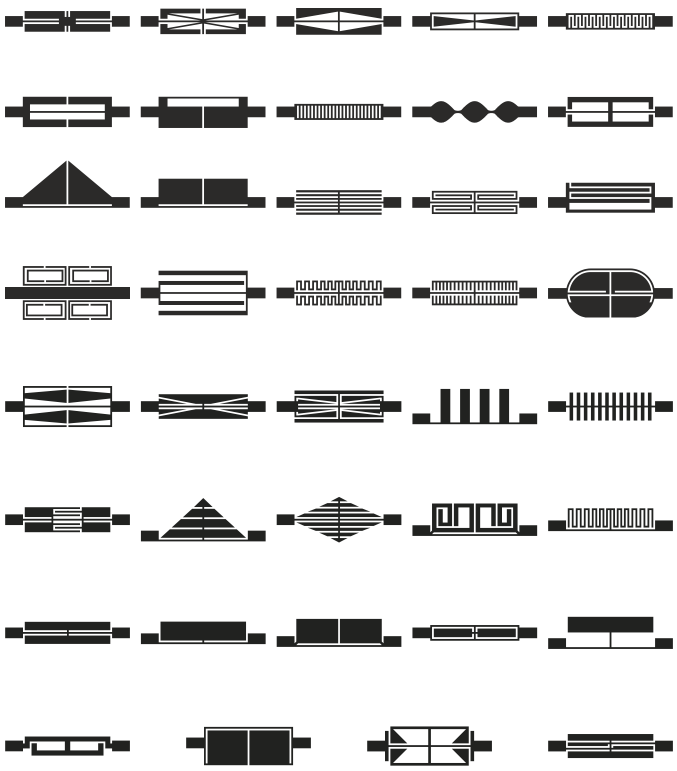

Figure 2.4: A catalogue of previously published compact cells [76].

2.3 Modeling of Compact Cells

Reliable modeling of compact cells is a necessary part of decomposition-based simulation-driven design of miniaturized hybrid couplers. In this work, much attention is directed towards physics-based low-fidelity models that are a simplified representation of the considered engineering problem. The main advantage of physics-based low-fidelity models is that they incorporate some knowledge about the problem at hand and, for that reason, exhibit decent generalization capabilities while being significantly cheaper (in the computational sense) than their high-fidelity EM-simulated counterparts. Such features are highly desired from the perspective of reliable and computationally efficient design methods. Here, equivalent circuits are primarily used as low-fidelity models of compact cells. In some cases, coarse-discretization EM models are employed in the design process. To perform a fine-tuning procedure for an approximate design solution produced by a low-fidelity model, local data-driven models may become handy. These typically require a rather small number of high-fidelity EM training samples associated with model development. Figure 2.6 shows several computational models of compact cells that are repeatedly utilized in this dissertation.

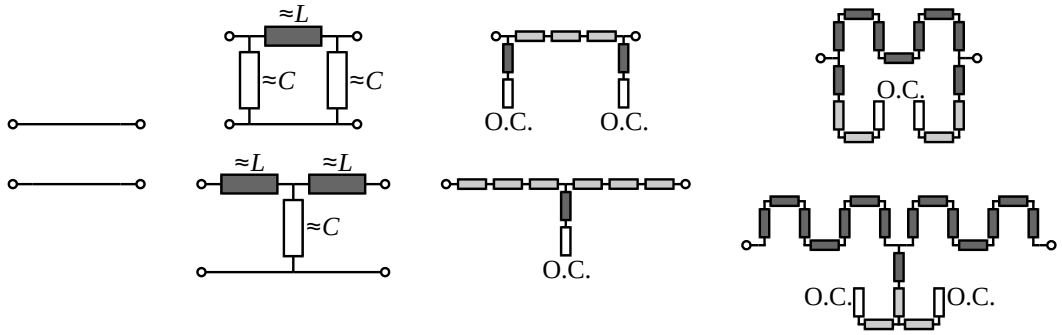

Figure 2.5: Conceptual evolution (from left to right) of a uniform transmission line through T- or π-networks into increasingly complex combinations of high- , low- or mixed-impedance lines (marked by dark grey, white, and light grey colors, respectively).

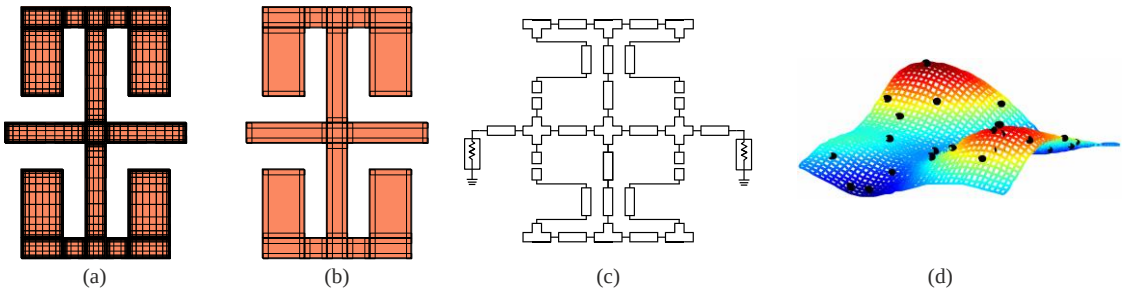

(a) (b) (c) (d)

Figure 2.6: Computational models of example compact cell: (a) fine-discretization EM model, (b) coarse-discretization EM model, (c) equivalent circuit, (d) local data-driven model.

3 Simulation-Driven Design of Microwave Circuits

This chapter introduces fundamental concepts of microwave circuit design using computer simulations. The microwave circuit design task is formulated as a nonlinear minimization problem with constraints. Typical objectives, constraints, and merit function definitions inherent to microwave engineering are discussed. A brief outline of conventional (direct) optimization routines is provided, including deterministic trajectory-based methods (both gradient-based and derivative-free) as well as stochastic population-based techniques. Selected design methods, utilized in the body of the dissertation, are covered in more detail. This includes the concept of surrogate-based optimization as well as model and/or response corrections based on space mapping technology.

3.1 Problem Formulation

Simulation-driven design of microwave circuits involves (i) developing a computer model of the structure under consideration, and (ii) adjusting its designable parameters to satisfy given design specifications. Stage (i) is typically realized with advanced design and simulation tools, which can be broadly categorized into circuit simulators (e.g., Agilent ADS [104]) and electromagnetic simulators (e.g, Sonnet ***em*** [95] or CST Microwave Studio [96]). The former are used to construct equivalent circuit models that, for a variety of complex design problems, are merely capable of yielding a rough estimate of the desired solution. The latter offer an ultimate modeling accuracy (particularly when using fine discretization of the structure at hand) and are widely utilized in both academia and industry for a reliable evaluation of the system performance [120]. Stage (ii) of the microwave circuit design process is normally accomplished either by repetitive parameter sweeps (usually with each parameter treated separately), supervised by an experienced designer, or by an automated procedure of numerical optimization. The first option is laborious, time-consuming, and practically limited to low-dimensional design problems. It also does not guarantee optimal solutions as they are often counter-intuitive in terms of parameter setups. This issue is addressed by the second strategy, which shifts the effort of searching for a satisfactory circuit solution from a designer to a computer-assisted optimization procedure.

It is assumed here that—for the sake of design reliability—conventional (or direct) optimization methods, outlined in Section 3.2, employ only high-fidelity EM simulation models for evaluating each candidate solution suggested by the optimizer. Thus, precise design optimization of microwave circuits can be stated as follows. Let $\boldsymbol{R}_f$ denote a function that accurately models the behavior of the structure under consideration. In other words, $\boldsymbol{R}_f$ is a so-called fine model of the device in question. Additionally, consider a vector $\boldsymbol{x} = [x_1\ x_2\ \ldots\ x_n]^T$ that represents design variables to be adjusted in the design process (most commonly these refer to geometry parameters of the given microwave structure). The value of the function $\boldsymbol{R}_f$ for a specified vector $\boldsymbol{x}$ is given by $\boldsymbol{R}_f(\boldsymbol{x})$. This represents a response of the fine model at a design $\boldsymbol{x}$, for instance, scattering parameters acquired by means of full-wave EM analysis. Normally, simulation models in microwave engineering are evaluated at a discrete set of frequency points, so in a general case, $\boldsymbol{R}_f(\boldsymbol{x})$ is a vector of responses of the fine model. The simulation-driven microwave circuit design task can be formulated as a nonlinear minimization problem of the following form [57]

$$\boldsymbol{x}^* = \arg\min_{\boldsymbol{x}\in X} U\left(\boldsymbol{R}_f\left(\boldsymbol{x}\right)\right) \tag{3.1}$$

where $\boldsymbol{x}^*$ is the optimum design solution to be determined by the optimization process, X is the n-dimensional search space (the objective function domain), and U is a scalar merit function that encodes design specifications (typically expressed in terms of the model response). The composition of U and $\boldsymbol{R}_f$ is referred to as an objective function, whereas $U(\boldsymbol{R}_f(\boldsymbol{x}))$ is a value of the objective function at a design $\boldsymbol{x}$. For the notation of (3.1), the merit function is implemented in such a way that a given design $\boldsymbol{x}$—for which the model response better satisfies design specifications—corresponds to a smaller value of the objective function. In microwave engineering, the typical design objectives include minimizing $|S_{11}|$ over a frequency band of interest or maintaining $|S_{21}|$ above a certain level for a given frequency range. In general, minimizing the selected scattering parameters can be implemented in the merit function in a straightforward manner, whereas keeping them below/above certain thresholds can be easily translated into U by means of the minimax function that returns the maximum violation of the specification vector by the model response [121]. Alternatively, U can be defined by the Euclidean norm that measures the distance between $\boldsymbol{R}_f(\boldsymbol{x})$ and the target (specification) vector [121].

In many practical instances, a proper formulation of U becomes far more challenging due to multiple design goals that are to be handled at the same time. A popular approach to this problem is the weighted sum method, which converts a multi-objective task into a single-objective one by constructing a linear aggregation of particular objectives prefixed with appropriate weighting factors [121]. Another possibility is to handle one design criterion directly and include auxiliary objectives through penalty functions that contribute to the aggregated objective function when certain specification thresholds are violated [121]. It should be mentioned—for the sake of completeness—that a comprehensive solution to the aforementioned issue is attained by means of genuine multi-objective optimization [89].

For the majority of realistic design cases, the process (3.1) takes the form of an optimization problem with constraints. These determine the feasibility or infeasibility of a given design with respect to design specifications. One example is obtaining a required phase shift, $\arg(S_{21})$, at the given operating frequency. Another one is keeping the layout size smaller or equal to the maximum real estate area available for the microwave structure under consideration. Formally, the optimization procedure (3.1) is subject to equality and/or inequality constraints, that is, $c_{eq.l}(\boldsymbol{x}) = 0$ and $c_{ineq.l}(\boldsymbol{x}) \le 0$, respectively, where $l = 1, 2, \ldots, N$, where N equals to the number of equality constraints, N_{eq}, or inequality constraints, N_{ineq}, depending on the particular case. In practice, the domain of problem (3.1) is also determined by the lower and upper bounds for design variables (e.g., expressing limitations of the selected fabrication technology).

In the series of articles presented in this dissertation, geometry constraints—such as those mentioned above, but also the ones that prevent certain parts of the circuit layout from overlapping—are handled explicitly as they are calculated directly from $\boldsymbol{x}$ and do not require an expensive evaluation of a model response. Conversely, performance-related constraints are controlled implicitly through penalty terms added to the primary objective function. Such constraints often emerge when a multi-objective design problem is converted into a single-objective one. It

should be emphasized that the discussed strategy of constraint handling results from the condition of computational efficiency, imperative for design procedures developed in the course of this work. However, it should also be mentioned that the literature provides efficient approaches to explicitly manage expensive constraints (e.g., [122], [123], which discuss design optimization problems in mechanical and aerospace engineering, respectively).

A general flowchart of EM-driven optimization-based design of microwave circuits is shown in Figure 3.1. The first stage of the design process is a manual problem setup involving model construction, definition of design specifications, etc. The second stage is an iterative optimization scheme that aims at finding the best candidate solution to satisfy design requirements. As already mentioned, each design produced by the optimizer is verified using a high-fidelity EM simulation. Depending on the type of the applied algorithm, the optimization process may be realized by a single agent or multiple agents. Likewise, the procedure may use only the model response or both the response and its gradient to produce an improved candidate solution. A short overview of conventional optimization routines is provided in Section 3.2.

3.2 Direct Optimization

Although the main focus of this dissertation is given to surrogate-based optimization partially relying on space mapping technology, some basic information on conventional optimization strategies are included here primarily for the comparison purposes. In addition, the selected conventional techniques (particularly local ones) are applied in the course of this work to solve low-cost optimization subproblems within the proposed surrogate-assisted design frameworks. A short overview of direct optimization techniques provided in this section includes gradient-based and derivative-free methods, as well as population-based metaheuristics. It should be noted that metaheuristics are also categorized as derivative-free methods; however, they are outlined here separately as majority of them operate on the principle of multiple agents as opposed to the previous techniques that use a single agent in the search for the optimum design. For a detailed exposition of conventional optimization algorithms, the interested reader is referred to the literature (e.g., [57], [121], [124]). To simplify notation, the symbol $f(\boldsymbol{x})$ is used throughout Section 3.2 as a scalar objective function instead of $U(\boldsymbol{R}_f(\boldsymbol{x}))$.

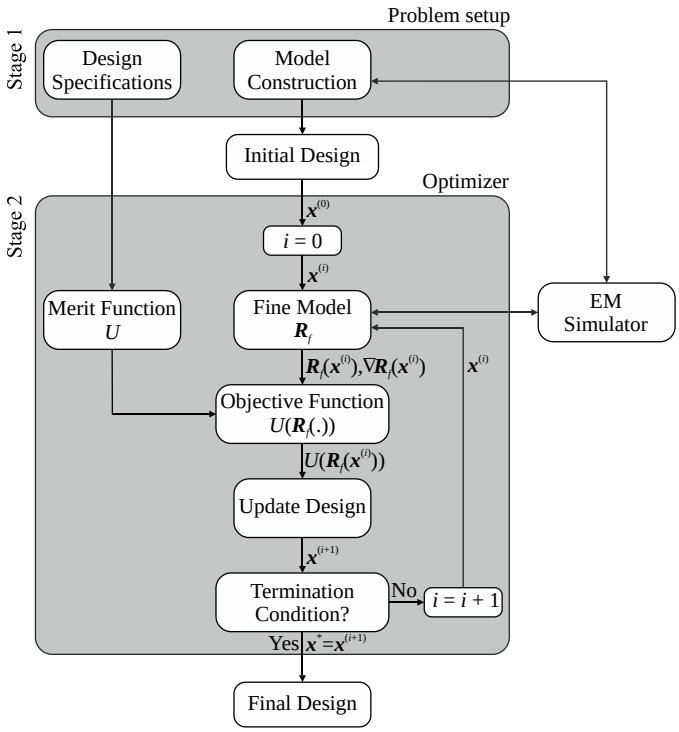

Figure 3.1: Simulation-driven design of microwave circuits based on numerical optimization and fine EM simulation models [125].

3.2.1 Gradient-Based Optimization Methods

Gradient-based algorithms belong to the most widespread and well-established optimization techniques today [121]. The search for a better design is directed by the gradient $\nabla f(\boldsymbol{x})$ of the objective function $f(\boldsymbol{x})$ defined as

$$\nabla f(\boldsymbol{x}) = \left[\frac{\partial f}{\partial x_1}(\boldsymbol{x}) \quad \frac{\partial f}{\partial x_2}(\boldsymbol{x}) \quad \ldots \quad \frac{\partial f}{\partial x_n}(\boldsymbol{x}) \right]^T \tag{3.2}$$

Assuming that the objective function $f(\boldsymbol{x})$ is sufficiently smooth, that is, at least continuously differentiable, the gradient (3.2) provides information about the local behavior of $f(\boldsymbol{x})$ in the vicinity of a design at which it is calculated. In more detail, for a sufficiently small vector $\boldsymbol{h}$, provided that $\nabla f(\boldsymbol{x}) \cdot \boldsymbol{h} < 0$, the following relation occurs

$$f(\boldsymbol{x} + \boldsymbol{h}) \cong f(\boldsymbol{x}) + \nabla f(\boldsymbol{x}) \cdot \boldsymbol{h} < f(\boldsymbol{x}) \tag{3.3}$$

Here, $\boldsymbol{h} = -\nabla f(\boldsymbol{x})$ determines the direction of the locally steepest descent. In general, gradient information can be utilized in the search process either by moving along the descent direction (e.g., the steepest descent) [121] or by exploiting a local approximation model of the objective function developed using ∇f [126]. A general flowchart embodying the concept of gradient-based descent methods is illustrated in Figure 3.2. From the practical perspective, using the steepest descent to navigate the search process leads to a poor performance of an optimization algorithm when in the close proximity to optimum [121], [127]. Algorithm performance can be improved by using a so-called conjugate-gradient method where the search direction $\boldsymbol{h}$ is established based on the current gradient as well as the previous direction $\boldsymbol{h}_{prev}$ as follows [127]

$$\boldsymbol{h} = -\nabla f(\boldsymbol{x}^{(i)}) + \gamma \boldsymbol{h}_{prev} \tag{3.4}$$

The most popular schemes for determining the value of coefficient γ of (3.4) are Fleecher-Reeves and Polak-Ribiére methods with the respective formulas given below

$$\gamma = \frac{\nabla f(\boldsymbol{x}^{(i)})^T \nabla f(\boldsymbol{x}^{(i)})}{\nabla f(\boldsymbol{x}^{(i-1)})^T \nabla f(\boldsymbol{x}^{(i-1)})} \tag{3.5}$$

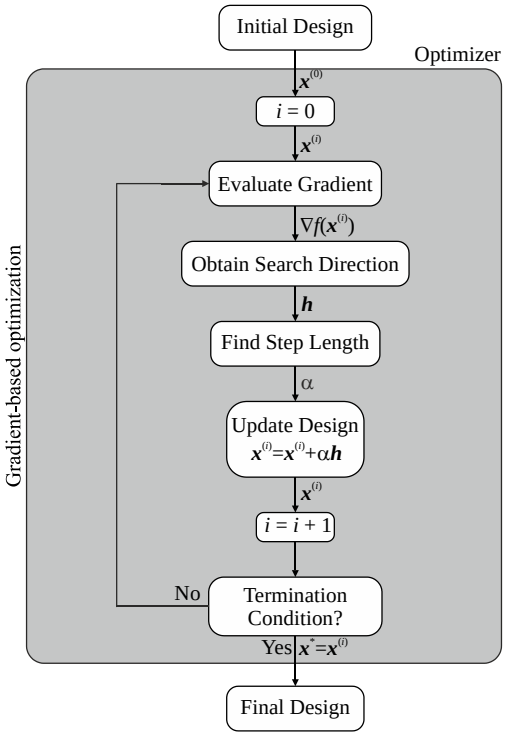

Figure 3.2: Generic gradient-based descent algorithm [121].

$$\gamma = \frac{(\nabla f(\boldsymbol{x}^{(i)}) - \nabla f(\boldsymbol{x}^{(i-1)}))^T \nabla f(\boldsymbol{x}^{(i)})}{\nabla f(\boldsymbol{x}^{(i-1)})^T \nabla f(\boldsymbol{x}^{(i-1)})} \tag{3.6}$$

Having obtained the search direction $\boldsymbol{h}$, the design is updated by adding $\alpha\boldsymbol{h}$ term, where a step size $\alpha > 0$ is found by performing a line search, so that $f(\boldsymbol{x}^{(i)}) < f(\boldsymbol{x}^{(i-1)})$ [121]. Note that the choice of a specific algorithm for identifying α is critical for the overall performance of the optimization algorithm.

A variety of conditions are used for terminating gradient-based optimization algorithms available in the literature. These include $\|\boldsymbol{x}^{(i+1)} - \boldsymbol{x}^{(i)}\| \le \varepsilon_1$ (convergence in the argument), $\|\nabla f(\boldsymbol{x}^{(i)})\| \le \varepsilon_2$ (vanishing of the gradient), $f(\boldsymbol{x}^{(i)}) - f(\boldsymbol{x}^{(i+1)}) \le \varepsilon_3$ (convergence in the function value), or a combination of the above.

The optimization process may also involve second-order derivatives, which is a characteristic feature of so-called Newton methods. Assuming that the objective function is at least twice continuously differentiable, one can consider a local representation of f in the form of its second-order Taylor expansion

$$f(\boldsymbol{x}+\boldsymbol{h}) \cong f(\boldsymbol{x}) + \nabla f(\boldsymbol{x}) \cdot \boldsymbol{h} + \frac{1}{2}\boldsymbol{h} \cdot \boldsymbol{H}(\boldsymbol{x}) \cdot \boldsymbol{h} \tag{3.7}$$

where $\boldsymbol{H}(\boldsymbol{x})$ is the Hessian of f at a design $\boldsymbol{x}$, defined as

$$\boldsymbol{H}(\boldsymbol{x}) = \begin{bmatrix} \dfrac{\partial^2 f}{\partial x_1 \partial x_1}(\boldsymbol{x}) & \cdots & \dfrac{\partial^2 f}{\partial x_1 \partial x_n}(\boldsymbol{x}) \\ \vdots & \ddots & \vdots \\ \dfrac{\partial^2 f}{\partial x_n \partial x_1}(\boldsymbol{x}) & \cdots & \dfrac{\partial^2 f}{\partial x_n \partial x_n}(\boldsymbol{x}) \end{bmatrix} \tag{3.8}$$

This infers, assuming that the current design $\boldsymbol{x}^{(i)}$ is sufficiently close to the minimum of f, that the consecutive approximation of the optimum can be determined as

$$\boldsymbol{x}^{(i+1)} = \boldsymbol{x}^{(i)} - [\boldsymbol{H}(\boldsymbol{x})]^{-1} \nabla f(\boldsymbol{x}) \tag{3.9}$$

The algorithm (3.9) converges at a very fast rate to the locally optimal design, provided that the starting point is sufficiently close to the optimum and the Hessian is positive definite [127]. In engineering practice, none of the aforementioned requirements is typically satisfied, so that different types of damped Newton techniques have to be used, e.g., the Levenberg-Marquardt method [121]. Another obstacle is that the Hessian of the objective function f is generally not available, which indicates the necessity of using Quasi-Newton methods, with Hessian approximation schemes based on various updating formulas [121].

The availability of some of the above outlined gradient-based optimization methods in commercial EM software (e.g., conjugate gradient method is implemented in Sonnet ***em*** [95], whereas interpolated Quasi-Newton is provided in CST Microwave Studio [96]) offers a chance of their practical application to current design problems of microwave engineering. However, this endeavor is hindered by several serious obstacles. The fundamental problem is the high computational cost of an accurate EM analysis, complemented by a large number of objective function evaluations required for convergence. Another issue is related to poor analytical properties of the EM-simulated objective function, which is normally noisy and discontinuous due to adaptive meshing techniques embedded in most of modern EM solvers. Additional problem pertinent to direct gradient-based optimization is a general lack of sensitivity information (or its high computational cost). Yet another drawback is the complexity of the objective function, which may feature multiple local optima. A possible solution to some of the above challenges are adjoint sensitivity techniques, available for example in CST Microwave Studio [96]). These enable calculation of sensitivities with little or no additional cost.

3.2.2 Derivative-Free Optimization Methods

Derivative-free techniques belong to a category of optimization methods that do not require derivative information in the search for the optimum design solution [128]. In many practical situations of EM-based CAD of microwave circuits, derivatives of the objective function are not available or are too expensive to compute (e.g., using finite differentiation of CPU-heavy objective function). Apart from that, gradient-based optimization methods exhibit poor performance in case of inherently noisy EM-simulated objective function. Derivative-free techniques aim at addressing the aforementioned issues.

The considered class of optimization methods include a variety of different routines such as pattern search algorithms [124], population-based metaheuristics [127], as well as SBO techniques [60]. This section, however, provides only a concise conceptual description of the first group of techniques from the above list, that is, local search algorithms. The remaining ones are outlined in Section 3.2.3 and 3.3, respectively.

Figure 3.3 illustrates the basic concept of the pattern search approach [124], which aims at identifying the optimum using a rectangular grid and an exploration scheme that searches for an improved solution only at the grid-restricted points. Failure in design improvement using the original grid results in its refinement, which in turn allows for obtaining steps with higher resolution. Note that by setting the original grid sufficiently large, one is capable of performing a quasi-global search. A typical criterion for the algorithm termination involves reaching a required used-defined resolution or the maximum number of iterations. It should be emphasized that the practical pattern search implementations use much more sophisticated strategies than the provided description suggests (cf. grid-restricted line search [124]).

The specialist literature offers a wide catalogue of numerous pattern search variations (see, e.g., [124]) as well as other local derivative-free optimization methods [128]. One of the most representative examples of the latter is the Nelder-Mead algorithm (also referred to as the simplex method) [127]. The search process of the discussed method is based on moving the vertices of the simplex in the design space in such a way that the vertex corresponding to the worst (highest) value of the objective function is replaced by the new one at the location where the value of the objective function is expected to be better.

Pattern search as well as other similar optimization methods exhibit partial immunity to the numerical noise characteristic to the EM-validated objective function. Their main disadvantage is a slower convergence rate when compared to the gradient-based optimization algorithms. One should note that the design difficulties related to the high computational cost of EM simulations, posing a challenge for all direct optimization methods, can be alleviated to some extent for the selected derivative-free routines (in particular pattern search algorithms) by problem parallelization using distributed computing.

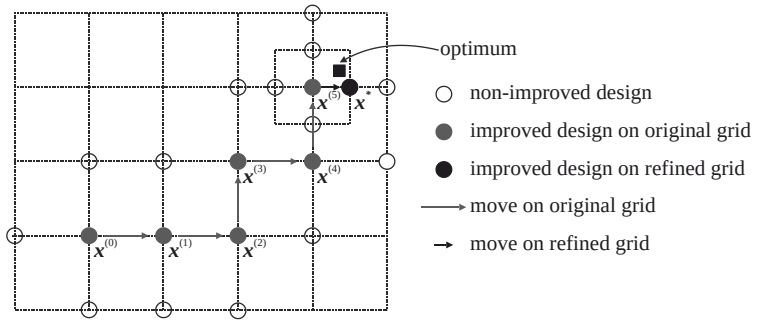

Figure 3.3: Conceptual illustration of pattern search [129]. The search is based on exploratory movements restricted to a rectangular grid. In each iteration i, only the grid-restricted neighborhood of design $\boldsymbol{x}^{(i)}$ is analyzed. Upon failure of making a successful move, the grid resolution is refined to allow smaller steps. Here, the consecutive approximations of the optimum are denoted as $\boldsymbol{x}^{(0)}$, $\boldsymbol{x}^{(1)}$, etc. The optimized design is given by $\boldsymbol{x}^*$.

3.2.3 Population-Based Optimization Methods

Population-based metaheuristics are global optimization methods that mimic processes occurring within biological or social systems. These algorithms concurrently process the entire sets (or populations) of candidate solutions (also referred to as individuals or agents) in such a way that—based on some nature-inspired operators—they adapt to the design environment at hand. The main advantages of population-based metaheuristics include (i) capability to avoid getting trapped in local minima, (ii) convergence to a global optimum with a reasonable probability, (iii) handling noisy, non-differentiable, and discontinuous objective functions, (iv) enabling hybridization with other optimization algorithms for operation improvement, and (v) explicitly considering multiple design objectives at the same time (refers to algorithm versions intended for multi-objective optimization) [89], [127]. The fundamental bottleneck here is a large number of objective function evaluations required for the convergence of the algorithm. This is indicated by a typical population size ranging between ten and one hundred, as well as the number of generations that may be between a few dozen and a few hundred. For this very reason, population-based metaheuristics are virtually prohibitive when utilized as direct optimization methods employing expensive EM simulations models. This shortcoming can be partially mitigated by using distributed computing, provided that massive CPU resources as well as multiple EM software licenses are available. Apart from the above, due to the stochastic nature of some of the mechanisms within the optimization algorithm, repeatability of results is limited. At the same time, the performance of a metaheuristic algorithm heavily depends on user-defined control parameters whose proper setup requires expertise and is generally problem-dependent.

The most popular types of population-based metaheuristic algorithms nowadays include genetic algorithms [130], evolutionary algorithms [131], particle swarm optimizers [132], differential evolution [133], and a firefly algorithm [127]. A typical flowchart of a population-based metaheuristic algorithm is presented in Figure 3.4. Its operation can be shortly described as follows. The initial phase of the algorithm involves (typically random) generation of the population of candidate design solutions. In the next stage, each individual is evaluated and the corresponding value of the objective function determines its fitness to the design environment. Subsequently, a subset of individuals is selected, either based on the quality of each candidate solution (in case of deterministic selection strategies) or on both the fitness value and stochastic operators that may allow for selecting even poorly adapted individuals. For other approaches, such as particle swarm optimizers or differential evolution, the selection phase is completely omitted and each candidate solution undergoes continuous modifications throughout consecutive generations. Next, the selected parent individuals are modified by stochastic nature-inspired mechanisms. These may include exploratory operators, such as crossover, that create next-generation individuals combining parts of information embedded in parent individuals, or

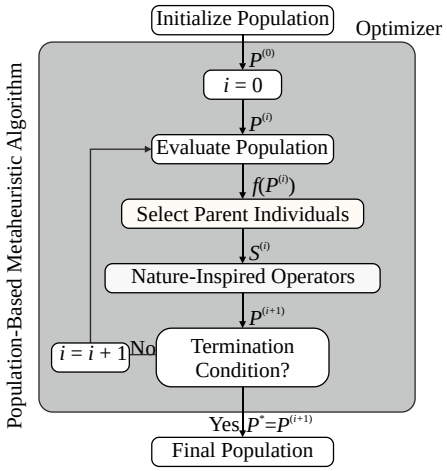

Figure 3.4: Flowchart of a typical population-based metaheuristic algorithm [103]. Here, P is used to denote a population of candidate solutions processed by the algorithm, f represents a fitness function, whereas S refers to the selected parent individuals.

exploitative operators, such as mutation, that introduce small perturbations to the individual at hand. The former operators enable far-reaching changes in the selected individuals, which translates into exploring new and potentially promising regions of the search space; the latter ones introduce only small changes to the candidate solutions, which improves local search properties of the algorithm. The entire process is repeated until the termination conditions are satisfied.

From the perspective of this work, population-based metaheuristics require too many objective function evaluations to be practically utilized for direct design optimization involving EM simulation models. A brief outline of metaheuristic algorithms provided in this section has been included as a context for the multi-objective design optimization method proposed in this dissertation as well as to make the descriptive part of this work on numerical optimization self-contained.

3.3 Surrogate-Based Optimization

Surrogate-based optimization is the primary methodology used in this work to handle expensive optimization problems pertinent to miniaturized hybrid coupler design. The present section introduces only these concepts of surrogate modeling and optimization that are relevant to this work and find direct application in the subsequent part of the dissertation. In particular, a generic SBO concept and optimization flow is discussed as well as fundamental space mapping techniques are elaborated on. References to the exhaustive body of up-to-date literature on SBO techniques that reside outside the scope of this work are also provided.

3.3.1 Surrogate-Based Optimization Concept

Conventional techniques of numerical optimization (as outlined in Sections 3.1 and 3.2) are well-established design tools in microwave engineering. Selected algorithms are implemented in major commercial EM software packages for CAD of microwave circuits and components, which is a clear indication of the real need for automated and reliable design procedures in this field. However, as pointed out in Sections 1.1.2, 1.1.3, and 3.2, their applicability for solving contemporary design problems is severely limited (or even prohibitive) primarily due to the high cost of high-fidelity EM simulations. Difficulties pertinent to direct optimization, considered from the standpoint of simulation-driven design of conventional microwave circuits and components, were the main incentives behind the development of alternative design approaches. Probably the most promising means of addressing the aforementioned challenges, that is, enabling computationally efficient parametric optimization of expensive EM simulation models, is surrogate-based optimization [50], [58], [60].

The fundamental concept of SBO is to replace direct optimization of an expensive EM simulation model by an iterative process that provides a sequence of increasingly precise approximations to the original problem (3.1) by optimizing a surrogate, that is, a fast and well-correlated representation of the high-fidelity model. In each iteration of the SBO algorithm, the surrogate is updated using data from the high-fidelity model evaluated at the current design (and possibly other designs) and re-optimized to find a better design. Formally, the surrogate-based optimization process can be formulated as [57]

$$\boldsymbol{x}^{(i+1)} = \arg\min_{\boldsymbol{x}} U\left(\boldsymbol{R}_s^{(i)}\left(\boldsymbol{x}\right)\right) \tag{3.10}$$

where $\boldsymbol{x}^{(i)}$, $i = 0, 1, \ldots$, is a sequence of approximate solutions to the original problem (3.1), whereas $\boldsymbol{R}_s^{(i)}$ is the surrogate model at the ith iteration. Here, $\boldsymbol{x}^{(0)}$ is the initial design, typically established based on engineering insight or by parametric optimization of a lower-fidelity model available for the design problem at hand. The surrogate $\boldsymbol{R}_s$ is assumed to be (i) much cheaper (in the computational sense) than the high-fidelity model $\boldsymbol{R}_f$ and (ii) sufficiently accurate, at least in the proximity of the current design $\boldsymbol{x}^{(i)}$. If these conditions are satisfied, the SBO algorithm (3.10) is inclined to quickly produce a good approximation of the high-fidelity optimum $\boldsymbol{x}^*$.

Typically, the high-fidelity model $\boldsymbol{R}_f$ is evaluated only once per iteration (to validate a new design $\boldsymbol{x}^{(i+1)}$ and to provide data for surrogate model update if the termination condition is not satisfied). A generic SBO flow used in microwave engineering is shown in Figure 3.5.

Provided that the surrogate model is much faster than its high-fidelity counterpart, the computational overhead related to solving (3.10) is negligible. Consequently, the overall cost of the SBO process is determined by the high-fidelity model evaluations. Normally, the number of iterations needed by the SBO algorithm to produce a good approximation of the high-fidelity model optimum is considerably smaller than for the vast majority of direct optimization methods (e.g., gradient-based routines) [50]. The above-mentioned premise concerning the speed of the surrogate model is generally met only for some of the SBO methods, particularly space mapping [64]. SM technology has been developed to solve conventional design problems of microwave engineering, where physics-based low-fidelity models (e.g., analytical formulas or equivalent circuits) are commonly used to construct efficient surrogates [61], [62]. The main SM approaches are discussed in Section 3.3.2.

Unfortunately, for a variety of contemporary design problems in microwave and antenna engineering, low-fidelity models that exhibit both suitable speed and reasonable accuracy are hardly available. The use of simplified means (e.g., analytical formulas) to describe the behavior of a complex engineering system under consideration may results in insufficient accuracy of the underlying low-fidelity model and lead to convergence problems of SBO algorithms [57]. On the other hand, the exploitation of EM simulations with coarse discretization of the structure at hand as low-fidelity models may diminish computational efficiency of the SBO process, with numerical operations associated with optimization and update of the surrogate model becoming a meaningful or even a major contributor to the overall cost of the SBO algorithm [125]. Addressing these issues by developing physics-based models of complex couplers that combine the advantages of equivalent circuits and EM simulations is one of the fundamental goals of this work.

It should be mentioned—for the sake of completeness—that the available literature provides possible solutions to this problem that require sensitive information [134] or use trust region convergence safeguards [126]. Alternative approaches involve adjoint sensitivities [135] or multi-level algorithms [136]. Note that convergence of some SBO algorithms can also be ensured by other strategies, for instance, manifold mapping [137] or surrogate management [138].

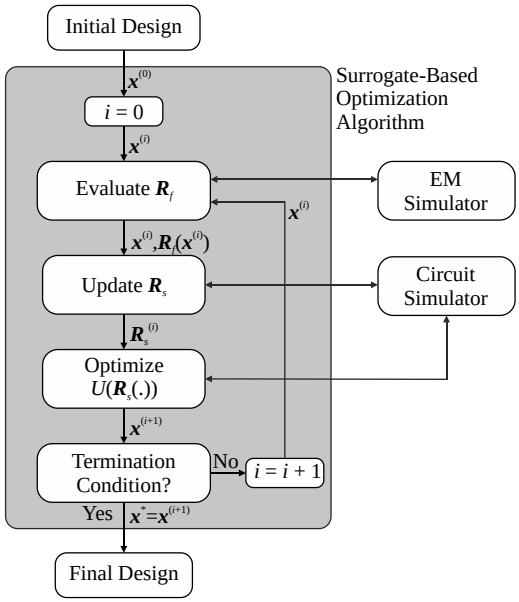

Figure 3.5: Surrogate-based optimization flow used in microwave engineering [125]. The surrogate $\boldsymbol{R}_s$ is iteratively updated and optimized to yield an approximate high-fidelity model optimum. The high-fidelity model $\boldsymbol{R}_f$ is evaluated to verify the design produced by surrogate optimization (in most cases only once per iteration). $\boldsymbol{R}_f$ simulation data is also used to improve the reliability of the surrogate model.

3.3.2 Space Mapping Technology

Space mapping is probably the most recognized SBO technique in microwave engineering today [62]. The majority of SM algorithms rely on physics-based low-fidelity models whose primary advantage lies in providing rather good generalization capabilities [129]. On the other hand, some SM versions allow for using physics-based as well as data-driven models.

SM exploits the algorithm (3.10) to generate a sequence of approximate solutions $\boldsymbol{x}^{(i)}$, i = 0, 1, 2, …, to high-fidelity model optimum given by (3.1). The surrogate model at the ith iteration, $\boldsymbol{R}_s^{(i)}$, is constructed from the underlying low-fidelity model by minimizing the misalignment between $\boldsymbol{R}_s^{(i)}$ and the fine model $\boldsymbol{R}_f$ at the current design $\boldsymbol{x}^{(i)}$ (and, in some cases, at other points established by appropriate design of experiment [129]). This process is referred to as a parameter extraction (PE) and is formulated as a nonlinear minimization task [61]. The surrogate is defined as [139]

$$\boldsymbol{R}_s^{(i)}(\boldsymbol{x}) = \boldsymbol{R}_{s.g}\left(\boldsymbol{x}^{(i)}, p^{(i)}\right) \tag{3.11}$$

where $\boldsymbol{R}_{s.g}$ is a generic SM surrogate composed of the low-fidelity model and suitable transformations, whereas

$$\boldsymbol{p}^* = \arg\min_{\boldsymbol{p}} \sum_{k=0}^{i} w_{i.k} \left\| \boldsymbol{R}_f\left(\boldsymbol{x}^{(k)}\right) - \boldsymbol{R}_{s.g}\left(\boldsymbol{x}^{(k)}, \boldsymbol{p}\right) \right\| \tag{3.12}$$

is a vector of auxiliary model parameters with $w_{i.k}$ being weighting factors (these determine the contribution of previous iteration points to PE process [139]).

The space mapping corrections available in the literature can be categorized into four main groups [62]:

1. Input space mapping [61]
   Input SM surrogate is defined as a distortion of the coarse model domain of the following form:
   $$\boldsymbol{R}_s(\boldsymbol{x}) = \boldsymbol{R}_c(\boldsymbol{B}\cdot\boldsymbol{x} + \boldsymbol{c}) \tag{3.13}$$
   where $\boldsymbol{B}$ and $\boldsymbol{c}$ are matrices to be established in the PE process.
2. Output space mapping [139]
   Output SM surrogate is based on a correction of the coarse model response given as:
   $$\boldsymbol{R}_s(\boldsymbol{x}) = \boldsymbol{A}\cdot\boldsymbol{R}_c(\boldsymbol{x}) + \boldsymbol{d} \tag{3.14}$$
   where $\boldsymbol{A}$ and $\boldsymbol{d}$ are output SM parameters obtained during the PE phase.
3. Implicit space mapping [140]
   Implicit SM surrogate is defined with respect to some additional model parameters that can be tuned for better alignment of the fine and coarse model responses:
   $$\boldsymbol{R}_s(\boldsymbol{x}) = \boldsymbol{R}_c(\boldsymbol{x};\boldsymbol{p}) \tag{3.15}$$
   In microwave engineering, $\boldsymbol{p}$ is typically a vector of substrate parameters (substrate permittivity and/or thickness) pertaining to the selected parts of equivalent circuit model.
4. Frequency space mapping [62]
   Considering a coarse model evaluated at a discrete set of m frequency points $\boldsymbol{R}_c(\boldsymbol{x})$ = $[R_c(\boldsymbol{x},\omega_1)\ R_c(\boldsymbol{x},\omega_2)\ \ldots\ R_c(\boldsymbol{x},\omega_m)]^T$, where $R_c(\boldsymbol{x},\omega_j)$ is evaluation of the model at a frequency ω_j, frequency SM surrogate is defined based on the affine scaling function $f(\omega) = f_0 + \omega\cdot f_1$
   $$\boldsymbol{R}_s(\boldsymbol{x}) = \left[R_c(\boldsymbol{x}; f_0 + \omega_1\cdot f_1)\ldots R_c(\boldsymbol{x}; f_0 + \omega_m\cdot f_1)\right]^T \tag{3.16}$$
   where f_0, f_1 are extractable parameters.

Figure 3.6 illustrates block diagrams of the main SM-based correction strategies formulated above. They may be used individually or in different combinations [cf. Figure 3.6(c)].

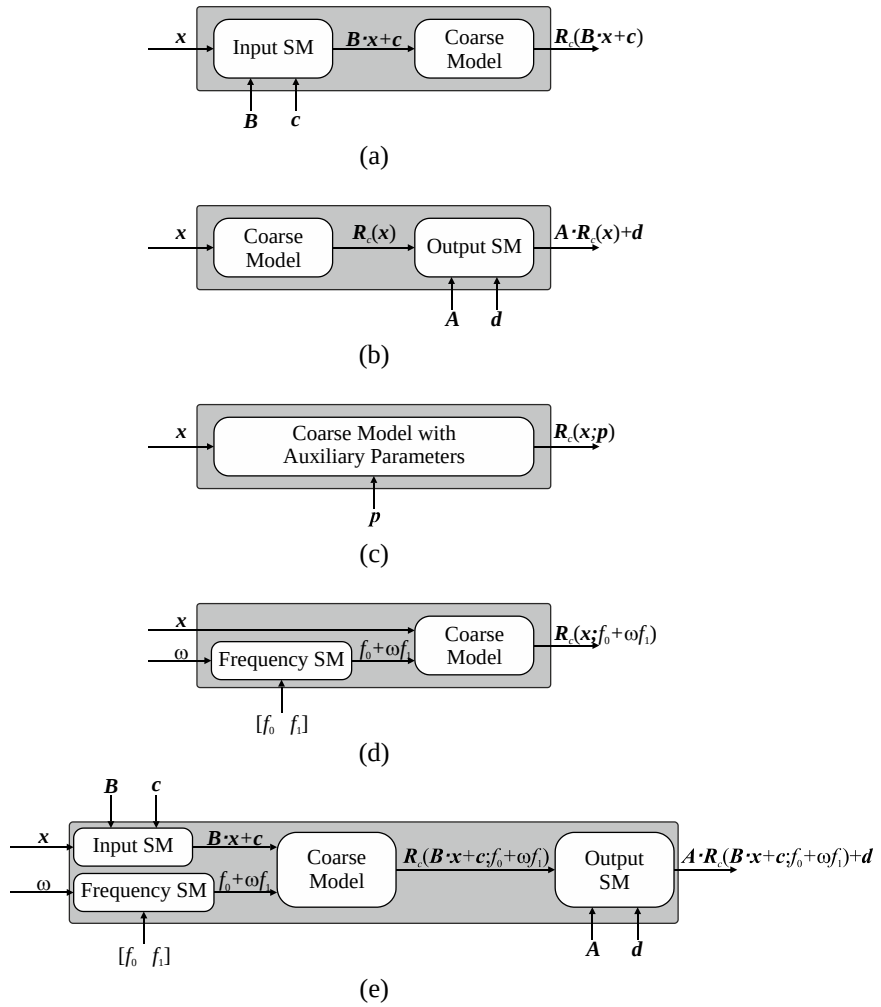

Figure 3.6: Fundamental SM correction types [57]: (a) input SM, (b) output SM, (c) implicit SM, (d) frequency SM, and (e) customized SM based on input, output and frequency SM.

REFERENCES

[1] R. Gilmore and L. Besser, *Practical RF Circuit Design for Modern Wireless Systems*. Norwood: Artech House, 2003.

[2] H.-R. Ahn, *Asymmetric Passive Components in Microwave Integrated Circuits*. New Jersey: John Wiley & Sons, Inc., 2006.

[3] H.-X. Xu, G.-M. Wang, and K. Lu, "Microstrip rat-race couplers," *IEEE Microw. Mag.*, vol. 12, no. 4, pp. 117–129, 2011.

[4] H.-R. Ahn and B. Kim, "Toward integrated circuit size reduction," *IEEE Microw. Mag.*, vol. 9, no. 1, pp. 65–75, 2008.

[5] J. Schiller, *Mobile Communications*. Pearson Education Limited, 2003.

[6] B. Fong, A. Fong, and C. Li, *Telemedicine Technologies: Information Technologies in Medicine and Telehealth*. Wiley, 2010.

[7] S. Khorram, C. van der Wiele, C. Koch, S. Nelson, and M. Potts, *Principles of Applied Remote Sensing*. Springer, 2016.

[8] F. Neri, *Introduction to Electronic Defense Systems, Second Edition*. Artech House, 2001.

[9] S. Ahn, "Electronic smart meter enabling demand response and method for demand response," US Patent 20090198384 A1, Aug. 6, 2009.

[10] D. James, "Moore's law continues into the 1x-nm era," in *Int. Conf. Ion Implant. Techn.*, pp. 1–10, 2016.

[11] G. Moore, "Cramming more components onto integrated circuits," *Electronics*, vol. 38, no. 8, pp. 114–117, 1965.

[12] D. M. Pozar, *Microwave Engineering*, 2nd ed. New York: John Wiley & Sons, Inc., 1998.

[13] J.-S. Hong and M. J. Lancaster, *Microstrip Filters for RF/Microwave Applications*, 1st ed. New York: John Wiley & Sons, Inc., 2001.

[14] IEEE Smart Grid Vision for Computing: 2030 and Beyond Roadmap, pp. 1-14, 2916.

[15] R. Mongia, I. Bahl, and P. Bhartia, *RF and Microwave Coupled-Line Circuits*. Boston: Artech House, 1999.

[16] S. Staras, R. Martavicius, J. Skudutis, V. Urbanavicius, and V. Daskevicius, *Wide-Band Slow-Wave Systems: Simulation and Applications*. Boca Raton: CRC Press, 2012.

[17] T. Hirota, A. Minakawa, and M. Muraguchi, "Reduced-size branch-line and rat-race hybrids for uniplanar MMIC's," *IEEE Trans. Microw. Theory Techn.*, vol. 38, no. 3, pp. 270–275, 1990.

[18] M. Gillick, I. Robertson, and J. Joshi, "Coplanar waveguide two-stage balanced MMIC amplifier using impedance-transforming lumped-distributed branchline couplers," *IEE Proc. Microw. Ant. Propag.*, vol. 141, no. 4, pp. 241–245, 1994.

[19] Y.-C. Chiang and C.-Y. Chen, "Design of a wide-band lumped-element 3-dB quadrature coupler," *IEEE Trans. Microw. Theory Techn.*, vol. 49, no. 3, pp. 476–479, 2001.

[20] Y. Li, Z. Zhang, Z. Li, J. Zheng, and Z. Feng, "High-permittivity substrate multiresonant antenna inside metallic cover of laptop computer," *IEEE Ant. Wireless Propag. Lett.*, vol. 10, pp. 1092–1095, 2011.

[21] Y.-C. Chen and C.-H. Hsu, "Inverted-E shaped monopole on high-permittivity substrate for application in industrial, scientific, medical, high-performance radio local area network, unlicensed national information infrastructure, and worldwide interoperability for microwave access," *IET Microw. Ant. Propag.*, vol. 8, no. 4, pp. 272–277, 2014.

[22] V. Radisic, Y. Qian, R. Coccioli, and T. Itoh, "Novel 2-D photonic bandgap structure for microstrip lines," *IEEE Microw. Guided Wave Lett.*, vol. 8, no. 2, pp. 69–71, 1998.

[23] F.-R. Yang, K.-P. Ma, Y. Qian, and T. Itoh, "A uniplanar compact photonic-bandgap (UC-PBG) structure and its applications for microwave circuit," *IEEE Trans. Microw. Theory Techn.*, vol. 47, no. 8, pp. 1509–1514, 1999.

[24] C.-S. Kim, J.-S. Park, D. Ahn, and J.-B. Lim, "A novel 1-D periodic defected ground structure for planar circuits," *IEEE Microw. Guided Wave Lett.*, vol. 10, no. 4, pp. 131–133, 2000.

[25] I. Awai, H. Kubo, T. Iribe, D. Wakamiya, and A. Sanada, "An artificial dielectric material of huge permittivity with novel anisotropy and its application to a microwave BPF," in *IEEE MTT-S Int. Microw. Symp. Dig.*, vol. 2, pp. 1085–1088, 2003.

[26] F. Elek and G. Eleftheriades, "On the slow wave behaviour of the shielded mushroom structure," in *IEEE MTT-S Int. Microw. Symp. Dig.*, pp. 1333–1336, 2008.

[27] F. Mbairi and H. Hesselbom, "Microwave bandstop filters using novel artificial periodic substrate electromagnetic band gap structures," *IEEE Trans. Compon. Packag. Technol.*, vol. 32, no. 2, pp. 273–282, 2009.

[28] Q. Xue, K. Shum, and C. Chan, "Novel 1-D microstrip PBG cells," *IEEE Microw. Guided Wave Lett.*, vol. 10, no. 10, pp. 403–405, 2000.

[29] T.-Y. Yun and K. Chang, "Uniplanar one-dimensional photonic-bandgap structures and resonators," *IEEE Trans. Microw. Theory Techn.*, vol. 49, no. 3, pp. 549–553, 2001.

[30] K. M. Shum, Q. Xue, and C. H. Chan, "A novel microstrip ring hybrid incorporating a PBG cell," *IEEE Microw. Wireless Comp. Lett.*, vol. 11, no. 6, pp. 258–260, 2001.

[31] Q. Xue, K. Shum, and C. Chan, "Low conversion-loss fourth subharmonic mixers incorporating CMRC for millimeter-wave applications," *IEEE Trans. Microw. Theory Techn.*, vol. 51, no. 5, pp. 1449–1454, 2003.

[32] B.-L. Ooi, "Compact EBG in-phase hybrid-ring equal power divider," *IEEE Trans. Microw. Theory Techn.*, vol. 53, no. 7, pp. 2329–2334, 2005.

[33] J. Gu and X. Sun, "Miniaturization and harmonic suppression rat-race coupler using C-SCMRC resonators with distributive equivalent circuit," *IEEE Microw. Wireless Comp. Lett.*, vol. 15, no. 12, pp. 880–882, 2005.

[34] C. Zhou and H.-Y. Yang, "Design considerations of miniaturized least dispersive periodic slow-wave structures," *IEEE Trans. Microw. Theory Techn.*, vol. 56, no. 2, pp. 467–474, 2008.

[35] C. M. Lin, H. H. Su, J. C. Chiu, and Y. H. Wang, "Wilkinson power divider using microstrip EBG cells for the suppression of harmonics," *IEEE Microw. Wireless Comp. Lett.*, vol. 17, no. 10, pp. 700–702, 2007.

[36] P. Kurgan, J. Filipcewicz, and M. Kitlinski, "Design considerations for compact microstrip resonant cells dedicated to efficient branch-line miniaturization," *Microw. Opt. Techn. Lett.*, vol. 54, no. 8, pp. 1949–1954, 2012.

[37] E. Gandini, M. Ettorre, R. Sauleau, and A. Grbic, "A lumped-element unit cell for beam-forming networks and its application to a miniaturized Butler matrix," *IEEE Trans. Microw. Theory Techn.*, vol. 61, no. 4, pp. 1477–1487, 2013.

[38] J.-A. Hou and Y.-H. Wang, "Design of compact 90° and 180° couplers with harmonic suppression using lumped-element bandstop resonators," *IEEE Trans. Microw. Theory Techn.*, vol. 58, no. 11, pp. 2932–2939, 2010.

[39] L. Brillouin, *Wave Propagation in Periodic Structures*, 1st ed. New York: McGraw-Hill Book Company, Inc., 1946.

[40] F. Martin, *Artificial Transmission Lines for RF and Microwave Applications*. Wiley, 2015.

[41] P. Kurgan and M. Kitlinski, "Novel doubly perforated broadband microstrip branch-line couplers," *Microw. Opt. Techn. Lett.*, vol. 51, no. 9, pp. 2149–2152, 2009.

[42] Y.-H. Chun and J.-S. Hong, "Compact wide-band branch-line hybrids," *IEEE Trans. Microw. Theory Techn.*, vol. 54, no. 2, pp. 704–709, 2006.

[43] J. Wang, B. Z. Wang, Y. X. Guo, L. C. Ong, and S. Xiao, "A compact slow-wave microstrip branch-line coupler with high performance," *IEEE Microw. Wireless Comp. Lett.*, vol. 17, no. 7, pp. 501–503, 2007.

[44] P. Kurgan and M. Kitlinski, "Doubly miniaturized rat-race hybrid coupler," *Microw. Opt. Techn. Lett.*, vol. 53, no. 6, pp. 1242–1244, 2011.

[45] P. Kurgan and M. Kitlinski, "Slow-wave fractal-shaped compact microstrip resonant cell," *Microw. Opt. Techn. Lett.*, vol. 52, no. 11, pp. 2613–2615, 2010.

[46] S. Koziel and P. Kurgan, "Rapid design of miniaturised branch-line couplers through concurrent cell optimisation and surrogate-assisted fine-tuning," *IET Microw. Ant. Propag.*, vol. 9, no. 9, pp. 957–963, 2015.

[47] P. Kurgan and S. Koziel, "Fast surrogate-assisted simulation-driven optimization of compact microwave hybrid couplers," *Eng. Opt.*, vol. 48, no. 7, pp. 1109–1120, 2016.

[48] S. Koziel and P. Kurgan, "Low-cost optimization of compact branch-line couplers and its application to miniaturized Butler matrix design," in *European Microw. Conf.*, pp. 227–230, 2014.

[49] S. Ogurtsov and S. Koziel, "Automated design of circularly polarized microstrip patch antennas with improved axial ratio," in *Loughborough Ant. Propag. Conf.*, pp. 1–5, 2016.

[50] S. Koziel, X. Yang, and Q. Zhang, Eds., *Simulation-Driven Design Optimization and Modeling for Microwave Engineering*. Imperial College Press, 2012.

[51] C. L. Hsu and J. T. Kuo, "Design of dual-band branch line couplers with circuit miniaturization," in *Asia-Pacific Microw. Conf.*, pp. 1–4, 2008.

[52] C. W. Wang, T. G. Ma, and C. F. Yang, "A new planar artificial transmission line and its applications to a miniaturized Butler matrix," *IEEE Trans. Microw. Theory Techn.*, vol. 55, no. 12, pp. 2792–2801, 2007.

[53] A. Bekasiewicz and P. Kurgan, "A compact microstrip rat-race coupler constituted by nonuniform transmission lines," *Microw. Opt. Techn. Lett.*, vol. 56, no. 4, pp. 970–974, 2014.

[54] S. Koziel and A. Bekasiewicz, "Novel structure and size-reduction-oriented design of microstrip compact rat-race coupler," in *Int. Rev. Prog. Appl. Comp. Electromagn.*, pp. 1–2, 2016.

[55] S. Koziel and A. Bekasiewicz, "Expedited geometry scaling of compact microwave passives by means of inverse surrogate modeling," *IEEE Trans. Microw. Theory Techn.*, vol. 63, no. 12, pp. 4019–4026, 2015.

[56] S. Koziel, A. Bekasiewicz, and P. Kurgan, "Rapid multi-objective simulation-driven design of compact microwave circuits," *IEEE Microw. Wireless Comp. Lett.*, vol. 25, no. 5, pp. 277–279, 2015.

[57] S. Koziel and X. Yang, Eds., *Computational Optimization, Methods and Algorithms*, series Studies in Computational Intelligence. Springer, 2011, vol. 356.

[58] N. V. Queipo, R. T. Haftka, W. Shyy, T. Goel, R. Vaidyanathan, and P. K. Tucker, "Surrogate-based analysis and optimization," *Prog. Aerosp. Scie.*, vol. 41, pp. 1–28, 2005.

[59] M. B. Yelten, T. Zhu, S. Koziel, P. D. Franzon, and M. B. Steer, "Demystifying surrogate modeling for circuits and systems," *IEEE Circ. Syst. Mag.*, vol. 12, no. 1, pp. 45–63, 2012.

[60] S. Koziel and L. Leifsson, Eds., *Surrogate-Based Modeling and Optimization: Applications in Engineering*. Springer, 2013.

[61] J. W. Bandler, Q. S. Cheng, S. A. Dakroury, A. S. Mohamed, M. H. Bakr, K. Madsen, and J. Sondergaard, "Space mapping: the state of the art," *IEEE Trans. Microw. Theory Techn.*, vol. 52, no. 1, pp. 337–361, 2004.

[62] S. Koziel, Q. S. Cheng, and J. W. Bandler, "Space mapping," *IEEE Microw. Mag.*, vol. 9, no. 6, pp. 105–122, 2008.

[63] P. Kurgan, A. Bekasiewicz, and M. Kitlinski, "On the low-cost design of abbreviated multisection planar matching transformer," *Microw. Opt. Techn. Lett.*, vol. 57, no. 3, pp. 521–525, 2015.

[64] S. Koziel, J. W. Bandler, and K. Madsen, "Quality assessment of coarse models and surrogates for space mapping optimization," *Opt. Eng.*, vol. 9, no. 4, pp. 375–391, 2008.

[65] S. Koziel, A. Bekasiewicz, and P. Kurgan, "Rapid EM-driven design of compact RF circuits by means of nested space mapping," *IEEE Microw. Wireless Comp. Lett.*, vol. 24, no. 6, pp. 364–366, 2014.

[66] S. Li, X. Fan, and P. D. Laforge, "Automated EM-based design of bandpass filter by sequential parameter extraction and space mapping technique," in *IEEE MTT-S Int. Conf. Num. Electromagn. Multiph. Model. Opt.*, pp. 1–4, 2015.

[67] S. Koziel and S. Ogurtsov, "Microwave design optimization using local response surface approximations and variable-fidelity electromagnetic models," in *European Microw. Conf.*, pp. 448–451, 2011.

[68] A. I. Forrester and A. J. Keane, "Recent advances in surrogate-based optimization," *Prog. Aerosp. Sci.*, vol. 45, no. 1-3, pp. 50–79, 2009.

[69] S. Koziel and A. Bekasiewicz, "Low-fidelity model considerations for EM-driven design of antenna structures," *J. Electromagnetic Waves Appl.*, vol. 30, no. 18, pp. 2444–2458, 2016.

[70] S. Koziel and S. Ogurtsov, "Multi-objective design of antennas using variable-fidelity simulations and surrogate models," *IEEE Trans. Ant. Prop.*, vol. 61, no. 12, pp. 5931–5939, 2013.

[71] R. K. Settaluri, G. Sundberg, A. Weisshaar, and V. K. Tripathi, "Compact folded line rat-race hybrid couplers," *IEEE Microw. Guided Wave Lett.*, vol. 10, no. 2, pp. 61–63, 2000.

[72] K.-O. Sun, S.-J. Ho, C.-C. Yen, and D. van der Weide, "A compact branch-line coupler using discontinuous microstrip lines," *IEEE Microw. Wireless Comp. Lett.*, vol. 15, no. 8, pp. 519–520, 2005.

[73] K. S. Chin, K. M. Lin, Y. H. Wei, T. H. Tseng, and Y. J. Yang, "Compact dual-band branch-line and rat-race couplers with stepped-impedance-stub lines," *IEEE Trans. Microw. Theory Techn.*, vol. 58, no. 5, pp. 1213–1221, 2010.

[74] P. Kurgan and A. Bekasiewicz, "A robust design of a numerically demanding compact rat-race coupler," *Microw. Opt. Techn. Lett.*, vol. 56, no. 5, pp. 1259–1263, 2014.

[75] C. H. Tseng and C. H. Wu, "Design of compact branch-line couplers using π-equivalent artificial transmission lines," *IET Microw. Ant. Propag.*, vol. 6, no. 9, pp. 969–974, 2012.

[76] P. Kurgan, J. Filipcewicz, and M. Kitlinski, "Development of a compact microstrip resonant cell aimed at efficient microwave component size reduction," *IET Microw. Ant. Propag.*, vol. 6, no. 12, pp. 1291–1298, 2012.

[77] K. W. Eccleston and S. H. M. Ong, "Compact planar microstripline branch-line and rat-race couplers," *IEEE Trans. Microw. Theory Techn.*, vol. 51, no. 10, pp. 2119–2125, 2003.

[78] C. W. Wang, T. G. Ma, and C. F. Yang, "Miniaturized branch-line coupler with harmonic suppression for RFID applications using artificial transmission lines," in *IEEE MTT-S Int. Microw. Symp.*, pp. 29–32, 2007.

[79] S. C. Jung, R. Negra, and F. M. Ghannouchi, "A design methodology for miniaturized 3-dB branch-line hybrid couplers using distributed capacitors printed in the inner area," *IEEE Trans. Microw. Theory Techn.*, vol. 56, no. 12, pp. 2950–2953, 2008.

[80] C. H. Tseng and H. J. Chen, "Compact rat-race coupler using shunt-stub-based artificial transmission lines," *IEEE Microw. Wireless Comp. Lett.*, vol. 18, no. 11, pp. 734–736, 2008.

[81] P. Mondal and A. Chakrabarty, "Design of miniaturised branch-line and rat-race hybrid couplers with harmonics suppression," *IET Microw. Ant. Propag.*, vol. 3, no. 1, pp. 109–116, 2009.

[82] J. T. Kuo, J. S. Wu, and Y. C. Chiou, "Miniaturized rat race coupler with suppression of spurious passband," *IEEE Microw. Wireless Comp. Lett.*, vol. 17, no. 1, pp. 46–48, 2007.

[83] S.-S. Liao, P.-T. Sun, N.-C. Chin, and J.-T. Peng, "A novel compact-size branch-line coupler," *IEEE Microw. Wireless Comp. Lett.*, vol. 15, no. 9, pp. 588–590, 2005.

[84] P. Kurgan and S. Koziel, "Design of high-performance hybrid branch-line couplers for wideband and space-limited applications," *IET Microw. Ant. Propag.*, vol. 10, no. 12, pp. 1339–1344, 2016.

[85] C. H. Tseng and C. L. Chang, "A rigorous design methodology for compact planar branch-line and rat-race couplers with asymmetrical T-structures," *IEEE Trans. Microw. Theory Techn.*, vol. 60, no. 7, pp. 2085–2092, 2012.

[86] C. W. Tang and M. G. Chen, "Synthesizing microstrip branch-line couplers with predetermined compact size and bandwidth," *IEEE Trans. Microw. Theory Techn.*, vol. 55, no. 9, pp. 1926–1934, 2007.

[87] T.-G. Ma, C.-W. Wang, C.-H. Lai, and Y.-C. Tseng, *Synthesized Transmission Lines. Design, Circuit Implementation, and Phased Array Applications.* Wiley, 2017.

[88] B.-Q. Lin, Q.-R. Zheng, and N.-C. Yuan, "A novel planar PBG structure for size reduction," *IEEE Microw. Wireless Comp. Lett.*, vol. 16, no. 5, pp. 269–271, 2006.

[89] K. Deb, *Multi-Objective Optimization Using Evolutionary Algorithms*. New York: John Wiley & Sons, 2001.

[90] Z. Michalewicz, *Genetic Algorithms + Data Structures = Evolution Programs*, 3rd ed. Berlin Heidelberg: Springer-Verlag, 1996.

[91] S. Chamaani, M. Abrishamian, and S. Mirtaheri, "Time-domain design of UWB Vivaldi antenna array using multiobjective particle swarm optimization," *IEEE Ant. Wireless Prop. Lett.*, vol. 9, pp. 666–669, 2010.

[92] C. Coello Coello, G. Lamont, and D. Van Veldhuizen, *Evolutionary Algorithms for Solving Multi-Objective Problems*. New York: Springer, 2007.

[93] A. Bekasiewicz and S. Koziel, "Structure and computationally efficient simulation-driven design of compact UWB monopole antenna," *IEEE Ant. Wireless Propag. Lett.*, vol. 14, pp. 1282–1285, 2015.

[94] M. John and M. Ammann, "Antenna optimization with a computationally efficient multiobjective evolutionary algorithm," *IEEE Trans. Ant. Prop.*, vol. 57, no. 1, pp. 260–263, 2009.

[95] Sonnet, v. 14.54, Sonnet Software, North Syracuse, NY, United States, 2013.

[96] CST Microwave Studio, v. 2013, CST AG, Bad Nauheimer Str. 19, D-64289 Darmstadt, Germany, 2013.

[97] S. Koziel, A. Bekasiewicz, and P. Kurgan, *Simulation and Modeling Methodologies, Technologies and Applications*. Springer, 2014, ch. Computationally-Efficient EM-Simulation-Driven Multi-Objective Design of Compact Microwave Structures, pp. 235–250.

[98] S. Koziel, A. Bekasiewicz, and P. Kurgan, *Solving Computationally Expensive Engineering Problems. Methods and Applications*. Springer, 2014, ch. Nested Space Mapping Technique for Design and Optimization of Complex Microwave Structures with Enhanced Functionality, pp. 53–86.

[99] P. Kurgan and A. Bekasiewicz, *Solving Computationally Expensive Engineering Problems. Methods and Applications.* Springer, 2014, ch. Atomistic Surrogate-Based Optimization for Simulation-Driven Design of Computationally Expensive Microwave Circuits with Compact Footprints, pp. 195–218.

[100] S. Koziel, P. Kurgan, and A. Bekasiewicz, *Computational Sustainability*. Springer, 2016, ch. Computationally Efficient Design Optimization of Compact Microwave and Antenna Structures, pp. 195–218.

[101] R. E. Amaya and C. J. Verver, "A 60 GHz CMOS balanced downconversion mixer with a layout efficient 90° hybrid coupler," in *IEEE Cust. Integr. Circ. Conf.*, pp. 235–238, 2009.

[102] M. Arrawatia, M. S. Baghini, and G. Kumar, "A CMOS power amplifier with 180° hybrid on-chip coupler for 4G applications," in *IEEE Int. Midwest Symp. Circ. Syst.*, pp. 1–4, 2015.

[103] S. Koziel, L. Leifsson, and X. Yang, Eds., *Solving Computationally Expensive Engineering Problems. Methods and Applications*. Springer, 2016.

[104] Agilent (Keysight) ADS, v. 2011.10, Agilent Technologies, 1400 Fountaingrove Parkway, Santa Rosa, CA 95403-1799, 2011.

[105] J. He, B. Z. Wang, and W. Shao, "Compact power divider embedded with zigzag microstrip slow-wave structures," *Electronics Lett.*, vol. 45, no. 1, pp. 62–63, 2009.

[106] A. Bekasiewicz and S. Koziel, "Cost-efficient simulation-driven design of compact impedance matching transformers," in *Int. Conf. Microw. Rad. Wireless Comm.*, pp. 1–4, 2016.

[107] A. Bekasiewicz, S. Koziel, and L. Leifsson, "Fast multi-objective design optimization of compact UWB matching transformers using variable-fidelity EM simulations and design space reduction," in *IEEE MTT-S Int. Conf. Num. Electromagn. Multiph. Model. Opt.*, pp. 1–3, 2015.

[108] D. Nesic, "A new type of slow-wave 1-D PBG microstrip structure without etching in the ground plane for filter and other applications," *Microw. Opt. Techn. Lett.*, vol. 33, no. 6, pp. 440–443, 2002.

[109] J. Gu and X. Sun, "Compact lowpass filter using spiral compact microstrip resonant cells," *Electronics Lett.*, vol. 41, no. 19, pp. 1065–1066, 2005.

[110] R. Chipman, *Theory and Problems of Transmission Lines*. New York: McGraw-Hill Book Company, Inc., 1968.

[111] W. Mason and R. Sykes, "The use of coaxial and balanced transmission lines in filters and wide band transformers for high radio frequencies," *The Bell Syst. Techn. J.*, vol. 16, no. 3, pp. 275–302, 1937.

[112] S. Ballantine, "Non-uniform lumped electric lines," *J. Franklin Institute*, vol. 203, pp. 849–853, 1927.

[113] C. Caloz and T. Itoh, *Electromagnetic Metamaterials: Transmission Line Theory and Microwave Applications*. Wiley, 2005.

[114] R. Gupta and W. Getsinger, "Quasi-lumped-element 3- and 4-port networks for MIC and MMIC applications," in *IEEE MTT-S Int. Microw. Symp.*, pp. 409–411, 1984.

[115] S. Opozda, P. Kurgan, and M. Kitlinski, "A compact seven-section rat-race hybrid coupler incorporating PBG cells," *Microw. Opt. Tech. Lett.*, vol. 51, no. 11, pp. 2910–2913, 2009.

[116] C. Caloz, "Dual composite right/left-handed (D-CRLH) transmission line metamaterial," *IEEE Microw. Wireless Comp. Lett.*, vol. 16, no. 11, pp. 585–587, 2006.

[117] R. Collin, *Foundations for Microwave Engineering*, 2nd ed., series IEEE Press Series on Electromagnetic Wave Theory. New York: John Wiley & Sons, Inc., 2001.

[118] S. Seki and H. Hasegawa, "Cross-tie slow-wave coplanar waveguide on semi-insulating GaAs substrates," *Electron. Lett.*, vol. 17, no. 25, pp. 940–941, 1981.

[119] J. Gu and X. Sun, "Miniaturization and harmonic suppression of branch-line and rat-race hybrid coupler using compensated spiral compact microstrip resonant cell," in *IEEE MTT-S Int. Microw. Symp. Dig.*, pp. 1211–1214, 2005.

[120] J. Rautio, "Planar electromagnetic analysis," *IEEE Microw. Mag.*, vol. 4, no. 1, pp. 35–41, 2003.

[121] J. Nocedal and S. Wright, *Numerical Optimization*. Springer Science, 2006.

[122] M. Kazemi, G. Wang, S. Rahnamayan, and K. Gupta, "Metamodel-based optimization for problems with expensive objective and constraint functions," *ASME J. Mech. Des.*, vol. 133, no. 1, pp. 014505–1–014505–7, 2011.

[123] A. Basudhar, C. Dribusch, S. Lacaze, and S. Missoum, "Constrained efficient global optimization with support vector machines," *Struct. Multidisc. Optim.*, vol. 46, pp. 201–221, 2012.

[124] T. Kolda, R. Lewis, and V. Torczon, "Optimization by direct search: new perspective and some classical and modern methods." *SIAM Rev.*, vol. 45, pp. 385–482, 2003.

[125] S. Koziel and L. Leifsson, *Simulation-Driven Design by Knowledge-Based Response Correction Techniques*. Springer, 2016.

[126] A. Conn, N. Gould, and P. Toint, *Trust Region Method*, series MOS-SIAM Series on Optimization. Springer Science, 2000.

[127] X. Yang, *Engineering Optimization: An Introduction with Metaheuristic Applications*. Wiley, 2010.

[128] A. Conn, N. Gould, and P. Toint, *Introduction to Derivative-Free Optimization*, series MOS-SIAM Series on Optimization. SIAM, 2009.

[129] S. Koziel and S. Ogurtsov, *Antenna Design by Simulation-Driven Optimization*. Springer, 2014.

[130] D. Goldberg, *Genetic Algorithms in Search, Optimization & Machine Learning*. New York: Pearson Education, 1989.

[131] T. Back, D. Fogel, and Z. Michalewicz, Eds., *Evolutionary Computation 1: Basic Algorithms and Operators*. New York: Taylor & Francis Group, 2000.

[132] J. Kennedy, R. Eberhart, and Y. Shi, *Swarm Intelligence*. New York: Academic Press, 2001.

[133] R. Storn and K. Price, "Differential evolution – a simple and efficient heuristic for global optimization over continuous spaces," *J. Global. Optim.*, vol. 11, pp. 341–359, 1997.

[134] N. Alexandrov and R. Lewis, "An overview of first-order model management for engineering optimization," *Opt. Eng.*, vol. 2, pp. 413–430, 2001.

[135] S. Koziel, S. Ogurtsov, J. Bandler, and Q. Cheng, "Reliable space mapping optimization integrated with em-based adjoint sensitivities," *IEEE Trans. Microw. Theory Tech.*, vol. 61, no. 10, pp. 3493–3502, 2013.

[136] S. Koziel and S. Ogurtsov, "Multi-level microwave design optimization with automated model fidelity adjustmenet," *Int. J. RF Microw. Comp. Aid. Eng.*, vol. 24, no. 3, pp. 281–288, 2014.

[137] D. Echeverria and P. Hemker, "Manifold mapping: a two-level optimization technique," *Comput. Visual. Sci.*, vol. 11, no. 4, pp. 193–206, 2008.

[138] A. Booker, J. Dennis, P. Frank, D. Serafini, V. Torczon, and M. Trosset, "A rigorous framework for optimization of expensive functions by surrogates," *Struct. Opt.*, vol. 17, no. 1, pp. 1–13, 1999.

[139] S. Koziel, J. Bandler, and K. Madsen, "A space mapping framework for engineering optimization: theory and implementation," *IEEE Trans. Microw. Theory Tech.*, vol. 54, no. 10, pp. 3721–3730, 2006.

[140] J. Bandler, Q. Cheng, N. Nikolova, and M. Ismail, "Implicit space mapping optimization exploiting preassigned parameters," *IEEE Trans. Microw. Theory Tech.*, vol. 52, no. 1, pp. 378–385, 2004.

4 SEQUENTIAL SPACE MAPPING

***

A. Bekasiewicz, P. Kurgan, and M. Kitliński

New Approach to a Fast and Accurate Design of Microwave Circuits With Complex Topologies

Published in: *IET Microwaves, Antennas & Propagation*, vol. 6, no. 14, pp. 1616–1622, 2012.

DOI: 10.1049/iet-map.2012.0434

***

Abstract: A robust simulation-driven design methodology of microwave circuits with complex topologies has been presented. The general method elaborated is suitable for a wide class of N-port unconventional microwave circuits constructed as a deviation from classic design solutions. The key idea of the approach proposed lies in an iterative redesign of a conventional circuit by a sequential modification and optimization of its atomic building blocks. The speed and accuracy of the method presented has been acquired by solving a number of simple optimization problems through surrogate-based optimization (SBO) techniques, which offer a satisfactory approximation of the optimal design solution. Two exemplary designs have been supplied to verify the method introduced. An abbreviated wideband quarter-wave impedance matching transformer and a miniaturized hybrid branch-line coupler have been developed. Diminished dimensions of the circuits under construction have been achieved by means of compact microstrip resonant cells. As an SBO engine, an implicit space mapping technique has been utilized. The final results have been acquired in only a fraction of time that is necessary for a direct electromagnetic (EM) optimization to generate competitive results. An experimental validation of the method proving its high utility has been provided.

4.1 Introduction

The design and optimization process of microwave circuits with unconventional topologies, which offer certain advantages over their classic counterparts, for example, an enhanced performance or a smaller real estate area, has been recently considered as an important and extremely challenging engineering issue. The general dogma for the synthesis of microwave circuits with improved functionality, for example, miniaturized couplers [1-5], abbreviated power dividers [6], [7] or compact filters [8-10], oscillates around a holistic EM-based optimization (EMBO) approach constituted by a laborious multi-parameter optimization of a high-fidelity EM model of the complete circuit. Such an approach has been found to be of limited use or even prohibitive when applied to computationally expensive microwave circuits with complex topologies that are described by a vast number of design variables.

This problem has been mitigated to some extent by the employment of surrogate-based optimization (SBO) techniques [11-21] that replace the direct optimization of a computationally demanding high-fidelity model by an iterative construction, optimization and updating of a computationally cheap low-fidelity surrogate model. The accuracy of the SBO design solution is achieved by a high-fidelity model evaluation that follows each surrogate model optimization. To date, a number of SBO methods, including explicit space mapping [11], aggressive space mapping [12], [13], neural space mapping [14], [15], implicit space mapping [16], [17], fuzzy space mapping [18], tuning space mapping [19], [20], manifold mapping [21] etc., have proven their vital usefulness in the process of a fast and accurate microwave circuit modeling.

In this paper, a new approach to the design of microwave circuits with complex topologies offering an enhanced functionality has been presented and showcased. The novelty of the method proposed lies in the reduction of the overall design cost by replacing a single complex optimization problem by a number of simple optimization problems that are solved sequentially to reach a satisfactory approximation of the optimal solution. Furthermore, the method presented exploits an SBO concept to capitalize on its high speed and accuracy. In the initial steps of the design scheme demonstrated, a logical decomposition of a conventional circuit into its atomic building blocks is performed. Next, each atomic building block constituting the circuit under construction is rebuilt in a sequential manner and undergoes an SBO (labeled here an atomistic SBO). In this work, the method proposed has been used to design two exemplary microwave circuits with unconventional topologies at a low computational cost. The substantial accuracy of the circuit optimization with only a handful of EM simulations has been achieved by means of an implicit space mapping technique. The enhanced functionality of the circuits has been acquired by using compact microstrip resonant cells as a substitution for initial atomic building blocks. However, it is noteworthy that the method proposed is also compatible with other SBO techniques as well as alternative means of circuit refinement (e.g. [6-10]), if only adequate computationally cheap surrogate models are available.

4.2 Design Methodology

Unconventional microwave circuits with enhanced functionality, because of their novelty and considerable complexity, lack accurate analytical models enabling their fast synthesis and, for that reason, indispensably require high-fidelity, but extremely time-consuming EM simulation tools in the process of their optimization. In order to address this inconvenience, the following design flow has been proposed.

4.2.1 General Design Flow

The new approach introduced in this work and illustrated in Figure 4.1 offers a robust simulation-driven design methodology enabling the achievement of an accurate design solution in relatively short time. The initial step of the diagram from Figure 4.1 is a definition of a design specification, for example, substrate parameters, frequency-dependent performance of the circuit (e.g. desired S_{11} and S_{21} over a given frequency band), physical dimension requirements etc. Subsequently, a conventional circuit is constructed from uniform transmission line (UTL) seg-

ments and various discontinuities. This can be done without major obstacles as conventional microwave circuits are supplied with good theoretical models ready to be used instantly after a few iterations of fine-tuning [22]. Next, a surrogate model of a conventional circuit is constructed (or re-used from the previous step). Afterwards, atomic building blocks of a conventional circuit are identified. The initial circuit is logically divided into n sets of equal UTLs and a $(n + 1)^{th}$ set of all discontinuities required. For example, a logical decomposition of a rat-race coupler would result in three sets ($n = 2$), the first one containing three UTLs of 90° electrical length and Z impedance, the second one containing one UTL of 270° electrical length and Z impedance and the third one containing four T-junctions. The following steps of the design flow are performed iteratively (from $i = 1$ to n). In each iteration, the circuit under consideration is updated, that is, the i^{th} set of equal UTL surrogate models is replaced with a set of equal non-UTL (n-UTL) surrogate models, after which a new circuit is composed from fixed and updated building blocks and undergoes an SBO aimed at the satisfaction of the desired design specification. In each iteration of the main algorithm, only design parameters corresponding to n-UTL surrogate models of the i^{th} set become optimization variables used during an SBO, whereas all other design parameters remain fixed. The main algorithm ends after a successful optimization of n updated circuits.

4.2.2 Circuit Surrogate Model Update

A UTL segment is an atomic building block of a conventional microwave circuit. In order to construct a circuit with improved functionality, one should substitute a UTL segment with its non-uniform counterpart (e.g. a discontinuous transmission line segment [2], a slow-wave resonant structure [3], a transmission line with perturbed ground plane metallization [1] etc.). Subsequently, an optimization of an n-UTL follows. In practice, an n-UTL segment is optimized to match the frequency-dependent parameters of a UTL segment (e.g. scattering parameters, characteristic impedance, electrical length etc.) in a given frequency range and to demonstrate an enhanced performance (e.g. out-of-band characteristics) or diminished dimensions. Moreover, in order to omit the final EM fine-tuning of the circuit, one should optimize the design parameters of an n-UTL segment as a part of the whole circuit and not as a stand-alone component. A general illustration of a circuit surrogate model update has been presented in Figure 4.2. An initial design is constituted by UTLs (collected in n sets, each of them containing at least one UTL element characterized by a certain electrical length and a characteristic impedance) and various discontinuities [gathered in the $(n + 1)^{th}$ set]. In the first iteration, the first set containing UTL_1 elements is replaced by a set containing n-UTL_1 elements, whereas all the other sets remain unchanged. In the i^{th} iteration, the i^{th} set is updated in a similar fashion and the circuit is composed of n-UTL_1, n-UTL_2, …, n-UTL_i, UTL_{i+1}, UTL_{i+2}, …, UTL_n elements and discontinuities collected in the $(n + 1)^{th}$ set. After the n^{th} update, no UTL segments remain and the whole circuit can be considered as completely refined.

4.2.3 Surrogate-Based Optimization

In order to develop an unconventional microwave circuit with a complex topology according to the specification prescribed, a non-linear minimization problem of the following form should be solved:

$$\boldsymbol{x}^* = \arg\min_{\boldsymbol{x}} U\left(\boldsymbol{R}_f\left(\boldsymbol{x}\right)\right) \tag{4.1}$$

where U denotes an objective function formulated on the basis of a design specification, $\boldsymbol{R}_f$ stands for a high-fidelity model evaluation (a fine model response), whereas $\boldsymbol{x}$ represents a vector of design variables. The optimal design solution vector is denoted by $\boldsymbol{x}^*$. The optimization problem from (4.1), when solved directly, is usually extremely CPU and time expensive and can be found impractical in case of circuits with a high computational cost. The SBO approach addresses this issue by using a computationally cheap surrogate model evaluation $\boldsymbol{R}_s$ and an iterative formulation that follows:

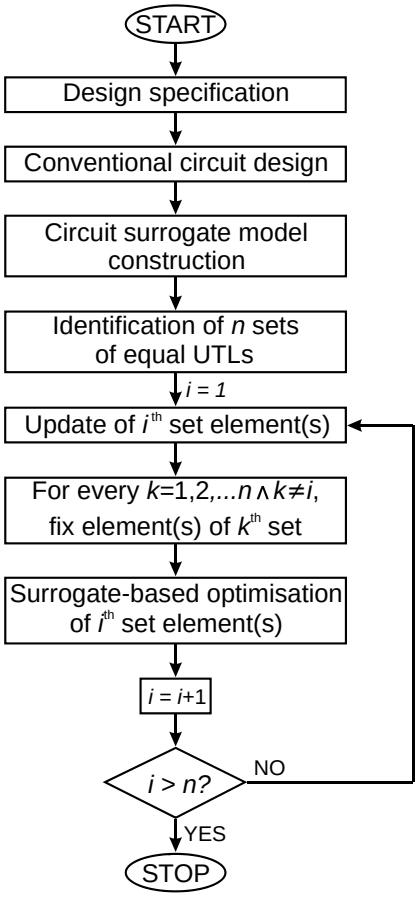

Figure 4.1: Design flow of an unconventional microwave circuit with a complex topology.

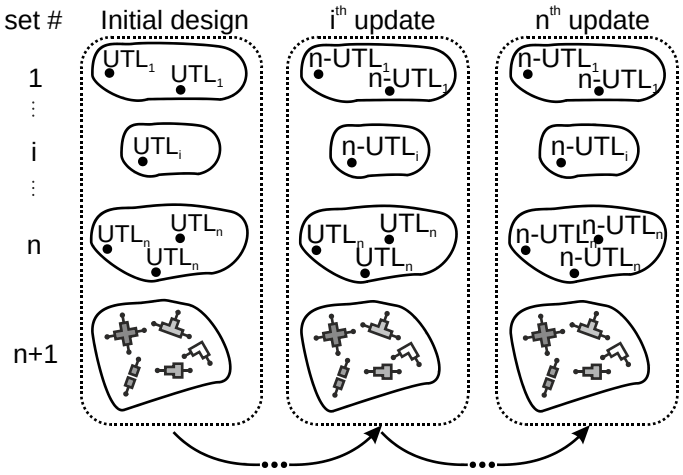

Figure 4.2: General scheme of circuit surrogate model update.

$$\boldsymbol{x}^{(j+1)} = \arg\min_{\boldsymbol{x}} U\left(\boldsymbol{R}_s^{(j)}(\boldsymbol{x})\right) \tag{4.2}$$

where $\boldsymbol{x}^{(j+1)}$ represents the optimal solution of the j^{th} iteration surrogate model $\boldsymbol{R}_s^{(j)}$, which is assumed to represent the fine model $\boldsymbol{R}_f$ in a relatively accurate manner [22]. Within these theoretical constraints, the algorithm formulated in (4.2) is aimed at approaching a quasi-optimal solution located in the vicinity of the global optimum $\boldsymbol{x}^*$. An SBO flowchart illustrating a general implementation of the theory described above is presented in Figure 4.3.

4.3 Design Examples

The general method described in Section 4.2 and schematically presented in Figure 4.1 has been applied to design two exemplary microwave circuits with complex topologies. A design flow of an exemplary two-port device, that is, an unconventional impedance matching transformer (MT) has been described in Section 4.3.1. A step-by-step design procedure of an exemplary four-port device, that is, a miniaturized branch-line coupler (BLC) has been discussed in Section 4.3.2. In both design examples, implicit space mapping (ISM) [16-17] has been used as an SBO engine due to the simplicity of its implementation [23]. A detailed flowchart of the ISM algorithm implemented in this work is depicted in Figure 4.4. The EM fine model evaluation has been performed by Momentum EM solver [24].

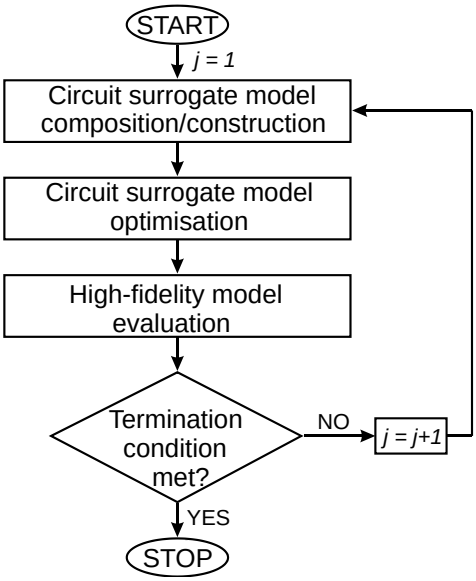

Figure 4.3: SBO flowchart.

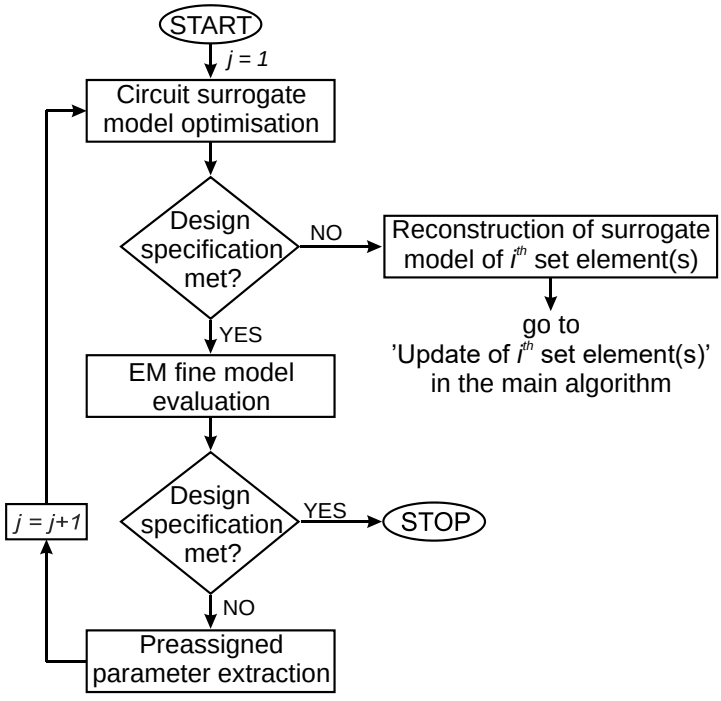

Figure 4.4: ISM algorithm flowchart.

It has been assumed that the circuit improvement in terms of its diminution (Section 4.3.1) and its miniaturization (Section 4.3.2) is to be obtained by means of metallization perforations, that is, intentional defects implemented in the signal line metallization plane (termed here compact microstrip resonant cells, CMRCs). Surrogate models of CMRCs used in this work are supplied with a geometric and preassigned parameter description of the following general form: $\boldsymbol{x}_i^{(j)} = [L_1\ H_1\ L_2\ H_2\ \ldots]^T$ and $\boldsymbol{p}_i^{(j)} = [h_1\ \varepsilon_1\ h_2\ \varepsilon_2\ \ldots]^T$, respectively ($i$ is an iteration index of the main algorithm and j denotes an iteration index of the ISM algorithm). The former parameters undergo the ISM optimization, while the latter auxiliary parameters (substrate height and relative permittivity) are used in the extraction process (see Figure 4.4).

In general, the ISM algorithm should successfully finish after the j^{th} iteration, when the EM circuit surrogate model evaluation satisfies the initially defined design specification. In such a case, the iteration counter i of the main algorithm is incremented and a novel refined circuit with the i^{th} UTL replaced by an n-UTL is developed in a similar fashion. Conversely, when no convergence of the ISM algorithm can be reached or the design specification is not met after a circuit optimization, surrogate model(s) under optimization should be reconstructed and the i^{th} iteration of the main algorithm repeated with a new n-UTL surrogate model.

4.3.1 Abbreviated Matching Transformer

The design specification has been defined as follows: (a) Rogers RO3210 substrate (ε_r = 10.2, h = 0.635 mm, tanδ = 0.0027); (b) circuit functionality ($|S_{11}| \leq -20$ dB over 1–2.5 GHz frequency band), Z_{source} = 50 Ω, Z_{load} = 6 Ω; (c) physical requirements (minimal length reduction equals 30%). Following the above stated design specification, a four-section conventional microstrip MT has been designed and fine-tuned using ADS software [25]. Subsequently, a simple MT surrogate model composed of four UTL components and several elements representing microstrip step discontinuities has been constructed in ADS circuit simulator. Next, four (n = 4) single-element sets of equal UTLs have been identified (46.8-Ω UTL_1, 33.6-Ω UTL_2, 17.3-Ω UTL_3, and 8.9-Ω UTL_4). Afterwards, as presented in detail in Figure 4.5, an iterative part of the main algorithm follows. In the first three iterations of the main algorithm, successive UTL surrogate models have been successfully substituted with a T-shaped CMRC surrogate model (termed here CMRC_A). However, in the fourth iteration of the main algorithm, no convergence of the ISM algorithm has been achieved owing to a very low impedance of the UTL_4 section. Therefore, a different CMRC model (named here CMRC_B) has been introduced for the circuit to meet the design specification. Both CMRC models have been presented in Figure 4.6. The initial design variable vector used in each iteration is $\boldsymbol{x}_i^{(0)} = [1\ 1\ 1\ 1\ \ldots]^T$ mm, whereas the initial preassigned parameter vector is $\boldsymbol{p}_i^{(0)} = [0.635\ 10.2\ 0.635\ 10.2\ \ldots]^T$, in which odd elements are in mm and even elements are unitless. After four iterations of the main algorithm, a completely refined MT design has been obtained revealing a satisfactory performance and a considerable 34% length reduction. A convergence plot for the ISM algorithm executed in each iteration of the main algorithm has been illustrated in Figure 4.7. Error functions from Figure 4.7 have been calculated at frequencies from 1 to 2.5 GHz with a 0.4 GHz step. The ISM algorithm has been set to terminate when the error function is less than 10^{-1}. Final geometric parameters of the abbreviated MT are listed in Table 4.1. A total design cost of the method proposed is presented in Table 4.2. In addition, the iterative method based upon multiple atomistic SBOs (this work) has been compared against several other approaches, that is, an iterative method based on multiple atomistic EM optimizations, a method based on a holistic SBO, and a method based on a holistic EM optimization. It should be concluded upon data collected in Table 4.2 that a multiple atomistic optimization approach requires less high-fidelity model evaluations than a direct holistic optimization. Moreover, a combination of a multiple atomistic optimization approach and an SBO technique results in a method that outclasses other competitive design methodologies included in this comparison. The atomistic SBO method introduced in this work presents a design cost of 20 EM simulations for the first example, which proves its considerable computational efficiency in comparison to a classic holistic EMBO method offering 2120 EM simulations for the same example. Average CPU time of a single 64-point EM model evaluation is ~51 s for the atomistic SBO approach and 61 s for the holistic EMBO approach (both methods used i7 2600k

8 GB RAM PC). Respective CPU times differ as the complexity of the circuit iteratively increases in case of the atomistic SBO approach, reaching the greatest complexity in the last iteration, whereas the holistic EMBO approach utilizes the most complex model in every iteration. For these reasons, the total time of EM model evaluations is 17 min for the atomistic SBO method and 36 h for the holistic EMBO approach.

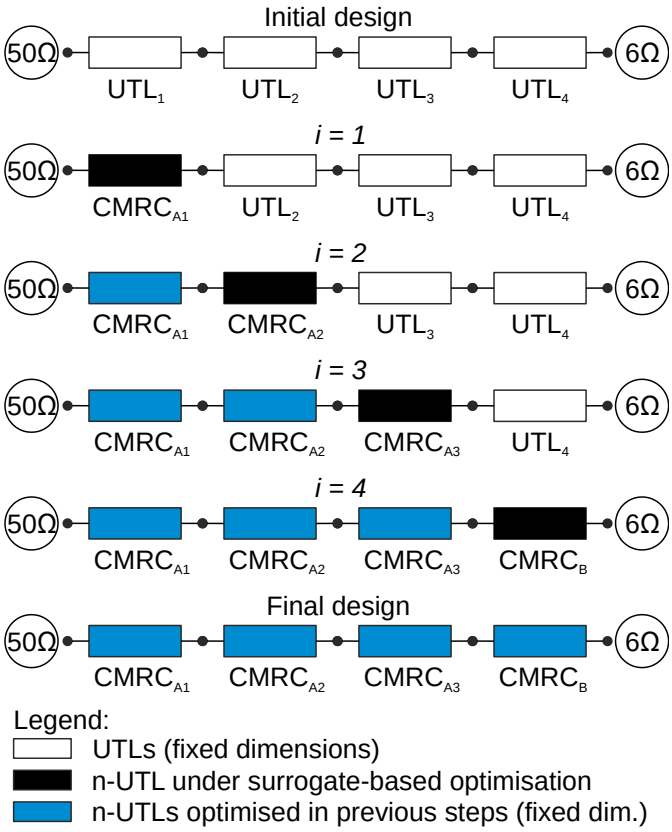

Figure 4.5: Schematic description of an MT under iterative construction.

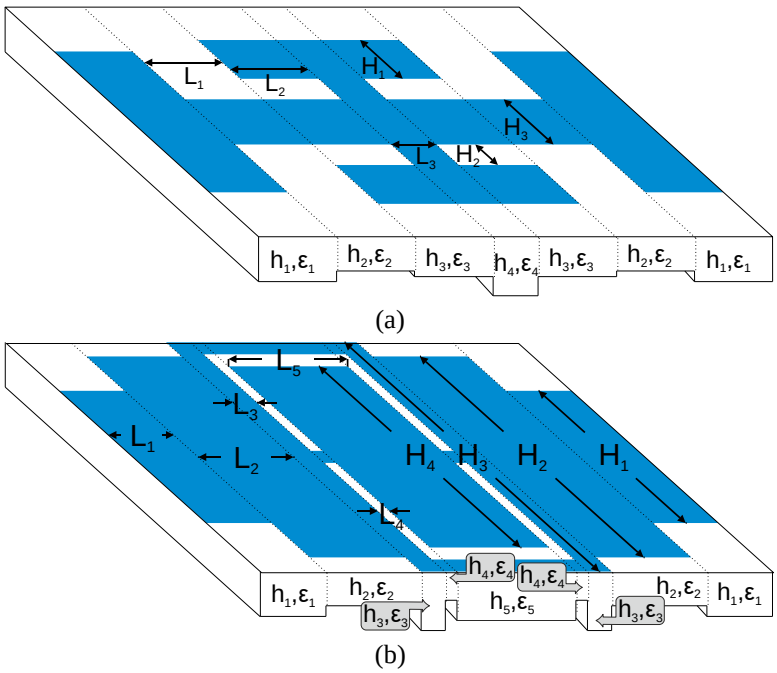

Figure 4.6: Surrogate model layout representation of: (a) $CMRC_A$, (b) $CMRC_B$.

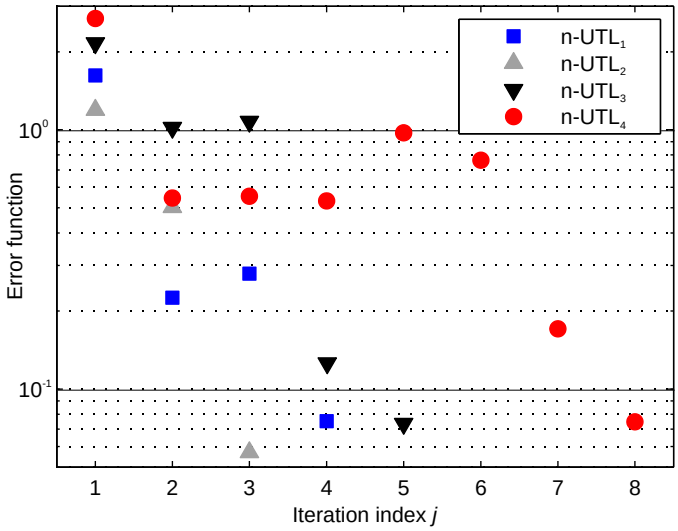

Figure 4.7: Matching transformer: a convergence plot for the ISM algorithm. Iteration index corresponds to the number of high-fidelity model evaluations.

TABLE 4.1: FINAL DESIGN GEOMETRIC DESCRIPTION

Final design dimensions		$CMRC_A$			$CMRC_B$
		n-UTL_1	n-UTL_2	n-UTL_3	n-UTL_4
x^* [mm]	L_1	0.4	0.8	0.4	1.05
	H_1	0.35	1.05	2.45	7.5
	L_2	2.4	1.4	1.4	1.6
	H_2	0.25	0.4	0.2	11.4
	L_3	0.25	0.4	0.2	0.4
	H_3	0.25	0.4	0.2	13
	L_4	-	-	-	0.2
	H_4	-	-	-	11.8

TABLE 4.2: ABBREVIATED MT: A TOTAL DESIGN COST

Total design cost	Optimization method			
	Holistic		Atomistic	
	EMBO	SBO	EMBO	SBO
Convergence	YES	NO	YES	YES
Total number of high-fidelity model evaluations	2120	N/A	746	20

4.3.2 Miniaturized Branch-Line Coupler

The design specification has been formulated as follows: (a) FR4 substrate (ε_r = 4.4, h = 0.508 mm, tanδ = 0.02); (b) circuit performance ($|S_{11}|$ and $|S_{41}| \leq -20$ dB over a 10% bandwidth with a 2.2 GHz operating frequency, $|S_{11}| \leq -40$ dB at 2.2 GHz frequency, and $|S_{21}| = |S_{31}|$ at 2.2 GHz frequency); (c) physical requirements (minimal circuit size reduction equals 30%). Using ADS simulation environment [25], a conventional BLC has been designed and fine-tuned to meet the above defined design specification. Next, a simple BLC surrogate model comprising two pairs of UTL components and four T-junctions has been built in ADS circuit simulator. Subsequently, two (n = 2) double-element sets of equal UTLs have been identified (35.35-Ω $UTLs_1$ and 50-Ω $UTLs_2$). Then, two iterations of the main algorithm have been performed in order to construct a completely refined BLC. A schematic illustration of the iterative part of the main algorithm is presented in Figure 4.8.

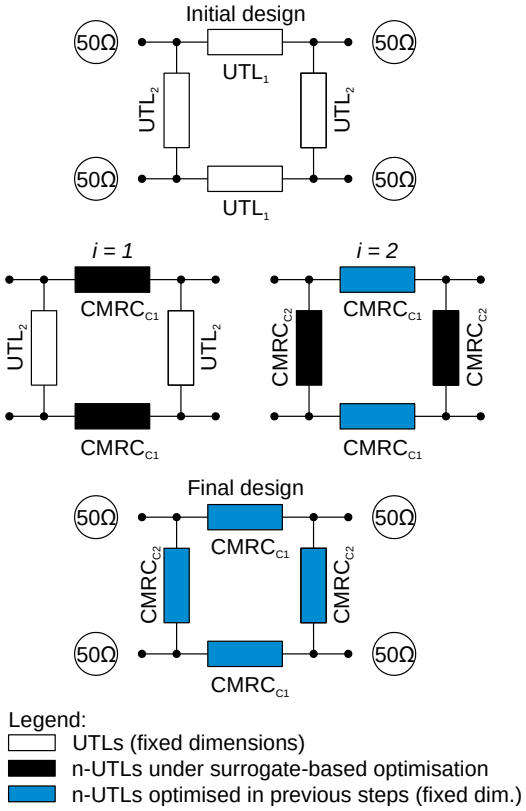

Figure 4.8: Schematic description of a BLC under iterative construction.

In each iteration i, the i^{th} pair of UTL surrogate models has been replaced with the i^{th} pair of n-UTL surrogate models. Each n-UTL surrogate model has been constituted by a cascade of two CMRCs (termed here CMRCs_{C}). A surrogate model layout representation described by a geometric and preassigned parameters is shown in Figure 4.9. The initial design variable vector used in each iteration is $\boldsymbol{x}_i^{(0)} = [1\ 1\ 1\ 1\ \ldots]^T$ mm, whereas the initial preassigned parameter vector is $\boldsymbol{p}_i^{(0)} = [0.508\ 4.4\ 0.508\ 4.4\ \ldots]^T$ (odd elements are in mm, while even elements are unitless). The final design demonstrates an acceptable performance and a notable 36% circuit area miniaturization. Error functions plotted against ISM algorithm iterations (see Figure 4.10) have been calculated at frequencies from 2.09 GHz to 2.31 GHz with a 20 MHz step and at the 2.2 GHz operating frequency alone. Final geometric parameters of the miniaturized BLC are listed in Table 4.3. Table 4.4 demonstrates a total design cost of the method implemented in this work in comparison to other competitive approaches. The ISM algorithm implemented in the atomistic SBO method has converged in 5 iterations total—two iterations for UTLs_1 (i = 1) and three iterations for UTLs_2 (i = 2)—which is more than eight times more efficient than a classic holistic EMBO method applied to the same example. Average CPU time of a single 64-point EM model evaluation is ~26 s for the atomistic SBO approach and 29 s for the holistic EMBO approach (both methods used i7 2600k 8 GB RAM PC), resulting in a total EM design cost of 2.16 min in case of the former approach and 20.3 min in case of the latter one.

4.4 Experimental Results

Both final design examples discussed in the previous section have been manufactured and measured (see Figure 4.11 and Figure 4.12). One should notice that the abbreviated MT has been fabricated in a back-to-back configuration [see Figure 4.11(b)] for the source and load impedance to be 50 Ω. Theoretical characteristics of the circuits designed, obtained by means of EM simulations, have been included for comparison purposes. It can be observed that the measured MT performance presents a reflection coefficient $|S_{11}| \leq -15$ dB in the specified frequency band. Furthermore, measured characteristics of the fabricated MT demonstrate an 8% bandwidth enlargement in comparison to the theoretical performance. Insertion loss $|S_{21}|$ is smaller

than 0.7 dB in 0.85–1.9 GHz frequency range and smaller than 1 dB in 1.9–2.65 GHz band. Lossless conductor used during EM simulations as well as the fabrication tolerance are accounted for differences in frequency characteristics between simulated and measured MT responses. The comparison between theory and experiment also reveals that ΔS_{21} is ranged between 0.3 and 0.6 dB in the predefined frequency range. In case of the miniaturized BLC, an agreement between theoretical and experimental characteristics has been found (see Figure 4.12). It is important to emphasize that the 36% rate of miniaturization has been achieved without major degradation in the performance of the circuit.

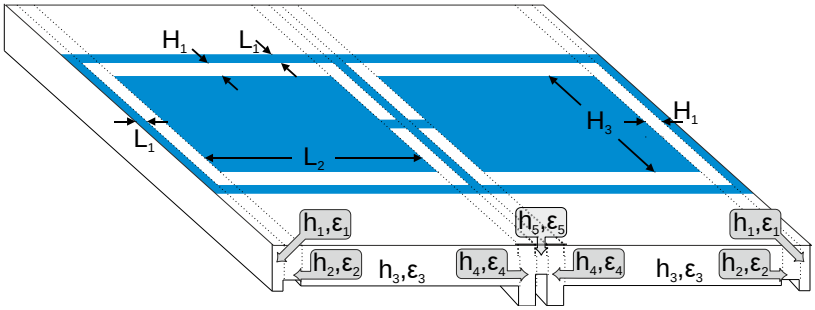

Figure 4.9: Surrogate model layout representation of a $CMRC_C$.

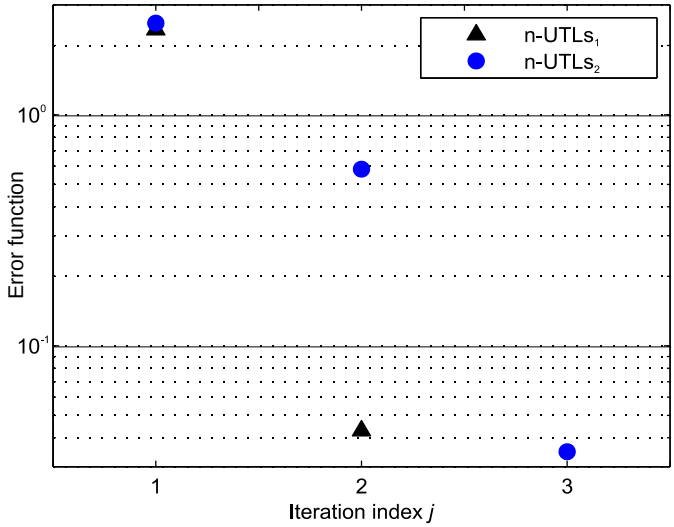

Figure 4.10: Miniaturized BLC: a convergence plot for the ISM algorithm. Iteration index corresponds to the number of high-fidelity model evaluations.

TABLE 4.3: FINAL DESIGN GEOMETRIC DESCRIPTION

Final design dimensions		$CMRC_C$	
		n-UTLs$_1$	n-UTLs$_2$
x^* [mm]	L_1	0.15	0.15
	H_1	0.15	0.15
	L_2	2.55	3.05
	H_2	1.8	0.65

TABLE 4.4: MINIATURIZED BLC: A TOTAL DESIGN COST

Total design cost	Optimization method			
	Holistic		Atomistic	
	EMBO	SBO	EMBO	SBO
Convergence	YES	YES	YES	YES
Total number of high-fidelity model evaluations	42	7	15	5

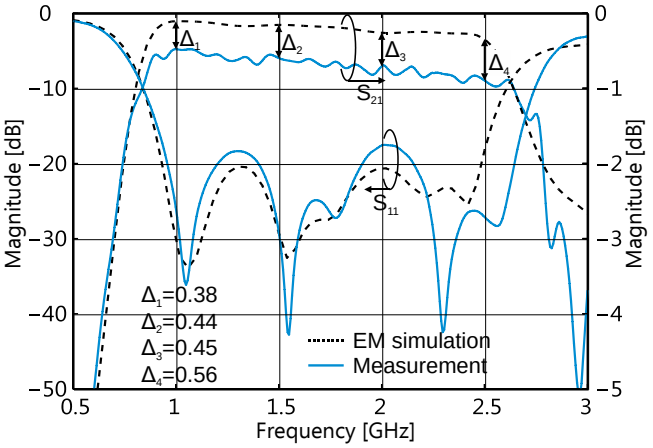

(a)

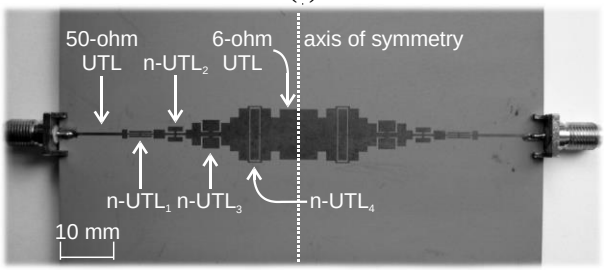

(b)

Figure 4.11: Abbreviated MT: (a) Frequency characteristics of the abbreviated MT (measurement) in comparison with its theoretical performance (simulation); (b) Photograph of the abbreviated MT in a back-to-back configuration.

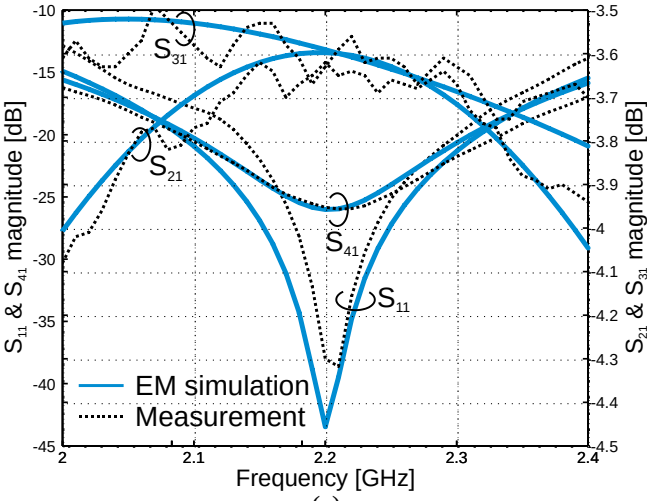

(a)

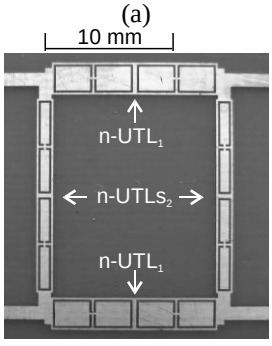

(b)

Figure 4.12: Miniaturized BLC: (a) Measurement vs. simulation performance of the miniaturized BLC; (b) Layout of the manufactured miniaturized BLC.

4.5 Conclusions

A computationally efficient design approach to microwave circuits with complex topologies has been presented and experimentally validated. The generality of the method discussed makes it suitable for a wide class of N-port unconventional microwave circuits conceived by a sequential alternation of a conventional design solution. The introduction of the atomistic optimization design approach as a vital alternative to a holistic optimization design methodology has been found useful in application to computationally demanding microwave circuits with unconventional topologies. Moreover, a combination of a sequential atomistic optimization approach and the ISM technique has resulted in a method that outclasses other competitive design methodologies mentioned in this work. The robustness and computational efficiency of the method elaborated in application to circuits with unconventional topologies has been obtained at the price of finding an approximation of the global optimum, rather than the global optimum itself. The computational gain from the application of the atomistic SBO concept promoted in this work is much more impressive in case of the circuit described by more design variables. The number of design variables, for which the utilization of this method is cost-efficient still remains an open issue.

Acknowledgement

This work was supported in part by National Science Centre, Poland, under grant no. 4699/B/T02/2011/40.

References

[1] P. Kurgan and M. Kitlinski, "Novel doubly perforated broadband microstrip branch-line couplers," *Microw. Opt. Tech. Lett*., vol. 51, no. 9, pp. 2149-2152, 2009.

[2] S. Opozda, P. Kurgan, and M. Kitlinski, "A compact seven-section rat-race hybrid coupler incorporating PBG cells," *Microw. Opt. Tech. Lett*., vol 51, no. 12, pp. 2910-2913, 2009.

[3] P. Kurgan and M. Kitlinski, "Slow-wave fractal-shaped compact microstrip resonant cell," *Microw. Opt. Tech. Lett*., vol. 52, no. 11, pp. 2613-2615, 2010.

[4] P. Kurgan and M. Kitlinski, "Doubly miniaturized rat-race hybrid coupler," *Microw. Opt. Tech. Lett*., vol. 53, no. 6, pp. 1242-1244, 2011.

[5] P. Kurgan, J. Filipcewicz, and M. Kitlinski, "Design considerations for compact microstrip resonant cells dedicated to efficient branch-line miniaturization," *Microw. Opt. Tech. Lett*., vol. 54, no. 8, pp. 1949-1954, 2012.

[6] H.L. Zhang, B.J. Hu, and X.Y. Zhang, "Compact equal and unequal dual-frequency power dividers based on composite right/left-handed transmission line," *IEEE Trans. Ind. Electron*., vol. 59, no. 9, pp. 3464-3472, 2012.

[7] H.-X. Xu, G.-M. Wang, C.-X. Zhang, Z.-W. Yu, and X. Chen, "Composite right/left-handed transmission line based on complementary single-split ring resonator pair and compact power dividers application using fractal geometry," *IET Microw. Ant. Propag.*, vol. 6, no. 9, pp. 1017-1025, 2012.

[8] P. Kurgan and M. Kitlinski, "Novel microstrip low-pass filters with fractal defected ground structures," *Microw. Opt. Tech. Lett*., vol. 51, no. 10, pp. 2473-2477, 2009.

[9] M. Smierzchalski, P. Kurgan, and M. Kitlinski, "Improved selectivity compact band-stop filter with Gosper fractal-shaped defected ground structures," *Microw. Opt. Tech. Lett*., vol. 52, no. 1, pp. 227-232, 2010.

[10] P. Kurgan, A. Bekasiewicz, M. Pietras, and M. Kitlinski, "Novel topology of compact coplanar waveguide resonant cell low-pass filter," *Microw. Opt. Tech. Lett*., vol. 54, no. 2, pp. 732-735, 2012.

[11] J.W. Bandler, R.M. Biernacki, S.H. Chen, P.A. Grobelny, and R.H. Hemmers, "Space mapping technique for electromagnetic optimization," *IEEE Trans. Microw. Theory Tech*., vol. 42, no. 12, pp. 2536-2544, 1994.

[12] M.H. Bakr, J.W. Bandler, R.M. Biernacki, S.H. Chen, and K. Madsen, "A trust region aggressive space mapping algorithm for EM optimization," *IEEE Trans. Microw. Theory Tech*., vol. 46, no. 12, pp. 2412-2425, 1998.

[13] M.H. Bakr, J.W. Bandler, N. Georgieva, and K. Madsen, "A hybrid aggressive space-mapping algorithm for EM optimization," *IEEE Trans. Microw. Theory Tech*., vol. 47, no. 12, pp. 2440-2449, 1999.

[14] J.W. Bandler, M.A. Ismail, J.E. Rayas-Sánchez, and Q.-J. Zhang, "Neuromodeling of microwave circuits exploiting space-mapping technology," *IEEE Trans. Microw. Theory Tech*., vol. 47, no. 12, pp. 2417-2427, 1999.

[15] M.H. Bakr, J.W. Bandler, M.A Ismail, J.E. Rayas-Sánchez, and Q.-J. Zhang, "Neural space-mapping optimization for EM-based design," *IEEE Trans. Microw. Theory Tech*., vol. 48, no. 12, pp. 2307-2315, 2000.

[16] J.W. Bandler, Q.S. Cheng, N.K. Nikolova, and M.A. Ismail, "Implicit space mapping optimization exploiting preassigned parameters," *IEEE Trans. Microw. Theory Tech*., vol. 52, no. 1, pp. 378-385, 2004.

[17] S. Koziel, Q.S. Cheng, and J.W. Bandler, "Implicit space mapping with adaptive selection of pre-assigned parameters," *IET Microw. Ant. Propag*., vol. 4, no. 3, pp. 361-373, 2010.

[18] S. Koziel and J.W. Bandler, "A space-mapping approach to microwave device modeling exploiting fuzzy systems," *IEEE Trans. Microw. Theory Tech*., vol. 55, no. 12, pp. 2539-2547, 2007.

[19] S. Koziel, J. Meng, J.W. Bandler, M.H. Bakr, and Q.S. Cheng, "Accelerated microwave design optimization with tuning space mapping," *IEEE Trans. Microw. Theory Tech*., vol. 57, no. 2, pp. 383-394, 2009.

[20] Q.S. Cheng, J.C. Rautio, J.W. Bandler, and S. Koziel, "Progress in simulator-based tuning – the art of tuning space mapping," *IEEE Microw. Mag*., vol. 11, no. 4, pp. 96-110, 2010.

[21] S. Koziel and S. Ogurtsov, "Robust design of UWB antennas using response surface approximations and manifold mapping," *European Conf. Ant. Propag.*, pp. 773-775, Prague, 2012.

[22] S. Koziel, C. Echeverría, and L. Leifsson, "Surrogate-based methods," in S. Koziel and X.-S. Yang, (Eds.): *Computational optimization, methods and algorithms*, Series: Studies in Computational Intelligence, vol. 356, pp. 33-59, Springer, 2011.

[23] S. Koziel, Q.S. Cheng, and J.W. Bandler, "Space mapping," *IEEE Microw. Mag*., vol. 9, no. 6, pp. 105-122, 2008.

[24] Agilent Momentum, ver. 2011.10, Agilent Technologies, 1400 Fountaingrove Parkway, Santa Rosa, CA 95403-1799, 2011.

[25] Agilent ADS, ver. 2011.10, Agilent Technologies, 1400 Fountaingrove Parkway, Santa Rosa, CA 95403-1799, 2011.

5 NESTED SPACE MAPPING

***

S. Koziel, A. Bekasiewicz, and P. Kurgan

Rapid EM-Driven Design of Compact RF Circuits By Means of Nested Space Mapping

Published in: *IEEE Microwave and Wireless Components Letters*, vol. 24, no. 6, pp. 364-366, 2014.

DOI: 10.1109/LMWC.2014.2313588

***

Hybrid coupler application example of nested space mapping is showcased in Appendix A.

***

Abstract: A methodology for rapid design of RF circuits constituted by compact microstrip resonant cells (CMRCs) is presented. Our approach exploits nested space mapping (NSM) technology, where the inner SM layer is used to correct the equivalent circuit model at the CMRC level, whereas the outer layer enhances the coarse model of the entire structure under design. We demonstrate that NSM dramatically improves performance of surrogate-based optimization of composite CMRC-based structures. It is validated using four examples of UWB microstrip matching transformers (MTs) and compared to previous attempts to surrogate-based compact structure design.

5.1 Introduction

Design optimization of RF passive components for space-limited applications is a challenging task constrained by rigorous specifications regarding size and the circuit performance. Typically, an initial design is obtained by replacing fundamental building blocks of a conventional circuit with composite structures of increased complexity, whose geometrical parameters are to be adjusted to reach a compact design with a satisfactory performance. Due to the physical complexity of the circuit, its reliable evaluation requires accurate, but CPU-intensive electromagnetic (EM) analysis. Classical EM-driven design approaches, based either on laborious parameter sweeps or direct optimization, are usually unfeasible [1], [2].

High cost of EM optimization can be alleviated by means of surrogate-based optimization (SBO) [3], where an improved design is obtained using computationally cheap replacement models. However, SBO success can be mainly contributed to a relatively small number of adjustable parameters and to generally well-suited physics-based low-fidelity models available for conventional RF circuits. In case of complex RF circuits, analytical coarse models are highly inaccurate and their utilization causes convergence problems of the SBO process [4].

In [5], a technique exploiting the SBO concept in combination with the design problem decomposition has been proposed. Despite its advantages, the method [5] requires an inconvenient manual setup of multiple optimization problems, which circumvents the necessity to handle a large number of parameters in a single optimization attempt. The method of [5] has been extended in [6] by fixing a number of designable parameters on the basis of theoretical premises and low-cost preliminary studies of a low-fidelity model. However, this approach is also hindered by the same drawback as [5].

Here, we propose a nested space mapping (NSM) approach for rapid design of compact CMRC-based RF circuits. NSM constructs a two-stage surrogate model, with the inner SM layer applied at the level of the decomposed components of the structure under design, and the outer SM layer applied for the entire circuit. NSM ensures excellent generalization capability of the surrogate model, which results in rapid design improvement. Our technique is demonstrated using several UWB microstrip MTs and compared with two benchmark SBO methods.

5.2 Design Methodology. Nested Space Mapping Modeling of CMRC Structures

5.2.1 Design Problem. Surrogate-Based Optimization

Let $\boldsymbol{R}_f$ denote the response vector of a fine EM-simulated model of the CMRC structure of interest. The task is to solve

$$\boldsymbol{x}^* = \arg\min_{\boldsymbol{x}} U\left(\boldsymbol{R}_f\left(\boldsymbol{x}\right)\right) \tag{5.1}$$

where U is an objective function implementing given design specifications. $\boldsymbol{R}_f$ is assumed to be computationally expensive, which makes a direct optimization of $U(\boldsymbol{R}_f(\boldsymbol{x}))$ prohibitive.

To solve (5.1), we exploit surrogate-based optimization (SBO) that generates a sequence of approximate solutions to (5.1), $\boldsymbol{x}^{(i)}$, $i = 0, 1, 2, \ldots$ as follows ($\boldsymbol{x}^{(0)}$ is an initial design) [7]:

$$\boldsymbol{x}^{(i+1)} = \arg\min_{\boldsymbol{x}} U\left(\boldsymbol{R}_s^{(i)}\left(\boldsymbol{x}\right)\right) \tag{5.2}$$

The surrogate model $\boldsymbol{R}_s^{(i)}$ is a fast representation of the fine model $\boldsymbol{R}_f$. In this work, $\boldsymbol{R}_s^{(i)}$ is created using a nested space mapping approach introduced in Section 5.2.2.

5.2.2 Nested Space Mapping Modeling

Figure 5.1 shows a typical CMRC component, its equivalent circuit representation, as well as an example CMRC-based structure. Let $\boldsymbol{R}_{f.cell}(\boldsymbol{y})$ and $\boldsymbol{R}_{c.cell}(\boldsymbol{y})$ denote the responses of the fine (EM-simulated) and coarse (circuit-simulated) models of the CMRC component; vector $\boldsymbol{y}$ represents geometry parameters of the component. Let $\boldsymbol{R}_f(\boldsymbol{x})$ and $\boldsymbol{R}_c(\boldsymbol{x})$ stand for the fine and coarse models of the entire CMRC structure with $\boldsymbol{x}$ being a corresponding vector of geometry parameters.

The nested SM approach proposed here builds up the surrogate model of the CMRC structure starting from the component level. Let $\boldsymbol{R}_{s.g.cell}(\boldsymbol{y},\boldsymbol{p})$ be a generic component surrogate, which is a composition of $\boldsymbol{R}_{c.cell}$ and suitable SM transformations; $\boldsymbol{p}$ denotes extractable SM parameters of the model. The SM surrogate $\boldsymbol{R}_{s.cell}$ of a component is obtained as

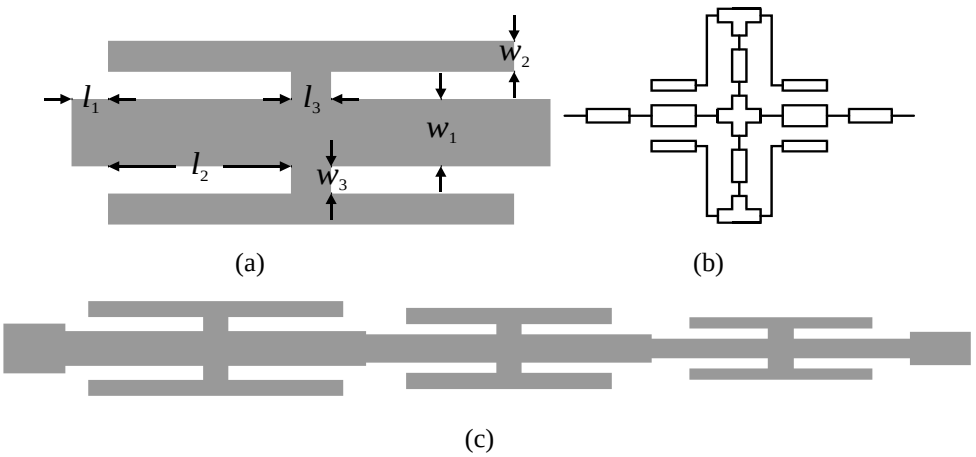

Figure 5.1: (a) Typical CMRC component (here, double-T), (b) its equivalent circuit, (c) exemplary CMRC-based matching transformer.

$$\boldsymbol{R}_{s.cell}\left(\boldsymbol{y}\right)=\boldsymbol{R}_{s.g.cell}\left(\boldsymbol{y},\boldsymbol{p}^{*}\right) \tag{5.3}$$

where

$$\boldsymbol{p}^{*}=\arg\min_{\boldsymbol{p}}\sum_{k=1}^{N_{cell}}\left\|\boldsymbol{R}_{s.g.cell}\left(\boldsymbol{y}^{(k)},\boldsymbol{p}\right)-\boldsymbol{R}_{f}\left(\boldsymbol{y}^{(k)}\right)\right\| \tag{5.4}$$

Here, $\boldsymbol{y}^{(k)}$, $k = 1, \ldots, N_{cell}$, are the training designs. We use the star-distributed base with $N_{cell} = 2n + 1$, where $n = \dim(\boldsymbol{y})$. For design cases shown in Section 5.3, $\boldsymbol{R}_{s.g.cell}$ is constructed using a combination of input, implicit and frequency SM [3]. The model $\boldsymbol{R}_{s.cell}$ is established to be valid in the entire range of parameters $\boldsymbol{y}$ used in the subsequent CMRC structure design.

Let $\boldsymbol{R}_{s.g}(\boldsymbol{x},\boldsymbol{P})$ be the generic SM surrogate of the entire CMRC structure, composed of the SM models of CMRC components, i.e., $\boldsymbol{R}_{s.g}(\boldsymbol{x},\boldsymbol{P}) = \boldsymbol{R}_{s.g}([\boldsymbol{y}_1; \ldots; \boldsymbol{y}_p],\boldsymbol{P}) = F(\boldsymbol{R}_{s.g.cell}(\boldsymbol{y}_1,\boldsymbol{p}^{*}),\ldots, \boldsymbol{R}_{s.g.cell}(\boldsymbol{y}_p,\boldsymbol{p}^{*}),\boldsymbol{P})$. In case of MTs considered in Section 5.3, the function F realizes cascade connection of S-parameters of individual components; the parameter vector $\boldsymbol{x}$ is a concatenation of component parameter vectors $\boldsymbol{y}_k$. The "global" SM parameter vector $\boldsymbol{P}$ is normally defined as perturbations (with respect to $\boldsymbol{p}^{*}$) of selected SM parameters of individual components.

The outer SM level is applied to the global model $\boldsymbol{R}_{s.g}(\boldsymbol{x},\boldsymbol{P})$, so that the final surrogate $\boldsymbol{R}_{s}^{(i)}$ utilized in the ith iteration of the SBO scheme (5.2) is defined as

$$\boldsymbol{R}_{s}^{(i)}\left(\boldsymbol{x}\right)=\boldsymbol{R}_{s.g}\left(\boldsymbol{x}^{(i)},\boldsymbol{P}^{(i)}\right) \tag{5.5}$$

where

$$\boldsymbol{P}^{(i)}=\arg\min_{\boldsymbol{P}}\left\|\boldsymbol{R}_{s.g}\left(\boldsymbol{x}^{(i)},\boldsymbol{P}\right)-\boldsymbol{R}_{f}\left(\boldsymbol{x}^{(i)}\right)\right\| \tag{5.6}$$

In practice, the number of parameters in $\boldsymbol{P}$ is much smaller than the combined number of SM parameters of CMRC components (i.e., multiple copies of a vector $\boldsymbol{p}^{*}$). This is sufficient because the inner SM layer already provides good alignment between the $\boldsymbol{R}_{s.cell}$ and $\boldsymbol{R}_{f.cell}$ so that the role of (5.5), (5.6) is to compensate for couplings between CMRC components that are not accounted for by the composing function F.

5.2.3 Generalization Properties of NSM. Algorithm Convergence

The fundamental advantage of NSM is that a globally accurate surrogate model of CMRC component obtained by (5.3), (5.4) (inner SM layer, see also Figure 5.2), ensures good generalization capability of the final NSM surrogate. Figure 5.3 shows the responses of the NSM surrogate before and after parameter extraction (PE) (5.5). The surrogate (i.e., $\boldsymbol{R}_{s.g}$) matches the fine model well even before PE. PE is executed using only a few parameters and allows us to quick-

ly compensate for the couplings between the CMRC components, which is not accounted for by the component models themselves. At the same time, NSM model exhibits excellent generalization as indicated in Figure 5.3(b).

Conventional SM modeling of the entire transformer (i.e., correction of its coarse model $\boldsymbol{R}_c$) is a much more complex process: (i) the coarse model of the entire transformer is much less accurate than $\boldsymbol{R}_{s.g}$ [cf. Figure 5.4(a)], (ii) large number of SM parameters is required, (iii) parameter extraction is more difficult and time consuming, and (iv) generalization capability of the model is poor [cf. Figure 5.4(b)]. Sufficient accuracy of the underlying coarse model and good generalization capability of the surrogate are essential for fast convergence of the SBO optimization process (5.2) [4]. The NSM model has both aforementioned features [here, the global model $\boldsymbol{R}_{s.g}$ is formally a coarse model for (5.2)], which results in rapid design of CMRC-based structures as demonstrated in Section 5.3.

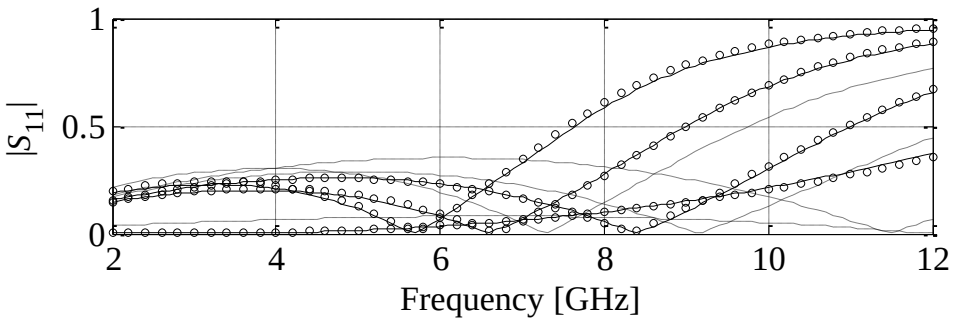

Figure 5.2: Nested SM modeling of double-T CMRC component. Responses at the selected test designs: coarse model (····), fine model (—), NSM surrogate (○).

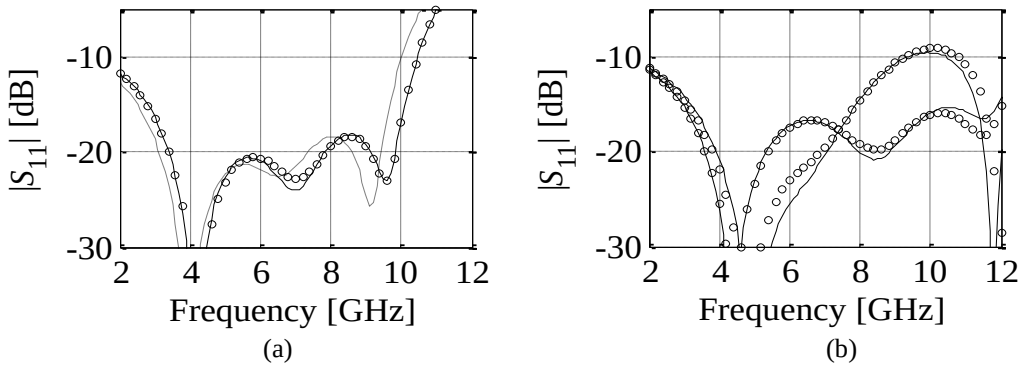

Figure 5.3: Nested SM modeling of double-T CMRC-based transformer: (a) fine (—), NSM surrogate before parameter extraction (····) and NSM surrogate after parameter extraction (○); (b) NSM surrogate extracted at the design of Figure 5.4(a) shown at other designs (○) as well as corresponding fine model responses (—). Generalization capability of the NSM surrogate is very good.

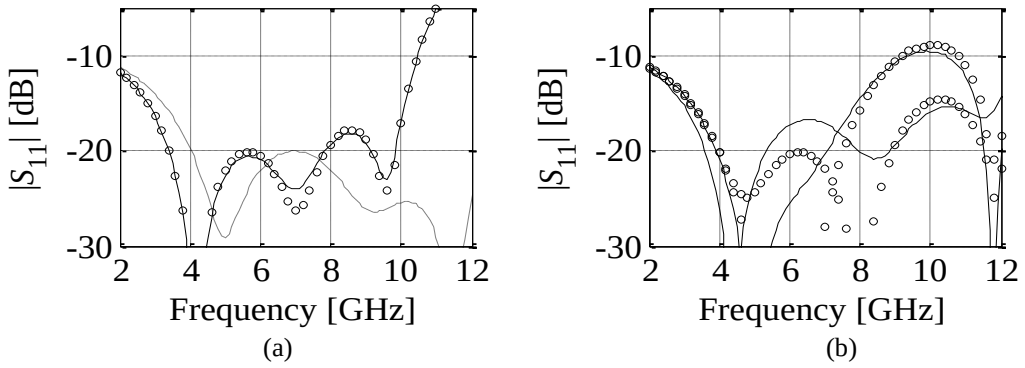

Figure 5.4: Conventional SM modeling of double-T CMRC-based MT: (a) fine (—), SM surrogate before parameter extraction (····) and SM surrogate after parameter extraction (○); (b) SM surrogate extracted at the design of Figure 5.4(a) shown at other designs (○) as well as corresponding fine model responses (—). Note poor generalization capability of the conventional SM surrogate.

5.3 Case Studies

In this section we validate a methodology of Section 5.2.2. For all cases, the generic SM surrogate takes the form of $\boldsymbol{R}_{s.g.cell}(\boldsymbol{y},\boldsymbol{p}) = \boldsymbol{R}_{c.F}(\boldsymbol{B}\cdot\boldsymbol{x}+\boldsymbol{c},p_I)$, where $\boldsymbol{B}$ and $\boldsymbol{c}$ are input SM parameters (we use diagonal matrix $\boldsymbol{B}$), $\boldsymbol{p}_I$ are implicit SM parameters (here, substrate parameters for individual microstrip models), and frequency scaling ($\boldsymbol{R}_{c.F}$ denotes frequency scaled $\boldsymbol{R}_c$ with the affine scaling function $F(\omega) = f_0 + \omega\cdot f_1$, where f_0, f_1 are extractable parameters).

A double-T structure [Figure 5.1(a)], described by 4 geometric parameters $\boldsymbol{y} = [l_1\ l_2\ w_1\ w_2]^T$ (dimensions $l_3 = 0.2$ and $w_3 = 0.2$ are fixed) with a total of 16 SM parameters, and a C-shaped cell [Figure 5.4(a)] with 5 geometric parameters: $\boldsymbol{y} = [l_1\ l_2\ w_1\ w_2\ w_3]^T$ (a total of 18 extractable SM parameters) have been used for verification (all geometry parameters are in mm).

The high-fidelity models $\boldsymbol{R}_{f.cell}$ of both structures and their SM surrogates $\boldsymbol{R}_{s.cell}$ [see Figure 5.1(a)-(b) and Figure 5.5(a)-(b)] are implemented in CST MWS [8] (RF-35 substrate with $h = 0.76$ mm) and Agilent ADS [9], respectively.

5.3.1 MTs Based on Double-T-shaped CMRCs

Consider a cascade of double-T CMRC components, Figure 5.1(c), used for a construction of three- and four-section MTs. The design objective is to achieve $|S_{11}| \le -15$ dB in UWB band (3.1 to 10.6 GHz). The vector of initial design parameters of each section is: $\boldsymbol{y} = [0.65\ 0.35\ 0.55\ 3.75]^T$.

A three-section MT (i) is designed to match 50 Ω to 100 Ω impedance. The final design: $\boldsymbol{x} = [0.5\ 4.36\ 0.76\ 0.2\ 0.5\ 3.73\ 0.49\ 0.2\ 0.5\ 3.22\ 0.24\ 0.2]^T$ is obtained after two iterations of the NSM technique ($|S_{11}| \le -17.5$ dB for 3.1 GHz to 10.6 GHz).

A cascade of four cells, constitutes a 50-to-130 Ω MT (ii). The final MT design denoted by: $\boldsymbol{x} = [1.0\ 3.52\ 0.85\ 0.2\ 0.8\ 4.10\ 0.58\ 0.05\ 0.8\ 3.09\ 0.1\ 0.25\ 1\ 2.315\ 0.13\ 0.05]^T$ is obtained after only three iterations of the proposed algorithm ($|S_{11}| \le -16.5$ dB for 3.1 GHz to 10.6 GHz). It should also be noted that the inner SM layer correction is used to build a generalized CMRC model that can be reused many times as a library component. Typically, the CPU cost of such process is not included in the overall design cost. Here, this cost is added in Table 5.1.

One should emphasize that for both MTs, the number of the outer layer SM parameters $\boldsymbol{P}$ is much smaller than the combined set of SM parameters for the inner layer (11 vs. 48 for the first MT and 14 vs. 64 for the second one) as only frequency scaling and selected implicit SM parameters are used (three substrate heights for each cell). The particular choice of the output SM layer parameters is not critical, however, it is recommended to have some parameters for each individual cell of the entire structure. Reduction of the number of parameters (possible because of excellent generalization capability of NSM) considerably speeds up the design process. The reflection characteristics of (i) and (ii) MTs are shown in Figure 5.6(a).

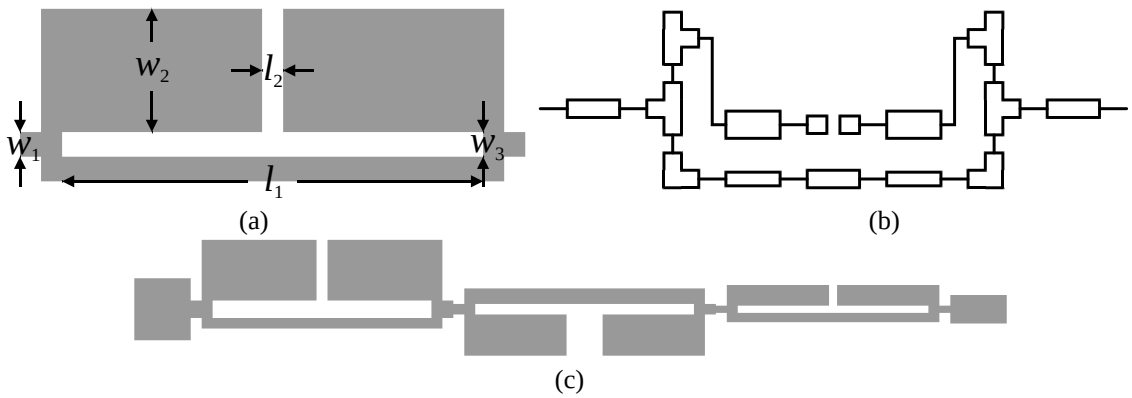

Figure 5.5: C-shaped CMRC component: (a) geometry; (b) equivalent circuit; (c) conceptual geometry of three-section MT.

5.3.2 MTs Based on C-Shaped CMRCs

Consider a three-section MT composed of cascaded C-shaped structures shown in Figure 5.5(c). The objective is to achieve $|S_{11}| \leq -15$ dB in the frequency band of interest.

The MT (iii) is designed to match 50 Ω to 100 Ω impedance within 3.1 to 10.6 GHz. The initial design variables of $\boldsymbol{R}_{s.cell}(\boldsymbol{y})$ are: $\boldsymbol{y} = [0.2\ 1\ 0.2\ 4\ 0.2]^T$, while vector $\boldsymbol{P}$ is set to 0. The final design, $\boldsymbol{x} = [3.0\ 0.5\ 0.4\ 0.997\ 0.15\ 4.58\ 0.45\ 0.33\ 0.175\ 0.16\ 4.37\ 0.198\ 0.15\ 0.15\ 0.15]^T$ [Figure 5.6(b)], is obtained after three iterations of NSM ($|S_{11}| \leq -14.7$ dB for 3.1 to 10.6 GHz).

The same C-shaped model is used for the design of a 50-to-130-Ohm MT (iv) desired to work in the 1 to 3.5 GHz band. Initial vector of $\boldsymbol{R}_{s.cell}(\boldsymbol{y})$ design parameters is: $\boldsymbol{y} = [0.5\ 1\ 0.2\ 10\ 0.2]^T$ and all SM perturbations $\boldsymbol{P}$ are set to 0. The optimized design, $\boldsymbol{x} = [10.0\ 0.3\ 0.5\ 1.21\ 0.177\ 8.98\ 0.3\ 0.19\ 1.5\ 0.20\ 10.0\ 0.3\ 0.15\ 0.97\ 0.15]^T$, Figure 5.6(b), is obtained after three iterations of NSM ($|S_{11}| \leq -17.0$ dB for 1.0 GHz to 3.5 GHz).

5.3.3 Comparison with Benchmark Methods

The computational efficiency of NSM is compared with implicit space mapping [3] and sequential space mapping [5], previously used for CMRC structure design. The proposed technique results in the smallest number iterations necessary to yield an optimized geometry (see Table 5.1) for all considered cases. The overall design cost, including high- and low-fidelity model simulations, is given in square brackets of Table 5.1. Additionally, a comparison with direct optimization of the EM transformer model is included (here, using pattern search) to show that the latter method is virtually impractical for the design of complex MTs.

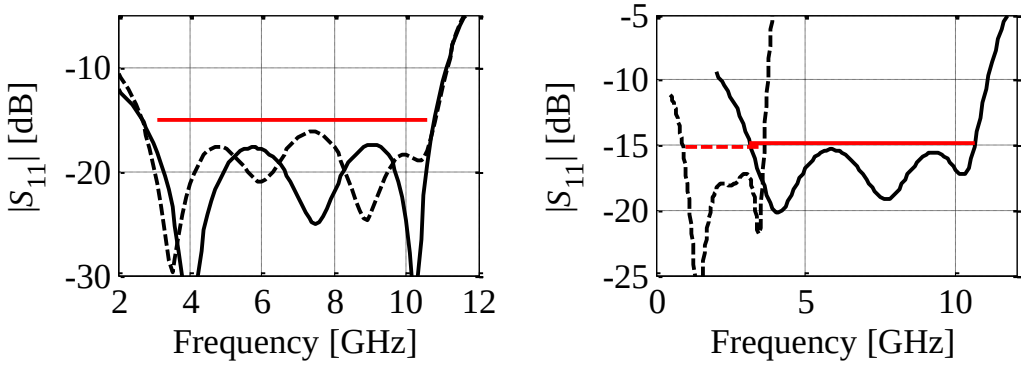

Figure 5.6: Reflection responses of the optimized MTs: (a) double-T CMRCs (i) (—), and (ii) (- - -); (b) C-shaped CMRCs (iii) (—), and (iv) (- - -).

TABLE 5.1: DESIGN OPTIMIZATION COST

SBO method	Design Cost (number of EM simulations)			
	MT (i)	MT (ii)	MT (iii)	MT (iv)
This work	2 [3.2]$^{+}$	3 [3.8]$^{+}$	3 [4.2]$^{+}$	3 [4.1]$^{+}$
Implicit SM [3]	8 [9.9]$^{\$}$	9 [12.1]$^{\$}$	10$^{\#}$ [13.7]$^{\$}$	7 [10]$^{\$}$
Sequential SM [5]	7 [8.2]$^{\$}$	10$^{\#}$ [11.7]$^{\$}$	8 [10.4]$^{\$}$	6 [7.3]$^{\$}$
Direct Search	406	500*	500*	520

$^{\#}$ The algorithm started diverging and was terminated after 10 iterations
* The algorithm failed to find a geometry satisfying performance specifications
$^{+}$ Including the inner SM layer cost (note: this cost would not be taken into account in practical situations where inner-SM-corrected cell models are treated as multiple-use library models
$^{\$}$ Includes the cost of parameter extraction and low-fidelity model refinement

5.4 Conclusion

In this work, a nested SM optimization technique is presented. The advantage of our approach lies in setting up a globally accurate surrogate model, which significantly decreases the overall design cost, reduces the number of extractable surrogate model parameters, and makes the optimization process more robust. NSM is validated using several test cases, resulting in average optimization cost of three iterations, which is a significant speedup compared to competitive surrogate-based methods.

References

[1] C.-H. Tseng and H.-J. Chen, "Compact Rat-Race Coupler Using Shunt-Stub-Based Artificial Transmission Lines," *IEEE Microw. Wireless Comp. Lett.*, vol. 18, no. 11, pp. 734-736, 2008.

[2] H.-W. Wu, S.-H. Huang, and Y.-F. Chen, "Design of New Quad-Channel Diplexer With Compact Circuit Size," *IEEE Microw. Wireless Comp. Lett.*, vol. 23, no. 5, pp. 240-242, 2013.

[3] J.W. Bandler, Q.S. Cheng, S.A. Dakroury, A.S. Mohamed, M.H. Bakr, K. Madsen, and J. Søndergaard, "Space mapping: the state of the art," *IEEE Trans. Microw. Theory Techn.*, vol. 52, no. 1, pp. 337-361, 2004.

[4] S. Koziel, J.W. Bandler, and K. Madsen, "Quality assessment of coarse models and surrogates for space mapping optimization," *Opt. Eng.*, vol. 9, no. 4, pp. 375-391, 2008.

[5] A. Bekasiewicz, P. Kurgan, and M. Kitlinski, "New approach to a fast and accurate design of microwave circuits with complex topologies," *IET Microw. Ant. Prop.*, vol. 6, no. 14, pp. 1616-1622, 2012.

[6] P. Kurgan and A. Bekasiewicz, "A robust design of a numerically demanding t rat-race coupler," *Microw. Opt. Tech. Lett.*, vol. 56, no. 5, pp. 1259–1263, 2014.

[7] S. Koziel, L. Leifsson, and X.S. Yang, "Surrogate-based optimization," S. Koziel, X.S. Yang, Q.J. Zhang (Eds.) *Simulation-Driven Design Optimization and Modeling for Microwave Engineering*, Imperial College Press, pp. 41-80, 2012.

[8] CST Microwave Studio, ver. 2013, CST AG, Bad Nauheimer Str. 19, D-64289 Darmstadt, Germany, 2013.

[9] Agilent ADS, ver. 2011.10, Agilent Technologies, 1400 Fountaingrove Parkway, Santa Rosa, CA 95403-1799, 2011.

6 EM-Driven Design and Surrogate-Assisted Fine-Tuning of Compact Hybrid Couplers

***

P. Kurgan and S. Koziel

Fast Surrogate-Assisted Simulation-Driven Optimization of Compact Microwave Hybrid Couplers

Published in: *Engineering Optimization*, vol. 48, no. 7, pp. 1109–1120, 2015.

DOI: 10.1080/0305215X.2015.1097098

***

Abstract: This work presents a robust methodology for expedited simulation-driven design optimization of compact microwave hybrid couplers. The technique relies on problem decomposition, and a bottom-up design strategy, starting from the level of basic building blocks of the coupler, and finishing with a tuning procedure that exploits a fast surrogate model of the entire structure. The latter is constructed by cascading local response surface approximations of coupler elementary elements. The cross-coupling effects within the structure are neglected in the first stage of the design process; however, they are accounted for in the tuning phase by means of space-mapping correction of the surrogate. The proposed approach is demonstrated through the design of a compact rat-race and two branch-line couplers. In all cases, the computational cost of the optimization process is very low and corresponds to just a few high-fidelity electromagnetic simulations of respective structures. Experimental validation is also provided.

6.1 Introduction

Hybrid directional couplers are essential building blocks implemented in numerous balanced-type applications of contemporary microwave engineering, such as balanced mixers or amplifiers [1]. Typical examples of equal-split couplers include branch-line couplers (BLCs) [2], and rat-race couplers (RRCs) [3]. These offer an equal power division between the output ports with a given phase shift—90° in the former case, and 0° or 180° in the latter. Unfortunately, this desired behavior can be obtained only at the center frequency of the operational bandwidth, in the vicinity of which the ideal performance is merely approximated. The narrowband character of these hybrids results from their modular architecture, primarily based on quarter-wavelength uniform transmission lines (UTLs). This, in turn, leads to excessively large layouts, usually violating the design guidelines of space-limited applications. To address this issue, many researchers focus on finding alternative realizations of microwave components with a non-deteriorated functionality and small-size footprints [4]. Most commonly, this is done through composite transmission lines featuring a slow-wave effect. Although constructing microwave couplers with abbreviated composite lines may offer circuit miniaturization, it also increases numerical complexity of the design problem to the point where the application of approximated theoretical analysis is no longer valid [5]. The intricate layouts of compact circuits may be accurately evaluated only by means of high-fidelity electromagnetic (EM) simulations. These, however, are extremely CPU-intensive, which is a serious bottleneck for design approaches that rely heavily on them [6]. A possible solution to this problem is surrogate-based optimization (SBO), in which a direct treatment of an expensive high-fidelity model is replaced by a sequence of optimization tasks that involve an iteratively corrected (using sparse high-fidelity simulation data) low-fidelity model [7]. This leads to a dramatic reduction in the computational cost of the optimization process [8]. Probably the most recognized SBO technique in contemporary microwave engineering is space mapping (SM) [9]. This method often requires fast and well-aligned equivalent circuit models, which are typically not available for compact circuits [10]. Such models usually exhibit poor generalization and susceptibility to non-unique results of the parameter extraction process, both hindering the effectiveness of SM applied to the given problem [11].

In this work, a methodology for a reliable and rapid design optimization of computationally expensive compact microwave couplers is presented. A modular architecture of these devices allows for problem decomposition, and expedited EM optimization of their individual building blocks. This is done at a low CPU cost compared to a single EM simulation of the entire coupler. Subsequently, SBO is used to compensate for cross-coupling effects between the adjacent elements that compose the device. The tuning is realized with the underlying surrogate built from response surface approximations (RSAs) of optimized coupler elements, and SM for model correction. The proposed approach is demonstrated by three design examples. Final solutions are obtained at a low computational cost, and occupy only a fraction of the initial area, while illustrating a perfect performance.

6.2 Surrogate-Assisted Coupler Design

In this section, the design optimization approach is described, including optimization of the coupler building blocks, construction of the RSA models and surrogate-assisted tuning of the entire device.

6.2.1 General Design Scheme Overview

The main challenge of a reliable simulation-driven design of compact couplers is the CPU cost associated with their high-fidelity EM analysis (typical simulation times varies from dozens of minutes to several hours per design, depending on the complexity [10]). On the other hand, an accurate EM simulation of coupler building blocks can be performed at a low computational cost (in practice, this corresponds to two to three orders of magnitude less than a single high-fidelity EM analysis of the entire coupler). In this article, this is exploited by

finding optimized geometries of the detached slow-wave cells, i.e., constitutive elements of the coupler under design. By doing so, perfect coupler performance is obtained, assuming a lack of interactions between its building blocks and the phase shifts introduced by the T-junctions that connect the cells within the coupler. In practice, however, these assumptions do not hold and the transmission characteristics of the coupler are degraded for the geometry parameter values obtained as above. To address this issue, a surrogate-assisted coupler fine-tuning is performed with the underlying low-fidelity model constructed from cascaded local RSAs of the optimized slow-wave cells. In general, this is an iterative process; however, as demonstrated by the case studies (cf. Section 6.3), one iteration is normally sufficient. One should note that the key advantage of the proposed approach lies in the ability to arrive at the optimized design within a single and fully automated process at the CPU cost equivalent to less than a few EM evaluations of the entire coupler (the coupler itself is simulated only at the tuning stage, i.e., at the initial design produced by cell optimization, and for the verification of the fine-tuning result).

6.2.2 Cell Optimization

Slow-wave cells are vital microwave components commonly used for the development of small-size couplers. Numerous examples of slow-wave cells can be found in the literature [4]. In general, compact couplers can be composed of more than one cell. Thus, two different approaches to cell optimization are considered here, i.e., sequential and concurrent.

6.2.2.1 Sequential Cell Optimization

The cells are optimized to satisfy certain design requirements, i.e., to obtain a required phase shift ϕ_c, $\arg(S_{21})$, at the operating frequency f_0, as well as to minimize the return loss $|S_{11}|$ at f_0 and around it. The task is formulated as

$$\boldsymbol{x}_c^* = \arg\min_{\boldsymbol{x}} U(\boldsymbol{x}) \tag{6.1}$$

where $U(\boldsymbol{x})$ is the objective function given by

$$U(\boldsymbol{x}) = \left\{ \max_{f_0 - df \le f \le f_0 + df} \left|S_{11}(\boldsymbol{x}; f)\right| + \beta \cdot \left[\arg\left(S_{21}(\boldsymbol{x}; f_0)\right) - \phi_c\right]^2 \right\} \tag{6.2}$$

Here, $\boldsymbol{x}$ is a vector of geometry parameters of the element under design. The electrical performance pertaining to a given cell depends on the dimensions (lengths and widths) of stripes and slots that constitute the cell. The components of the vector $\boldsymbol{x}$ are all relevant dimensions of a given cell. The primary objective is to reduce the so-called return loss $|S_{11}|$ over a specific frequency band. In (6.2), $S_{11}(\boldsymbol{x};f)$ and $S_{21}(\boldsymbol{x};f)$ denote explicit dependence of S-parameters on frequency. Thus, the first component of (6.2) is the maximum value of $|S_{11}|$ in the frequency range $f_0 - df$ to $f_0 + df$. In other words, the process (6.1) aims at minimizing $|S_{11}|$ in the vicinity of f_0 (in practice, the three frequency points: $f_0 - df$, f_0, and $f_0 + df$ are utilized). The second term in (6.2) is a penalty function, with β being a penalty factor. It aims at forcing $\arg(S_{21})$ to the required phase shift ϕ_c. The value of β is set to ensure that even a small violation of the phase requirement results in a meaningful contribution to the penalty function. Here, for $\beta = 10^4$, deviation of $\arg(S_{21})$ from ϕ_c by 0.01 degree results in the penalty function value of 1, which is a few percent of the primary cost function value; for deviation by 0.1 degree, the penalty function becomes a dominant component of U. Thus, formulation (6.2) allows for obtaining the required phase shift with good accuracy.

The problem (6.1) is solved using a pattern search algorithm [12]. The optimization process (6.1) is done sequentially, i.e., it is repeated for each type of elementary cell of a coupler under design.

6.2.2.2 Concurrent Cell Optimization

Another approach to cell optimization assumes that the specific building blocks of a compact coupler under development are physically complementary, meaning that some of their geometry parameters are interdependent to ensure tight fit of the cells inside the target structure. The aforementioned dependence can be formally expressed as $\boldsymbol{x}_1 = f_1(\boldsymbol{x})$, $\boldsymbol{x}_2 = f_2(\boldsymbol{x})$, …, $\boldsymbol{x}_i = f_i(\boldsymbol{x})$, where $\boldsymbol{x}$ is a composite vector of all geometry parameters, and $\boldsymbol{x}_i$, $i = 1, 2, \ldots$, is a vector of geometry parameters pertaining to the ith slow-wave cell. In practice, f_i may be a projection, in which case $\boldsymbol{x}_i$ contains selected components of the vector $\boldsymbol{x}$; otherwise, it is composed of both independent geometry parameters of a given cell, and geometry constraints that ensure layout consistency. Specific realizations of such functions are provided in Section 6.3.3.

For the purpose of concurrent cell optimization, a different formulation of the objective function $U(\boldsymbol{x})$ of (6.2) is used. Here, $U(\boldsymbol{x})$ is the aggregated cost function, whose value depends on the given design specifications and response vectors pertaining to high-fidelity models of all slow-wave cells involved in the design process, $R_i(\boldsymbol{x}_i)$. Note that all high-fidelity EM models—evaluated during each iteration of the optimization algorithm—include only internal EM effects present within each cell, and neglect cross-coupling phenomena between them to keep the cost of the corresponding EM analysis low. The aggregated objective function for concurrent optimization of two complementary cells is defined as

$$U(\boldsymbol{x}) = \max_{f_0 - df \le f \le f_0 + df} \left\{ \left| S_{11.1}(\boldsymbol{x}_1; f) \right|, \left| S_{11.2}(\boldsymbol{x}_2; f) \right| \right\} + \beta \sum_{i=1}^{2} \left[\arg\left(S_{21.i}(\boldsymbol{x}_i; f_0) \right) - \phi_c \right]^2 \qquad (6.3)$$

Analogically to (6.2), $S_{11.i}(\boldsymbol{x};f)$ and $S_{21.i}(\boldsymbol{x};f)$ denote explicit dependence of S-parameters on frequency for the ith cell. Parameters β and ϕ_c are defined exactly as in Section 6.2.2.1.

6.2.3 Response Surface Approximation Models

The local RSA model of the cell, utilized in the tuning process (cf. Section 6.2.4), is constructed in the vicinity of its optimized design, $\boldsymbol{x}_c^*$, defined as $[\boldsymbol{x}_c^* - d\boldsymbol{x}, \boldsymbol{x}_c^* + d\boldsymbol{x}]$. The model uses $2n + 1$ ($n = \dim(\boldsymbol{x})$) EM simulations of the cell at $\boldsymbol{x}_c^{(0)} = \boldsymbol{x}_c^*$ and at the perturbed designs $\boldsymbol{x}_c^{(k)} = [\boldsymbol{x}_{c.1}^* \ldots x_{c.\lceil k/2 \rceil}^* + (-1)^k dx_{.\lceil k/2 \rceil} \ldots x_{c.n}^*]^T$, $k = 1, \ldots, 2n$, where $x_{c.k}^*$ and dx_k are kth components of the vectors $\boldsymbol{x}_c^*$ and $d\boldsymbol{x}$, respectively. The RSA model $\boldsymbol{R}_c(\boldsymbol{x})$ of the cell is a simple second-order polynomial without mixed terms:

$$\boldsymbol{R}_c(\boldsymbol{x}) = c_0 + \sum_{k=1}^{n} c_k x_k + \sum_{k=1}^{n} c_{n+k} x_k^2 \qquad (6.4)$$

with the parameters identified as least-square solution to the linear regression problem $\boldsymbol{R}_c(\boldsymbol{x}_c^{(k)}) = \boldsymbol{R}_f(\boldsymbol{x}_c^{(k)})$, $k = 0, 1, \ldots, 2n$, where $\boldsymbol{R}_f$ denotes the high-fidelity (fine) EM model of the cell. The above process is repeated for each type of the elementary cell present in the coupler. The RSA model $\boldsymbol{R}_c$ of the entire structure is subsequently constructed by cascading the RSA cell models using ABCD matrix representation.

The truncated form of the polynomial model is chosen here primarily because of the small number of the training points required for its setup (increasing linearly with the design space dimension), as opposed to the models with cross-terms that scale with a polynomial rate (equal to the polynomial order).

6.2.4 Surrogate-Assisted Design Refinement

To account for EM couplings between the cells, as well as other phenomena, e.g., T-junction phase shifts, final tuning of the coupler is required. The tuning procedure is realized as SBO process:

$$\boldsymbol{x}^{(i+1)} = \arg\min_{\boldsymbol{x}} H\left(\boldsymbol{R}_s^{(i)}(\boldsymbol{x}) \right) \qquad (6.5)$$

The vectors $\boldsymbol{x}^{(i)}$, i = 0, 1, …, approximate the solution to the coupler design problem $\boldsymbol{x}^* = \text{argmin}\{\boldsymbol{x} : H(\boldsymbol{R}_f(\boldsymbol{x}))\}$ (H encodes design specifications for the coupler), whereas $\boldsymbol{R}_s^{(i)}$ is the surrogate model at iteration i. $\boldsymbol{R}_s^{(i)}$ is constructed from the RSA model $\boldsymbol{R}_c$ using input SM [8]:

$$\boldsymbol{R}_s^{(i)}(\boldsymbol{x}) = \boldsymbol{R}_c\left(\boldsymbol{x} + \boldsymbol{q}^{(i)}\right) \tag{6.6}$$

where $\boldsymbol{q}^{(i)}$ is the input SM shift vector obtained using the usual parameter extraction procedure of the form

$$\boldsymbol{q}^{(i)} = \text{argmin}\left\{\boldsymbol{q} : \left\|\boldsymbol{R}_f\left(\boldsymbol{x}^{(i)}\right) - \boldsymbol{R}_c\left(\boldsymbol{x}^{(i)} + \boldsymbol{q}\right)\right\|\right\} \tag{6.7}$$

that aims at reduction of misalignment between $\boldsymbol{R}_c$ and the EM coupler model $\boldsymbol{R}_f$. Note that the high-fidelity model $\boldsymbol{R}_f$ is not evaluated until the tuning stage. In practice, a single iteration (6.5) is sufficient. The overall cost of the coupler design process is therefore very low and usually corresponds to a few simulations of the entire coupler including cell optimization and construction of the RSA models.

6.3 Case Studies

In this section, the methodology of Section 6.2 is showcased using the most popular equal-split couplers, namely, RRCs and BLCs. In each case, a compact coupler is constructed as a deviation from a classic design solution. A conventional RRC, shown in Figure 6.1(a), comprises six quarter-wavelength UTLs of $\sqrt{2}\cdot Z_0$ impedances, where Z_0 is the system impedance [1]. Hence, the cell optimization stage of the proposed method aims at reaching only one cell solution. On the other hand, a conventional BLC [Figure 6.1(b)] is built from four quarter-wavelength UTLs, but described by two different impedances, i.e., Z_0 and $Z_0/\sqrt{2}$. Thus, one deals here with the optimization problem of two separate cells. It is worth noting that exact definitions of coupler elements in Figure 6.1 determine a perfect performance of the respective components at the center frequency, i.e., an equal power division between output ports 2 and 3, infinite isolation at port 4, and perfect matching at port 1 [2]. For all design cases, the high-fidelity EM models have been implemented in Sonnet ***em*** using a 0.025 mm × 0.025 mm grid setup [13], and simulated on a personal computer with 8-core Intel Xeon 2.5 GHz processor and 6 GB RAM.

6.3.1 Rat-Race Coupler Design

The task here is to perform design optimization of a compact RRC. A Taconic RF-35 dielectric substrate (ε_r = 3.5, h = 0.762 mm) is selected for the physical realization (Z_0 = 50 Ω). The circuit is assumed to work over a 20% fractional bandwidth defined for the return loss and isolation $|S_{11}|$, $|S_{41}| \le -20$ dB, with an equal power split ($|S_{21}| = |S_{31}|$) at f_0 = 1 GHz center frequency. For comparison purposes, a conventional RRC is also designed according to the theoretical solution of Figure 6.1(a). Its exterior dimensions are: 47.7 mm × 96 mm.

The above requirements can be translated into design specifications pertaining to the basic building block of a compact RRC. Thus, the objective of the first stage of the design process is to find the best layout of a slow-wave cell that offers a –90° phase shift, ϕ_c, at f_0, and $|S_{11}| \le -20$ dB over the operational bandwidth, when terminated with 70.7-Ω ports. The specific realization of the slow-wave cell is shown in Figure 6.2(a). It is described by a vector of six designable parameters $\boldsymbol{x}_c = [x_1\ x_2\ x_3\ x_4\ x_5\ x_6]^T$. Cell optimization is executed as given in Section 6.2.2.1. Starting from the initial design solution, $\boldsymbol{x}_c^{(0)}$, the task aims at minimizing the return loss $|S_{11}|$ in the neighborhood of f_0, more precisely at 0.9 GHz, 1 GHz, and 1.1 GHz, which covers the entire operational bandwidth. The penalty function (6.2) is used to arrive at the final result, $\boldsymbol{x}_c^*$, for the specified phase shift $\phi_c = -90°$ at 1 GHz. Next, an RSA model of the optimized cell is developed, as described in Section 6.2.3. It is subsequently used to assemble an RRC surrogate for the purpose of circuit fine-tuning and cross-coupling compensation (coupling between the adjacent cells is neglected in the first stage of the design process). This procedure, realized according to Section 6.2.4, returns the final design solution, $\boldsymbol{x}^*$, after a single iteration.

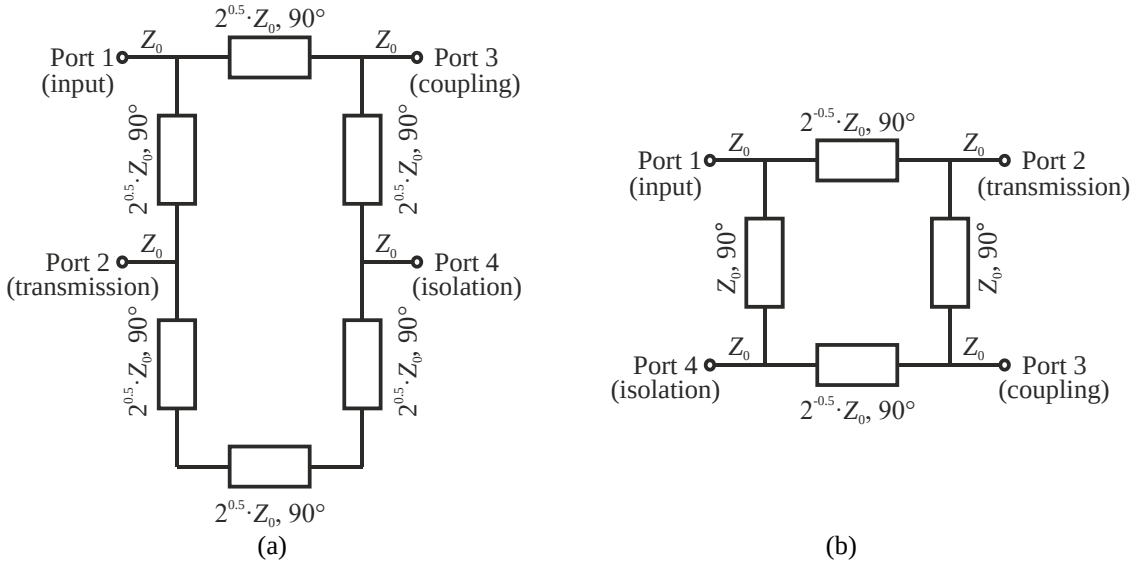

Figure 6.1: Typical hybrids: (a) rat-race coupler and (b) branch-line coupler.

The lower/upper bounds ***l***/***u*** of designable parameters, as well as the initial and final design solutions for each design step are listed in Table 6.1. The EM analysis of the entire structure at $\boldsymbol{x}_c^*$ shows a 5-MHz alteration of the center frequency, due to neglecting of cross-coupling and T-junction phase effects in the assembled RSA model of the given coupler. This is successfully fine-tuned, resulting in a compact RRC with an ideal performance as shown in Figure 6.2(b). The entire design process is negligible CPU-wise when compared to excessive computational expenses of classical EM-based optimization methods. Here, the total design cost is about 25 hours, which corresponds to less than three high-fidelity EM analyses of the compact RRC. The overall cost can be broken down into the following components: slow-wave cell optimization (80 EM cell simulations at three frequencies, ~164 min of CPU time), RSA model construction (13 EM cell simulations with adaptive frequency sweep, ~89 min), and two EM analyses of the entire RRC (at $\boldsymbol{x}_c^*$ and at $\boldsymbol{x}^*$, ~1280 min; adaptive frequency sweep, 10 frequencies per simulation). The estimated cost of direct optimization exploiting a high-fidelity EM model of the compact RRC is approximately 100 EM simulations of the structure at hand (>1000 hours of CPU time).

To validate theoretical predictions, the final design has been fabricated and measured. Experimental characteristics, included in Figure 6.2(b), are slightly degraded in comparison to the performance of the high-fidelity EM model. This can be attributed to the idealized nature of conducted simulations, where the fabrication tolerances, the substrate anisotropy or the influence of SMA connectors have not been involved. The exterior dimensions of the final design are 21.5 mm × 37.9 mm, which is only 17.8% of the substrate area dedicated for the conventional circuit.

Table 6.2 shows a comprehensive comparison of the compact RRC presented in this article, with state-of-the-art designs from the literature. Based on two figures of merit, i.e., the fractional bandwidth, and miniaturization, one can see that the fabricated RRC presented here offers a broader operational bandwidth with comparable or superior miniaturization than competitive results. The only exception is the structure proposed in [16], which stands out as the smallest RRC in the literature. However, the performance of this coupler is far from ideal, especially in terms of $|S_{21}|$ and $|S_{31}|$, which can be attributed to the lack of EM design closure of the structure of interest.

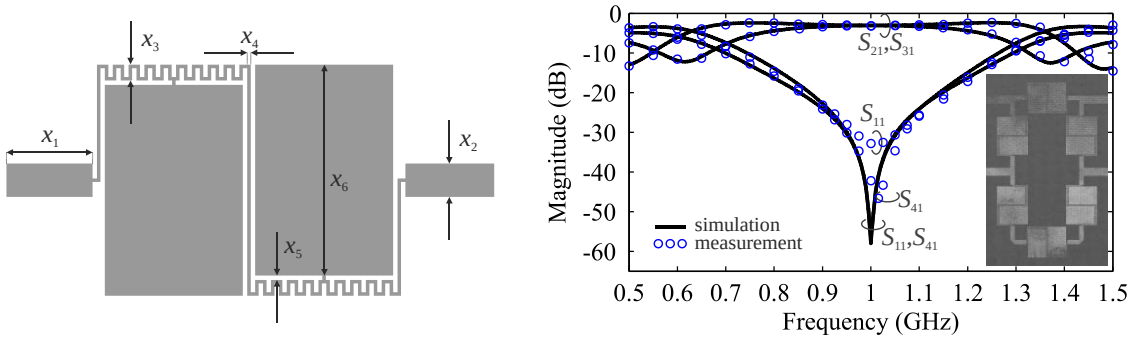

(a) (b)

Figure 6.2: Design case no. 1: (a) Parameterized layout of the composite cell proposed in [5]; Simulated (—) vs. measured (○) frequency characteristics of the compact rat-race coupler.

TABLE 6.1: DESIGN CASE NO. 1: DESIGN BOUNDS AND SOLUTIONS (ALL DIMENSIONS IN MM)

	x_1	x_2	x_3	x_4	x_5	x_6
$\boldsymbol{l}$	0.1	0.8	0.2	0.1	0.1	1
$\boldsymbol{u}$	3	1.1	2	0.5	0.5	8
$\boldsymbol{x}_c^{(0)}$	1	0.95	0.4	0.1	0.1	5
$\boldsymbol{x}_c^*$	2.15	0.95	0.275	0.1	0.125	6.275
$\boldsymbol{x}^*$	2.225	0.95	0.45	0.1	0.125	6.1

TABLE 6.2: DESIGN CASE NO. 1: COMPARISON OF COMPACT RRCS: BANDWIDTH (BW), ELECTRICAL SIZE AND MINIATURIZATION

Reference	BW[a] (%)	Electrical size ($\lambda_g \times \lambda_g$)	Miniaturization[b] (%)
Conventional	26	0.26 × 0.52	none
[14]	19.7	0.26 × 0.26	50
[15]	9.6	0.22 × 0.22	64.2
[16]	29.1	0.07 × 0.13	93.3
[17]	6.4	0.08 × 0.09	94.7
[18]	18.5	0.11 × 0.20	83.7
[19]	9.5	0.13 × 0.23	77.9
[20]	16.8	0.14 × 0.14	85.5
[21]	7.5	0.24 × 0.25	55.6
[22]	17.2	0.19 × 0.19	73.3
This work	27.2	0.12 × 0. 20	82.2

[a] Bandwidth is defined as a symmetrical intersection of $|S_{11}|$ and $|S_{41}| \leq -20$ dB
[b] Miniaturization is computed based on the electrical size of a conventional RRC of this work

6.3.2 Branch-Line Coupler Design with Sequential Cell Optimization

The goal is to design a compact BLC following the methodology of Section 6.2. A Taconic RF-35 dielectric substrate (ε_r = 3.5, h = 0.508 mm) is chosen for circuit implementation with Z_0 = 50-Ω ports. The design specification is: center frequency f_0 = 1 GHz, $|S_{11}|$, $|S_{41}| \leq -20$ dB for 0.96 GHz to 1.04 GHz (this corresponds to an 8% fractional bandwidth), and an equal power division ($|S_{21}| = |S_{31}|$) at f_0. For the sake of size comparison, a conventional BLC is designed using the above criteria. The area of this component is 45.65 mm × 48.15 mm.

As given in Figure 6.1(b), the first stage of the design process is aimed at obtaining the best layouts of slow-wave cells that illustrate a –90° phase shift, ϕ_c, at f_0, and $|S_{11}| \leq -20$ dB within the prescribed frequency range when loaded with 35.36-Ω and 50-Ω resistances, respectively. The specific implementation of the cells is presented in Figure 6.3(a). Each structure is described by seven designable parameters: $\boldsymbol{x}_{ci} = [x_1\ x_2\ x_3\ x_4\ x_5\ x_6\ x_7]^T$, where i is the index of the respective element. In the given example, cell optimization is performed sequentially, with the upper bounds of Cell_2 adjusted to prevent layout overlapping (see Section 6.2.2.1). Starting from the respective initial design, $\boldsymbol{x}_{ci}^{(0)}$, each cell is optimized individually to reach the minimal

return loss in the vicinity of f_0, having in mind that Cell_1 and Cell_2 are terminated with 35.36 Ω and 50 Ω, respectively. The objective function is computed at three frequency points around f_0 with df = 40 MHz, which covers the entire operational bandwidth. Having obtained the final results of Cell_1, $\boldsymbol{x}_{c1}^*$, the upper bounds for Cell_2 parameters are limited to $\boldsymbol{u}_{c2}^{limit}$ as a precautionary measure for possible layout overlapping. The final optimization results of Cell_2 are given by $\boldsymbol{x}_{c2}^*$. Next, RSA models are developed in the vicinity of previously optimized designs. These are subsequently combined into a fast model of the entire BLC, whose SM-enhanced version is later exploited as the underlying surrogate for the SBO-like fine-tuning procedure. Note that the $\boldsymbol{x}_{c1}^*$ and $\boldsymbol{x}_{c2}^*$ coupler design solution requires compensating for interactions between the adjacent cells, as its EM simulation shows a ~15-MHz deviation from ideal BLC characteristics. However, after only one cycle of the tuning procedure, the final structure of $\boldsymbol{x}_1^*$ and $\boldsymbol{x}_2^*$ demonstrates perfect frequency characteristics, as shown in Figure 6.4(a), while occupying a 16.25 mm × 16.95 mm area, which translates into 12.4% of the conventional coupler size. The measurement results, included in Figure 6.4(a) for validation purposes, are in agreement with simulated characteristics, with minor discrepancies caused by a simplified setup of simulations (e.g., lack of SMA connectors, smooth metallization). A complete list of results is gathered in Table 6.3.

The entire design procedure has been conducted within a low computational budget of ~526 min, which translates into ~4.8 high-fidelity EM evaluations of the entire compact BLC. The detailed breakdown of this process is as follows: sequential slow-wave cell optimization takes ~216 min (every cell needs 120 EM simulations at three frequency points each), RSA model construction requires ~90 min (in total 30 EM simulations with adaptive frequency sweep), and two EM evaluations of the entire BLC take 220 min. In comparison to the estimated cost of direct EM optimization (>400 hours of CPU time), the proposed design method provides reliable results about 50 times faster.

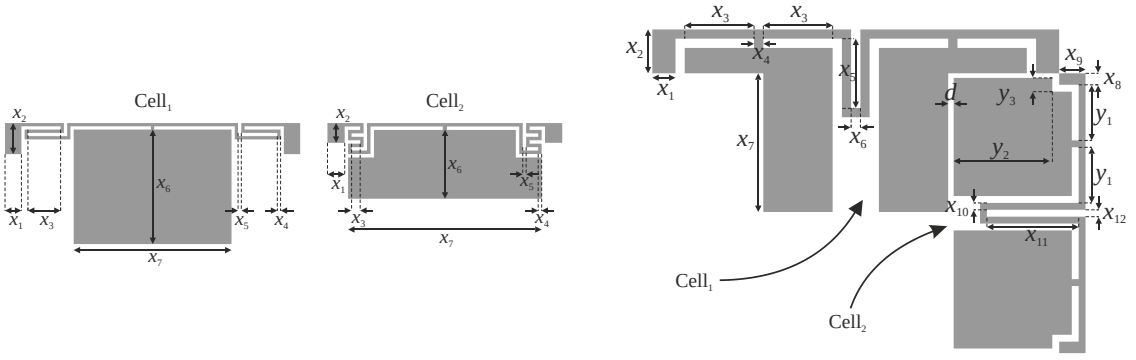

(a) (b)

Figure 6.3: Parameterized layouts of composite cells, where Cell_1 and Cell_2 are 35.36-Ω and 50-Ω cells, respectively: (a) design case no. 2; (b) design case no. 3.

TABLE 6.3: DESIGN CASE NO. 2: DESIGN BOUNDS AND SOLUTIONS (ALL DIMENSIONS IN MM)

	x_1	x_2	x_3	x_4	x_5	x_6	x_7
$\boldsymbol{l}_{c1}$	0.1	1.8	0.1	0.1	0.1	1	5
$\boldsymbol{u}_{c1}$	3	2	3	0.5	0.5	10	15
$\boldsymbol{l}_{c2}$	0.1	1	0.1	0.1	0.1	1	5
$\boldsymbol{u}_{c2}^{init.}$	3	1.3	3	0.5	0.5	10	15
$\boldsymbol{u}_{c2}^{limit.}$	3	1.3	3	0.45	0.45	4	15
$\boldsymbol{x}_{c1}^{(0)}$	1	1.9	1	0.2	0.2	10	8
$\boldsymbol{x}_{c2}^{(0)}$	1	1.15	2	0.2	0.2	3.55	15
$\boldsymbol{x}_{c1}^*$	0.225	1.9	2	0.2	0.175	7.975	6.95
$\boldsymbol{x}_{c2}^*$	0.925	1.15	1.1	0.2	0.375	3.9	11.35
$\boldsymbol{x}_1^*$	0.6	1.9	1.95	0.2	0.15	7.925	6.7
$\boldsymbol{x}_2^*$	0.5	1.15	1.125	0.2	0.325	3.85	11.5

6.3.3 Branch-Line Coupler Design with Concurrent Cell Optimization

In the previous case study, the constitutive elements of the compact BLC have been optimized sequentially using suitably selected upper bounds for the second structure to avoid layout overlapping. In many practical instances, this approach can reduce the design space to the point where no desirable solution can be found. To address this issue, concurrent optimization of the slow-wave cells is carried out in the present case study. This way, the lower and upper bounds of designable parameters may be sufficiently large, so that the target solution is located inside the design space pertaining to each cell. Moreover, geometrical dependence of the selected designable parameters is used as a precautionary measure against layout conflicts and to ensure a high compression of the layout.

The main task here is to find an optimized design solution of a compact BLC that satisfies design specifications defined in Section 6.3.2, using complementary slow-wave cells of Figure 6.3(b). Note that these slow-wave cells are arranged according to their intended placement in the target BLC. The geometry of Cell_1 and Cell_2 is defined by vectors $\boldsymbol{x}_1 = [x_1\ x_2\ x_3\ x_4\ x_5\ x_6\ x_7]^T$ and $\boldsymbol{x}_2 = [x_8\ x_9\ x_{10}\ x_{11}\ x_{12}\ y_1\ y_2\ y_3]^T$, respectively. All parameters $x_1 – x_{12}$ are independent, whereas parameters $y_1 – y_3$ depend on specific elements of vector $\boldsymbol{x}_1$ as well as the parameter d, which represents a predefined distance between the cells. In this example, geometry constraints put on Cell_2 to force its good fit into a compact layout of the coupler under design are as follows: $y_1 = 0.5\cdot(x_7 + d/2 – x_8 – 2\cdot x_{10} – 2.5\cdot x_{12})$, $y_2 = x_1 + x_3 + x_4 + x_6 – d – x_{12}$ and $y_3 = x_8 + x_{12} – d$, where d is set to 0.2 mm. Concurrent cell optimization is executed according to Section 6.2.2.2. Starting from $\boldsymbol{x}_c^{(0)}$, the optimization process reaches final design solution $\boldsymbol{x}_c^*$. The latter corresponds to the constrained optima for individual cells as follows: $f_1(\boldsymbol{x}_c^*) = [0.375\ 1.9\ 3.35\ 0.225\ 1.55\ 0.125\ 8.05]^T$ mm and $f_2(\boldsymbol{x}_c^*) = [0.375\ 1.15\ 0.1\ 0.35\ 1\ 3.65\ 2.875\ 0.95]^T$ mm. Despite perfect frequency characteristics of the optimized cells, the initial BLC design of the fine-tuning stage, given by $\boldsymbol{x}^{(0)} = \boldsymbol{x}_c^*$, shows a ~25-MHz shift in the return loss and isolation. Again, this deterioration is caused by T-junction and cross-coupling effects that are neglected at the initial design stage. One can observe that the after-tuning BLC design solution, described as $f_1(\boldsymbol{x}^*) = [0.475\ 1.9\ 3.25\ 0.225\ 1.5\ 0.125\ 8.05]^T$ mm and $f_2(\boldsymbol{x}^*) = [0.125\ 1.15\ 0.125\ 0.375\ 0.95\ 2.7\ 2.925\ 0.875]^T$ mm, shows the desired transmission characteristics as presented in Figure 6.4(b). The final circuit consumes a 17.78 mm × 20.1 mm layout area, which corresponds to only 16.3% of the dielectric substrate needed for accommodating a conventional BLC designed for the same specifications and operating frequency. The measurement characteristics of the fabricated BLC, included in Figure 6.4(b) for the validation of numerical result, are comparable to the performance of the simulated BLC, where minor discrepancies are probably due to the lack of metal surface roughness and dielectric anisotropy in EM simulation, as well as geometrical differences (fabrication tolerance) between the EM model and the prototype. The detailed results of the design process are summarized in Table 6.4.

The entire procedure has been carried out rapidly at the CPU cost corresponding to about 4.4 high-fidelity EM analyses of the final BLC. In detail, concurrent cell optimization takes ~150 minutes (200 evaluations at three frequency points), the construction of RSA models lasts ~63 minutes (25 evaluations at 10 frequencies), and the evaluation of the entire compact coupler takes ~180 minutes (2 EM simulations, i.e., at the initial and final designs of the tuning phase). One should bear in mind that direct optimization would require several hundred such evaluations, which is virtually infeasible.

Additionally, compact BLCs of Section 6.3.2 and 6.3.3 are compared with state-of-the-art small-size hybrids from the literature, as given in Table 6.5. The assessment of these couplers, based on the fractional bandwidth and circuit miniaturization, reveals that the obtained designs offer not only an ideal performance, but also one of the best miniaturization coefficients (only one out of ten designs has a smaller relative size, but at the same time its bandwidth is dramatically degraded [23].

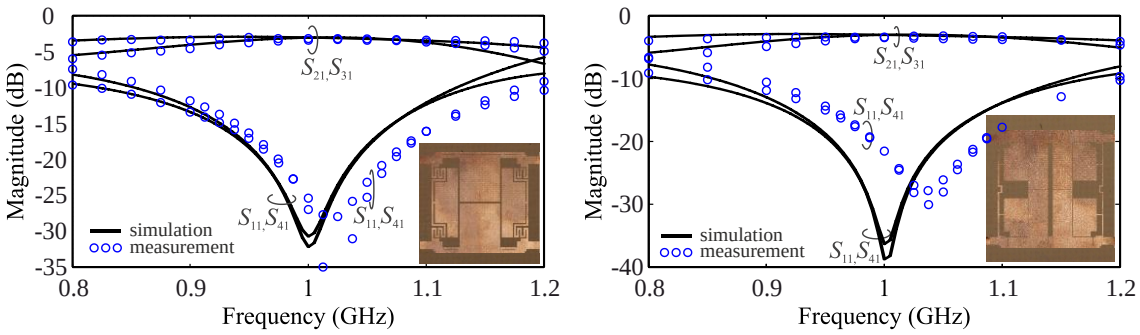

Figure 6.4: Simulated (—) vs. measured (○) frequency characteristics of the compact branch-line couplers: (a) design case no. 2; (b) design case no. 3.

TABLE 6.4: DESIGN CASE NO. 3: DESIGN BOUNDS AND SOLUTIONS (ALL DIMENSIONS IN MM)

	x_1	x_2	x_3	x_4	x_5	x_6	x_7	x_8	x_9	x_{10}	x_{11}	x_{12}
$\boldsymbol{l}$	0.1	1.8	0.5	0.1	0.1	0.1	2	0.1	1	0.1	0.1	0.1
$\boldsymbol{u}$	1	2	6	0.5	6	0.5	12	1	1.2	0.5	6	0.5
$\boldsymbol{x}_c^{(0)}$	0.1	1.9	4	0.1	1	0.1	4	0.1	1.15	0.1	1	0.1
$\boldsymbol{x}_c^*$	0.375	1.9	3.35	0.225	1.55	0.125	8.05	0.375	1.15	0.1	0.35	1
$\boldsymbol{x}^*$	0.475	1.9	3.25	0.225	1.5	0.125	8.05	0.125	1.15	0.125	0.375	0.95

TABLE 6.5: COMPARISON OF COMPACT BLCS: BANDWIDTH (BW), ELECTRICAL SIZE AND MINIATURIZATION

Reference	BW[a] (%)	Electrical size ($\lambda_g \times \lambda_g$)	Miniaturization[b] (%)
Conventional	10	0.26 × 0.27	0
[23]	2	0.06 × 0.08	92.3
[24]	3	0.14 × 0.14	72.1
[25]	4	0.14 × 0.18	64.1
[26]	5	0.16 × 0.16	63.5
[27]	5	0.03 × 0.46	80.3
[28]	6	0.15 × 0.15	67.7
[29]	6	0.18 × 0.21	46.2
[30]	8	0.16 × 0.22	49.9
[31]	9	0.09 × 0.10	87.2
[32]	10	0.18 × 0.21	46.2
This work (design case no. 2)	9	0.09 × 0.09	88.5
This work (design case no. 3)	9	0.10 × 0.11	84.3

[a] Bandwidth is defined as a symmetrical intersection of $|S_{11}|$ and $|S_{41}| \leq -20$ dB around f_0
[b] Miniaturization is computed based on the electrical size of conventional RRC of this work

6.4 Conclusions

This article presents a rigorous design methodology for compact microwave couplers. The proposed approach features simplicity, cost-efficiency, automation, and reliability. This work addresses fundamental issues of conventional simulation-driven techniques applied to compact circuit design, namely, the susceptibility to inaccurate equivalent circuit models (neglecting complex high-frequency phenomena such as cross-coupling effects), and the high computational cost of EM-based design closure. The numerical efficiency of this technique is ensured by the ability to arrive at the optimal design solution (assuming the lack of cross-coupling effects within the coupler), and, subsequently, including all the initially neglected phenomena by performing an SBO-like tuning of the entire structure. Both these components are computationally cheap, as the former involves EM models of separate coupler elements, while the latter utilizes aggregated RSA models. Comprehensive numerical and experimental validation of the method-

ology demonstrates its consistent performance across the range of compact hybrid couplers. The proposed method is also suitable for handling other decomposable design problems, such as Wilkinson power dividers in microwave engineering or coupler micro-rings in photonics. A potential limitation of this technique is when the couplings between the adjacent building blocks are so strong that discrepancies between the aggregated approximation model and EM model of the entire structure might not be accommodated through SM. The future work will be focused on handling such situations.

Acknowledgements

The authors thank Sonnet Software, Inc., Syracuse, NY, for making ***em***™ available. This work was partially supported by National Science Centre of Poland [grant 2014/15/B/ST7/04683].

References

[1] D. M. Pozar, *Microwave Engineering*, John Wiley & Sons, New York, 1998.

[2] R. Mongia, I. Bahl, and P. Bhartia, *RF and Microwave Coupled-Line Circuits*, Artech House Publishers, Norwood, MA, 1999.

[3] H.-X. Xu, G.-M. Wang, and K. Lu, "Microstrip Rat-Race Couplers," *IEEE Microw. Mag*., vol. 12, no. 4, pp. 117–129, 2011.

[4] P. Kurgan, J. Filipcewicz, and M. Kitlinski, "Development of a compact microstrip resonant cell aimed at efficient microwave component size reduction, " *IET Microw. Ant. Propag.*, vol. 6, no. 12, pp. 1291–1298, 2012.

[5] A. Bekasiewicz and P. Kurgan, "A compact microstrip rat-race coupler constituted by nonuniform transmission lines," *Microw. Opt. Techn. Lett*., vol. 56, no. 4, pp. 970–974, 2014.

[6] S. Koziel, "Computationally efficient multi-fidelity multi-grid design optimization of microwave structures," *Appl. Comp. Electromagn. Soc. J.*, vol. 25, no. 7, pp. 578–586, 2010.

[7] S. Koziel and X.S. Yang (Eds.), "Computational optimization, methods and algorithms," Series: *Studies in Computational Intelligence*, vol. 356, Springer, 2011.

[8] S. Koziel, J.W. Bandler, and K. Madsen, "Towards a rigorous formulation of the space mapping technique for engineering design," *Proc. Int. Symp. Circ., Syst*., vol. 1, pp. 5605–5608, 2005.

[9] J.W. Bandler, Q.S. Cheng, S.A. Dakroury, A.S. Mohamed, M.H. Bakr, K. Madsen, and J. Søndergaard, "Space mapping: the state of the art," *IEEE Trans. Microw. Theory Techn*., vol. 52, no. 1, pp. 337–361, 2004.

[10] A. Bekasiewicz, P. Kurgan, and M. Kitlinski, "New approach to a fast and accurate design of microwave circuits with complex topologies", *IET Microw. Ant. Propag*., vol. 6, no. 14, pp. 1616–1622, 2012.

[11] S. Koziel, A. Bekasiewicz, and P. Kurgan, "Rapid EM-driven design of compact RF circuits by means of nested space mapping," *IEEE Microw. Wireless Comp. Lett*., vol. 24, no. 6, pp. 364–366, 2014.

[12] S. Koziel, L. Leifsson, and Q.J. Zhang (Eds.), "Surrogate-based optimization", S. Koziel, X.S. Yang, Q.J. Zhang (Eds.), *Simulation-driven design optimization and modeling for microwave engineering*, Imperial College Press, pp. 41–80, 2012.

[13] Sonnet ***em***, version 14.54. Sonnet Software, North Syracuse, NY, Unites States, 2013.

[14] P. Mondal and A. Chakrabarty, "Design of miniaturised branch-line and rat-race hybrid couplers with harmonics suppression," *IET Microw. Ant. Propag*., vol. 3, no. 1, pp. 109–116, 2009.

[15] J.-T. Kuo, J.-S. Wu, and Y.-C. Chou, "Miniaturized rat race coupler with suppression of spurious passband," *IEEE Microw. Wireless Comp. Lett*., vol. 17, no. 1, pp. 46–48, 2007.

[16] C.-H. Tseng and C.-L. Chang, "A rigorous design methodology for compact planar branch-line and rat-race couplers with asymmetrical T-structures," *IEEE Trans. Microw. Theory Techn*., vol. 60, no. 7, pp. 2085–2092, 2012.

[17] C.-H. Tseng and H.-J. Chen, "Compact rat-race coupler using shunt-stub-based artificial transmission lines," *IEEE Microw. Wireless Comp. Lett*., vol. 18, no. 11, pp. 734–736, 2008.

[18] P. Kurgan and A. Bekasiewicz, "A robust design of a numerically demanding compact rat-race coupler," *Microw. Opt. Tech. Lett*., vol. 56, no. 5, pp. 1259–1263, 2014.

[19] P. Kurgan and M. Kitlinski, "Doubly miniaturized rat-race hybrid coupler," *Microw. Opt. Tech. Lett*., vol. 53, no. 6, pp. 1242–1244, 2011.

[20] J. Wang, B.-Z. Wang, Y.-X. Guo, L.C. Ong, and S. Xiao, "Compact slow-wave microstrip rat-race ring coupler," *Electron. Lett*., vol. 43, no. 2, pp. 111–113, 2007.

[21] S. Opozda, P. Kurgan, and M. Kitlinski, "A compact seven-section rat-race hybrid coupler incorporating PBG cells," *Microw. Opt. Tech. Lett*., vol. 51, no. 12, pp. 2910–2913, 2009.

[22] W. Shao, J. He, and B.-Z. Wang, "Compact rat-race ring coupler with capacitor loading, " *Microw. Opt. Tech. Lett*., vol. 52, no. 1, pp. 7–9, 2010.

[23] C.-H. Tseng and C.-H. Wu, "Design of compact branch-line couplers using π-equivalent artificial transmission lines," *IET Microw. Ant. Propag*., vol. 6, no. 9, pp. 969–974, 2012.

[24] K.-Y. Tsai, H.-S. Yang, J.-H. Chen, and Y.-J. Chen, "A miniaturized 3 dB branch-line hybrid coupler with harmonics suppression," *IEEE Microw. Wireless Comp. Lett*., vol. 21, no. 10, pp. 537–539, 2011.

[25] S.-S. Liao and J.-T. Peng, "Compact planar microstrip branch-line couplers using the quasi-lumped elements approach with nonsymmetrical and symmetrical T-shaped structure," *IEEE Trans. Microw. Theory Techn*., vol. 54, no. 9, pp. 3508–3514, 2006.

[26] W.-L. Chen and G.-M. Wang, "Exact design of novel miniaturised fractal-shaped branch-line couplers using phase-equalising method," *IET Microw. Ant. Propag*., vol. 2, no. 8, pp. 773–780, 2008.

[27] L.K. Yeung, "A compact dual-band 90° coupler with coupled-line sections," *IEEE Trans. Microw. Theory Techn*., vol. 59, no. 9, pp. 2227–2232, 2011.

[28] J. Wang, B.-Z. Wang, Y.-X. Guo, L.C. Ong, and S. Xiao, "A compact slow-wave microstrip branch-line coupler with high performance," *IEEE Microw. Wireless Comp. Lett*., vol. 17, no. 7, pp. 501–503, 2007.

[29] S.-S. Liao, P.-T. Sun, N.-C. Chin, and J.-T. Peng, "A novel compact-size branch-line coupler," *IEEE Microw. Wireless Comp. Lett*., vol. 15, no. 9, pp. 588–590, 2005.

[30] C.-W. Tang, M.-G. Chen, and C.-H. Tsai, "Miniaturization of microstrip branch-line coupler with dual transmission lines," *IEEE Microw. Wireless Comp. Lett*., vol. 18, no. 3, pp. 185–187, 2008.

[31] H.-R. Ahn and S. Nam, "Compact microstrip 3-dB coupled-line ring and branch-line hybrids with new symmetric equivalent circuits," *IEEE Trans. Microw. Theory Techn*., vol. 61, no. 3, pp. 1067–1078, 2013.

[32] K.W. Eccleston and S.H.M. Ong, "Compact planar microstripline branch-line and rat-race couplers," *IEEE Trans. Microw. Theory Techn*., vol. 51, no. 10, pp. 2119–2125, 2003.

7 HIERARCHICAL EM-DRIVEN SURROGATE-ASSISTED DESIGN OF COMPACT WIDEBAND COUPLERS

***

P. Kurgan and S. Koziel

Design of High-Performance Hybrid Branch-Line Couplers for Wideband and Space-Limited Applications

Published in: *IET Microwaves Antennas & Propagation*, vol. 10, no. 12, pp. 1339–1344, 2016.

DOI: 10.1049/iet-map.2016.0188

***

Abstract: This study presents a new design method of high-performance broadband equal-split branch-line couplers with compact footprints. Size reduction as well as wideband operation are achieved here by using cascaded slow-wave cells in place of conventional transmission lines that are basic building blocks of a reference structure. The initial stage of the design process involves numerical optimization of the reference coupler equivalent circuit model to enhance its performance and account for practical design limitations. The next stage concerns determination of a repetition factor of the recurrent slow-wave structure that provides sufficient bandwidth and phase characteristics to be a suitable substitute for a conventional line. The subsequent steps include cell optimization using fine electromagnetic simulations, local response surface modeling of the single cell, and surrogate-based optimization of the recurrent slow-wave structure composed of cascaded cell approximation models. Additionally, minor T-junction and proximity effects that deteriorate the performance of the compact coupler are compensated by means of surrogate-assisted design closure. The proposed method is demonstrated by two numerical examples. The

compact couplers obtained in this study illustrate the highest bandwidth-to-size ratio when compared against state-of-the-art wideband couplers from the literature. Experimental verification of one of the examples confirms the reliability of the proposed design approach.

7.1 Introduction

Hybrid branch-line couplers (BLCs) are vital microwave components widely used in balanced-type applications to provide an equal power split between the output ports with a 90° phase shift [1]. Planar BLCs are usually preferred over other popular hybrids, i.e., rat-race couplers, as the latter have non-adjacent output arms and require a crossover to be used in practice [2]. Unfortunately, conventional two-branch BLCs exhibit inherently narrow bandwidth of about 10% [3]. To address this issue, several bandwidth enhancement techniques for BLC structures have been proposed in the literature, including various applications of $\lambda/4$ transmission lines (TLs), e.g., as matching transformers [4], open-circuited coupled lines [5], short-circuited stubs [6], or additional branches [7]. These techniques offer bandwidth widening, but do not ensure small dimensions. Size reduction is predominantly achieved by circuit decomposition and replacement of its conventional building blocks, i.e., uniform TLs, with intricate slow-wave structures that offer a reduced physical length without altering their electrical length [8-10]. As a consequence, the corresponding design problem becomes particularly complex, with issues such as the high computational cost of an electromagnetic (EM) analysis, the lack of accurate equivalent circuit models, multi-dimensional and wide-ranged search spaces, as well as counter-intuitive parameter setups pertaining to high-performance circuit solutions [11-13]. Hence, the solution to the design problem of compact structures is either roughly approximated by analytical methods [14], [15] (and, thus, requires fine-tuning) or too expensive to accomplish by means of standard simulation-driven design procedures, solely based on repetitive EM simulations (e.g., parameter sweeps and numerical optimization). To date, only a few works on the design of compact microwave couplers have attempted to alleviate the aforementioned obstacles by exploiting the concept of surrogate-based optimization (SBO) [16-21]. SBO methods such as space mapping (SM) [21] benefit from executing vast majority of numerical operations using a cheap surrogate instead of an expensive fine model. The latter is utilized only occasionally to verify the solution produced by the surrogate or to refine it. The works of [9] and [11] have been specifically tailored to deal with computational demands of narrowband compact couplers, whose constitutive building blocks can be successfully replaced by single-element slow-wave cells. A decomposition-based SM technique relying on fast (yet sufficiently accurate) equivalent circuit models has been proposed in [9] to address the issue of a large number of designable parameters for a compact coupler design. A different approach has been presented in [11], combining direct EM-based optimization of structure's building blocks with surrogate-assisted fine-tuning procedure that utilizes an aggregated surrogate model composed of local response surface approximations (RSAs). None of these methodologies can be efficiently applied to solve the problem at hand due to the wideband operation requirements that imply utilization of multi-element slow-wave structures as building blocks of a compact broadband coupler. This leads to excessive computational costs of their repeated EM simulations (related to sequential verifications of the entire structure as in [9] or direct optimization and data acquisition for approximation model construction as in [11]). In addition, the referred methods are not suitable for establishing the topology of the recurrent slow-wave structure, namely, the number of its elements, which is critical in design of compact wideband couplers.

This work aims at mitigating the aforementioned issues by combining cheap equivalent circuit models with EM and RSA models embedded in a customized SBO procedure for rapid and reliable design of cascaded slow-wave structures. An expedited design closure technique is applied here to compensate the effects that deteriorate the performance of the entire structure. The proposed method is demonstrated by two numerical examples. A comparison with state-of-the-art BLCs as well as experimental validation of one of the examples is provided.

7.2 Methodology

In this section, we discuss the design methodology of compact wideband BLCs. The main stages of the design process include: (i) optimizing the reference coupler circuit model, (ii) determining the repetition factor of the quasi-periodic slow-wave structure, and (iii) performing SBO of the recurrent slow-wave structure.

7.2.1 Design Flow Overview

To date, the prevailing approach to miniaturization of microwave devices is based on the decomposition of a conventional circuit, and subsequent replacement of its building blocks (i.e., uniform TLs) with slow-wave structures that are specifically designed to mimic electrical properties of the former in a given frequency range, while offering a diminished physical length [8]. In general, slow-wave structures are periodic TLs with series inductance and shunt capacitance loadings [22]. Practical implementations follow the concept of spatially separated storage of magnetic and electric energy realized by high-impedance strips and low-impedance stubs [23]. From the perspective of transmission characteristics, the discussed structures are inherently low pass, with slow-wave propagation within the passband, which translates into a higher propagation coefficient with respect to a conventional TL. In practice, the repetition factor of a slow-wave line is established based on engineering insight, with consideration of the target bandwidth [8]. The rule of the thumb is that the repetition factor of 1–2 is used for narrowband applications; in case of a wideband operation, the repetition factor above 3 is more preferable. The reason is the location of the cut-off frequency, which is usually restrictively low for small values of the repetition factor, thus limiting the width of the usable passband.

The fundamental challenge of reliable simulation-driven design of wideband BLCs—miniaturized by means of slow-wave structures—is the CPU-cost associated with numerous high-fidelity EM simulations required to accomplish a typical parameter sweep or optimization process. In that context, evaluation time varies between dozens of minutes to several hours per design, depending on circuit complexity [8-10]. A parallel problem can be formulated regarding EM-driven design of multi-section slow-wave structures. In this work, we propose a three-stage method that alleviates the aforementioned difficulties. Firstly, we execute a gradient-based optimization algorithm with constraints to maximize the performance of the underlying equivalent circuit model with consideration of practical design restrictions, such as lower/upper fabrication limits. This becomes particularly handy for wideband BLCs of three or more sections, whose exterior branches usually exceed upper limits of their physical realization [7]. Once the reference structure is established, we apply circuit decomposition and translate design specifications pertaining to the entire coupler into design specs for its building blocks [8]. The latter design criteria are used in the second stage of the design process, where an iterative optimization scheme is executed to find the smallest repetitive factor of a hand-picked slow-wave structure, for which certain performance thresholds are not violated. Stages 1 and 2 rely entirely on equivalent circuit models, thus are computationally cheap. The principal design process of quasi-periodic slow-wave structures is realized in the third stage of the proposed method. We use here an SBO scheme to alleviate the excessive CPU cost related to the direct EM optimization of a multi-element slow-wave line. The surrogate model exploited in the SBO process is a space-mapping-corrected low-fidelity model, con6structed from cascaded local RSAs of the optimized unitary slow-wave elements. The latter are numerically cheap when compared with the high-fidelity model of the entire coupler, and their direct EM optimization is feasible. The proposed design procedure enables a cost-efficient determination a suitable number of elements within a quasi-periodic slow-wave structure, and adjustment of designable parameters of the latter to satisfy performance goals at the high-fidelity level, which to date has not been reported in the literature. This method is also compatible with a rapid fine-tuning technique of [11] that can be applied in case of minor discrepancies attributed to T-junction or cross-coupling effects, unaccounted for during the design process. The above-summarized methodology is conceptually presented by the design flow shown in Figure 7.1.

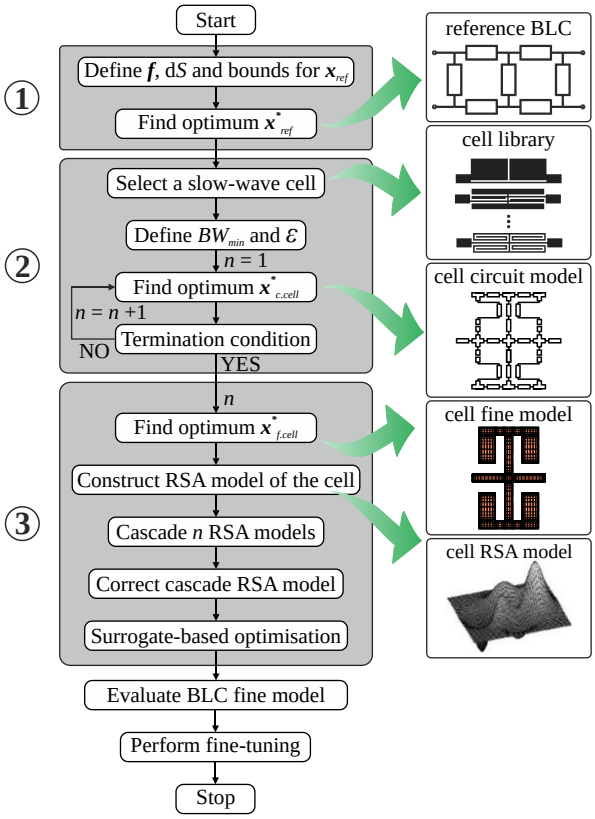

Figure 7.1: Design flow of compact wideband BLCs. Stage 1: optimization of the reference circuit; Stage 2: optimization-based process aimed at finding the smallest slow-wave structure repetition factor; Stage 3: surrogate-assisted optimization of the slow-wave structure.

7.2.2 Reference Coupler Optimization

The main drawback of the known bandwidth enhancement techniques lies in a considerable size enlargement of the resulting components (three-fold [4], [5] to even nine-fold [5]). Conversely, the multi-section concept [7] seems more beneficial in that regard as a two-section BLC only doubles its initial size. Although the proposed methodology can be applied to other reference structures, the scope of the following discussion is limited—for simplicity—to a two-section BLC topology.

Consider a standard two-section BLC model of Figure 7.2(a), composed of seven quarter-wavelength TLs of Z_1–Z_3 impedances. Practical figures of merit for microwave couplers with a wideband operation include (i) fractional bandwidth (*BW*), defined here as symmetrical—with respect to the center frequency f_0—intersection of the return loss and isolation that remain below the level of –20 dB, and (ii) d*S*, denoting the absolute difference between the transmission and coupling at f_0. For illustration purposes, we use these quantities to evaluate conventional design solutions of the Butterworth and Chebyshev [2] type, as shown in Figure 7.2(b). Both designs exhibit non-zero d*S* which is a deviation from the desired performance. In addition, conventional design solutions of Figure 7.2(b) do not account for any practical design limitations, such as the constraints put on characteristic impedances to determine ranges of TL physical realization in available fabrication technology. In this work, we address the aforementioned issues by means of numerical optimization, i.e., the BLC model of Figure 7.2(a) is optimized to obtain the maximum *BW* together with an equal power split between the output ports at the operating frequency f_0, i.e., d*S* = 0. The optimization task of the reference BLC is formulated as:

$$\boldsymbol{x}_{ref}^{*} = \arg\min_{x} \left\{ -BW\left(\boldsymbol{x}; f\right) + \beta \cdot \left[\mathrm{d}S\left(\boldsymbol{x}; f_0\right) / 0.1 \right]^2 \right\} \tag{7.1}$$

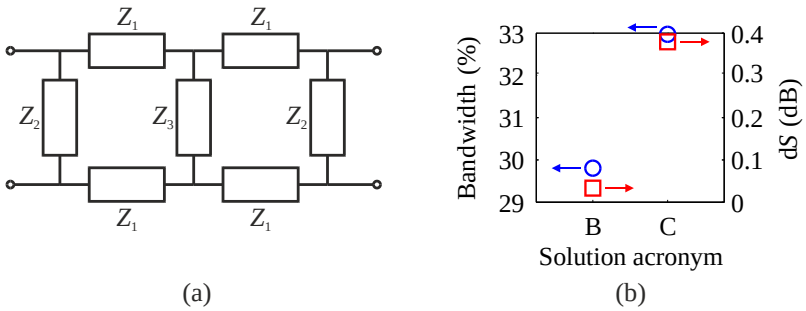

(a) (b)

Figure 7.2: (a) Conventional two-section BLC circuit model (each TL is 90° at f_0); (b) bandwidth (circle) and dS (square) for two conventional BLC design solutions: B – Butterworth type (Z_1 = 36.3 Ω, Z_2 = 120.5 Ω, Z_3 = 37.2 Ω), and C – Chebyshev type (Z_1 = 26.9 Ω, Z_2 = 105.2 Ω, Z_3 = 24.3 Ω).

where $\boldsymbol{x}$ represents a vector of optimization arguments (more precisely, a vector of adjustable parameters of the structure at hand, i.e., Z_1–Z_3 impedances), $\boldsymbol{x}^*_{ref}$ is the optimized reference BLC design solution, β denotes the penalty factor, while $BW(\boldsymbol{x};f)$ and $dS(\boldsymbol{x};f_0)$ are the above-defined bandwidth and transmission-coupling imbalance, respectively. Problem (7.1) is solved directly using a standard gradient optimization algorithm with constraints. In practice, constraints are related to fabrication limitations (as the upper impedance bounds) and slow-wave structure design restrictions (as the lower impedance bounds). The latter result from great transverse dimensions of slow-wave TLs (typically much larger than the width of a conventional line [8]).

7.2.3 Determination of the Slow-Wave Structure Repetition Factor

The reference BLC (either taken from the literature as in Figure 7.2(b) or obtained via optimization as in Section 7.2.2) is composed of high- and low-impedance TLs that require length diminution to achieve circuit size reduction. The high-impedance branches can be shortened by line folding [8], [24], which is probably the most efficient technique of contracting narrow TLs and maintaining their wideband operation. On the other hand, abbreviation of quarter-wavelength low-impedance TLs for small-size and broadband applications is far from trivial. As mentioned before, it can be accomplished by exploiting quasi-periodic slow-wave lines. One should bear in mind that single-element 90° slow-wave structures are inherently narrowband [8], which typically excludes them from use in wideband applications. The utilization of multiple slow-wave elements (the so-called cells) instead of one results in shifting of the cut-off frequency upwards and, in turn, leads to bandwidth widening. General guidelines for establishing the number of slow-wave elements, n, are the following: (i) n should be as small as possible because the increase of n corresponds to the increase of CPU cost associated with slow-wave structure EM analysis, and (ii) n should be sufficiently large so that the given n-element cascade is capable of imitating the behavior of its conventional counterpart in a specified frequency range. The determination of a suitable repetition factor of the recurrent slow-wave structure is accomplished here by means of an iterative process set up in ADS [25] with port impedances set to the low impedance obtained by (7.1), e.g., Z_1. In each iteration, starting from n = 1, we solve a slow-wave cell optimization task aimed at minimizing the return loss $|S_{11}|$ at f_0, while forcing phase shift, arg(S_{21}), to $\phi_c = -90°/n$ at f_0. The process optimizes a slow-wave cell equivalent circuit model and increments n until the following termination conditions are simultaneously satisfied: (i) BW of the cascaded n-element recurrent network is larger or equal to the BW of the reference coupler, and (ii) the absolute difference between the transmission phase of a conventional TL and n-element cascade, $\Delta\varphi$, is less than a certain threshold value ε. The latter condition is verified only at the high BW limit, f_h. This is sufficient, as the discrepancy between the conventional and slow-wave TLs increases with frequency [8]. Formally, the optimization task is defined as:

$$\boldsymbol{x}^*_{c.cell} = \arg\min_{\boldsymbol{x}} \left\{ \max_{f=f_0} \left| S_{11}(\boldsymbol{x};f) \right| + \beta \cdot \left[\arg\left(S_{21}(\boldsymbol{x};f_0) \right) - \phi_c \right]^2 \right\} \tag{7.2}$$

where $\boldsymbol{x}$ is substituted by $\boldsymbol{x}_{cell}$, which is a vector of designable parameters of the slow-wave cell, $\boldsymbol{x}_{c.cell}^{*}$ is the optimized design solution pertaining to the slow-wave cell coarse model (equivalent circuit); $S_{11}(\boldsymbol{x};f)$ and $S_{21}(\boldsymbol{x};f)$ denote explicit dependence of S-parameters on frequency, whereas β is the penalty factor. Note that the equivalent circuit representation of slow-wave structures is typically too inaccurate to be directly used in the main design process, but it may be useful to find initial design solutions for further EM analysis or to establish certain features of circuit topology such as the smallest number n that satisfies the aforementioned requirements.

7.2.4 Optimization of Quasi-Periodic Slow-Wave Structures

The principal stage of the proposed design process involves adjustment of geometry parameters of the quasi-periodic slow-wave structure to satisfy performance requirements imposed by conventional coupler building blocks. The final goal is to reduce the size of the reference BLC without degrading its frequency characteristics. The main challenge here is that reliable EM analysis of multi-element slow-wave lines is numerically expensive, which prohibits the use of standard simulation-driven design strategies. To address this issue, we build a surrogate model of the quasi-periodic slow-wave structure to be subsequently used in a cost-efficient SBO routine. First, we decompose the cascaded slow-wave line and execute (7.2) using an EM model of the single slow-wave cell, assuming $\phi_c = -90°/n$, with n established in the previous design stage. The problem (7.2) is solved directly using a pattern search algorithm (cf. [26]). Having obtained the optimized design solution pertaining to the slow-wave cell fine model, $\boldsymbol{x}_{f.cell}^{*}$, we construct a local RSA model, $\boldsymbol{R}_{c.cell}$, in the vicinity of $\boldsymbol{x}_{f.cell}^{*}$ defined as $[\boldsymbol{x}_{f.cell}^{*} - d\boldsymbol{x}, \boldsymbol{x}_{f.cell}^{*} + d\boldsymbol{x}]$. It is developed at the cost of $2m + 1$ EM simulations ($m = \dim(\boldsymbol{x}_{cell})$) at $\boldsymbol{x}_{f.cell}^{(0)} = \boldsymbol{x}_{f.cell}^{*}$ and at the perturbed designs $\boldsymbol{x}_{f.cell}^{(k)} = [x_{f.cell.1}^{*} \ldots x_{f.cell.\lceil k/2 \rceil}^{*} + (-1)^k dx_{\lceil k/2 \rceil} \ldots x_{f.cell.m}^{*}]^T$, $k = 1, \ldots, 2m$, where $x_{f.cell.k}^{*}$ and dx_k are kth components of the vectors $\boldsymbol{x}_{f.cell}^{*}$ and $d\boldsymbol{x}$, respectively. $\boldsymbol{R}_{c.cell}(\boldsymbol{x})$ is a second-order polynomial without mixed terms

$$\boldsymbol{R}_{c.cell}(\boldsymbol{x}) = c_0 + \sum_{k=1}^{n} c_k x_k + \sum_{k=1}^{n} c_{n+k} x_k^2 \tag{7.3}$$

The parameters c_k in (7.3) are identified by solving the linear regression problems

$$\boldsymbol{R}_{c.cell}\left(\boldsymbol{x}_{f.cell}^{(k)}\right) = \boldsymbol{R}_{f.cell}\left(\boldsymbol{x}_{f.cell}^{(k)}\right), \quad k = 0,1,\ldots,2m \tag{7.4}$$

where $\boldsymbol{R}_{f.cell}$ denotes a high-fidelity (fine) EM model of the cell. Next, a coarse model of the entire recurrent slow-wave structure, $\boldsymbol{R}_{c.cas}$, is developed by cascading n $\boldsymbol{R}_{c.cell}$ models, i.e., local RSAs of the individual slow-wave cell, and adding a cheap fine model $\boldsymbol{R}_{f.TL}$ of a short TL of Z_1 impedance and l_{TL} length at both ends of the cascade. A conceptual illustration of the cascaded coarse model is shown in Figure 7.3. Lastly, the surrogate model of the recurrent slow-wave structure, used in each iteration i of the SBO process, is a space-mapping-corrected [16], [21] version of the cascade coarse model $\boldsymbol{R}_{c.cas}$ and is given by

$$\boldsymbol{R}_{s.cas}^{(i)}(\boldsymbol{x}) = \boldsymbol{R}_{c.cas}\left(\boldsymbol{x} + \boldsymbol{q}^{(i)}\right) \tag{7.5}$$

where $\boldsymbol{q}^{(i)}$ is the input SM shift vector obtained using a standard parameter extraction procedure [16]

$$\boldsymbol{q}^{(i)} = \arg\min_{\boldsymbol{q}} \left\| \boldsymbol{R}_{f.cas}\left(\boldsymbol{x}^{(i)}\right) - \boldsymbol{R}_{c.cas}\left(\boldsymbol{x}^{(i)} + \boldsymbol{q}\right) \right\| \tag{7.6}$$

which aims at the reduction of the misalignment between the coarse and fine cascade models—$\boldsymbol{R}_{c.cas}$ and $\boldsymbol{R}_{f.cas}$. Note that $\boldsymbol{R}_{c.cas}$ does not account for cross-coupling effects between the cells, which calls for further tuning. This may be realized as the following SBO process [16]

$$\boldsymbol{x}_{cas}^{(i+1)} = \arg\min_{\boldsymbol{x}} U\left(\boldsymbol{R}_{s.cas}^{(i)}(\boldsymbol{x})\right) \tag{7.7}$$

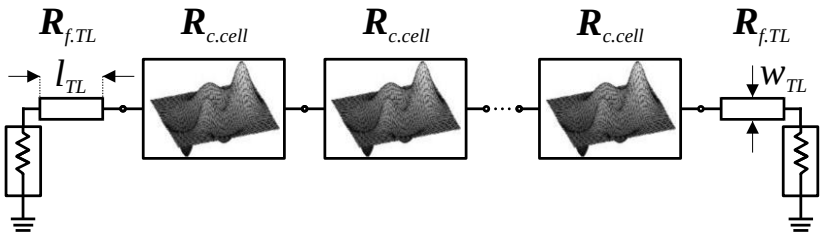

Figure 7.3: Schematic diagram of the cascaded slow-wave structure composed of n RSA models of the cell and two fine EM models of feeding lines of variable length l_{TL} (w_{TL} is fixed and corresponds to Z_1 obtained by process (7.1)). The circuit is loaded with Z_1 impedance.

The vectors $\boldsymbol{x}_{cas}^{(i)}$, i = 0, 1, …, approximate the solution to the cascaded slow-wave structure direct EM-driven design problem of the form $\boldsymbol{x}_{cas}^{*}$ = argmin{$\boldsymbol{x}$: $U(\boldsymbol{R}_{f.cas}(\boldsymbol{x}))$}, where U encodes design specifications for the recurrent slow-wave structure, and $\boldsymbol{x}$ is a vector of optimization arguments (in practice, it is substituted by a vector of cascade designable parameters). The process (7.7) is cost-effective as the fine cascade model is evaluated only at the beginning and end of each iteration i [16].

7.3 Case Studies

In this section, we use the methodology of Section 7.2 to showcase complete design cycles of compact wideband couplers. The proposed approach is demonstrated by two design examples of BLCs whose conventional high-impedance lines are folded, whereas low-impedance lines are replaced by cascaded slow-wave cells to achieve size reduction. The specific geometries of the latter are hand-picked from a wide collection of slow-wave elements found in the literature [8].

The reference coupler of Figure 7.2(a) is additionally simplified by assuming $Z_3 = Z_1$. This is done to shorten the following design cycles, as a typical miniaturization procedure requires that each different element of the reference coupler is substituted by a unique slow-wave structure. Thus, the CPU cost of the design process is increased with the number of different TLs in the reference circuit [8], [9].

For the following design cases, all fine EM models are implemented in Sonnet ***em*** [27] using 0.01 mm × 0.01 mm grid and fine meshing. Note that for these settings only the slow-wave cell fine model is relatively cheap (simulation time of ~1 min/freq.) as opposed to the cascade (~10 min/freq.) and the entire coupler (~5 h/freq.) fine models. Slow-wave cell equivalent circuit models are implemented and optimized using ADS [25].

Practical design constraints for reference circuit optimization are typically established based on engineering insight. We assume here that the lower and upper limits of microstrip TL realization are 0.1 mm and 3.25 mm, respectively. The former corresponds to the minimal width of a microstrip in our fabrication process, while the latter is chosen arbitrary, considering that the slow-wave cells are most commonly much wider than their conventional counterparts, which could pose a difficulty in coupler reassembly.

7.3.1 Design Case 1: Compact BLC with T-shaped Slow-Wave Structures

The task here is to design a compact BLC using the TLC-32 dielectric substrate of ε_r = 3.2 and h = 0.787 mm. The operating frequency is f_0 = 1 GHz. The first stage of the design process concerns numerical optimization of the reference BLC of Fig. 2(a). For the selected dielectric material and the lower/upper limits of TL realization, the available impedance range lies within the limits of 34.6 and 157 Ω. After model simplification, the vector of designable parameters is given by $\boldsymbol{x}_{ref}$ = $[Z_1\ Z_2]^T$. Solving (7.1) subjected to the above constraints, with the penalty factor β set to 10^4, enables maximization of BW while enforcing dS = 0. The optimized reference BLC design solution, given by $\boldsymbol{x}_{ref}^{*}$ = $[34.6\ 118.16]^T$ Ω, outperforms conventional designs by provid-

ing an ideal power split at f_0 together with BW = 31%. Its microstrip implementation occupies an excessively large area of 93.23 mm × 51.17 mm.

The second stage of the design process is commenced with the selection of a slow-wave cell for the construction of a quasi-periodic structure to replace low-impedance (Z_1 = 34.6 Ω) quarter-wavelength TLs of the optimized reference BLC. Here, we use a unit cell of Figure 7.4(a), whose geometry is described by the vector $\boldsymbol{x}_{cell} = [l_1\ l_2\ l_3\ l_4\ w_1\ w_2]^T$. Subsequently, an equivalent circuit model of Figure 7.4(b), representing the selected slow-wave cell, is used to find the smallest number of the elements in the slow-wave cascade so that the BW of the n-part structure is larger or equal to BW_{ref} = 31%, as well as the absolute difference between the transmission phase of a conventional TL and the n-element cascade, $\Delta\varphi$, is less than ε = 0.5°. This is accomplished by executing process (7.2). The family of resulting quasi-periodic slow-wave structures is compared w.r.t. the above figures of merit. The inspection of Figure 7.4(c) reveals that the first condition excludes only the case of n = 1. Note that for n = 3, 4, 5, the BW—which is defined as being symmetrical around f_0—reaches the maximum value of 200%. Considering the second condition, we can see that only the five-element cascade offers $\Delta\varphi$ below 0.5° in the entire bandwidth. Thus, we terminate the iteration process (7.2) and choose n = 5 for the next design stage. The optimized design solution for n = 5 is used as the starting point for the following design process: $\boldsymbol{x}_{cell}^{(0)} = [0.41\ 0.12\ 0.14\ 3.15\ 0.38\ 1.78]^T$ mm.

The principal design stage is an SBO process that requires a fast and well-aligned surrogate model of the recurrent slow-wave structure. To obtain accurate results, we first solve the problem (7.2) using the fine EM model of the cell. The target phase shift is ϕ_c = –18° given a five-cell setup for constructing the 90° TL of 34.6-Ω impedance. The lower/upper bounds $\boldsymbol{l}$/$\boldsymbol{u}$ of the search space are given by $\boldsymbol{l} = [0.05\ 0.1\ 0.1\ 0.1\ 0.1\ 0.1]^T$ mm, and $\boldsymbol{u} = [1\ 1\ 1\ 5\ 0.5\ 5]^T$ mm. The EM model evaluated at the initial point $\boldsymbol{x}_{cell}^{(0)}$ returns $|S_{11}|$ = –25.2 dB, and $\arg(S_{21})$ = –23.9° at f_0, while the final solution, obtained after ~100 EM simulations, $\boldsymbol{x}_{cell}^{*} = [0.16\ 0.14\ 0.13\ 3.93\ 0.42\ 1.15]^T$ mm, yields $|S_{11}|$ = –59.5 dB, and $\arg(S_{21})$ = –18.0° at f_0. Next, we construct the local RSA model of the slow-wave cell in the vicinity of its optimized design by (7.3) and (7.4), and use it to build a coarse model of the cascade. The vector of cascade designable parameters is given by $\boldsymbol{x}_{cas} = [\boldsymbol{x}_{cell}\ l_{TL}]^T$. Design specifications for the SBO process, i.e., minimal $|S_{11}|$, and $\arg(S_{21})$ = –90° at f_0, are encoded in U function. In this example, only one iteration of (7.5) is needed to satisfy the design specs with $\boldsymbol{x}_{cas}^{*} = [0.14\ 0.14\ 0.12\ 3.89\ 0.42\ 1.04\ 3.34]^T$ mm. Finally, we adjust the dimensions of the folded high-impedance line (Z_2 = 118.16 Ω) by (7.2) assuming ϕ_c = –90°.

Subsequently, we assemble the compact BLC and perform EM verification of the design. The performance of the compact BLC developed using the proposed method is shown in Figure 7.5(a). One can see a 40-MHz shift of the $|S_{11}|$ and $|S_{41}|$ frequency characteristics and a non-ideal dS = 0.2 dB. This can be explained by the T-junction effects, omitted during the design process. However, we can easily fine-tune the structure by means of a rapid design closure of [11]. By applying minor corrections given by $\Delta\boldsymbol{x}_{cas} = [0\ 0\ 0.01\ 0\ 0\ –0.06\ 0]^T$, perfect BLC performance is achieved, with a BW of 31% and dS=0. The entire process, including the design closure, takes less than three evaluations of the high-fidelity BLC model. More specifically, the overall design cost can be broken down into the following components: direct optimization of the slow-wave cell (100 EM simulations of the cell at f_0, ~100 min of CPU time), direct optimization of the high-impedance branch (50 EM simulations of the branch at f_0, ~75 min of CPU time), construction of RSA models (13 EM simulations of the cell with adaptive frequency sweep, ~130 min, and 7 EM simulations of the branch with adaptive frequency sweep, ~105 min), two EM evaluations of the cascade using adaptive frequency sweep (at $\boldsymbol{x}_{cas}^{(0)}$ and $\boldsymbol{x}_{cas}^{*}$, ~100 min), and two EM simulations of the entire BLC for the purpose of method numerical validation and final design fine-tuning (~50 h). The estimated cost of direct optimization exploiting a high-fidelity EM model of the compact BLC is—approximately—150 EM simulations of the structure, which corresponds to 3750 h of CPU time.

For validation, the fine-tuned design has been fabricated and measured. The final BLC layout of Figure 7.5(b) occupies 46.58 mm × 33.92 mm area, which is only 1/3 of the area of the reference device. Experimental results confirm our numerical predictions. Small misalignments may be explained by the susceptibility of compact components to the fabrication tolerance as well as idealized nature of conducted simulations (e.g., substrate anisotropy has not been included [28]). The measured values of $|S_{21}|$ and $|S_{31}|$ at f_0 are –3.38 dB and –3.41 dB, respectively. The phase difference between the output ports of the fabricated BLC is ~90.1° at f_0.

7.3.2 Design Case 2: Compact BLC with Dumbbell-Shaped Slow-Wave Structures

The second design example is realized in accordance to the methodology of Section 7.2. We choose the Taconic RF-35 dielectric substrate of ε_r = 3.5 and h = 0.762 mm for microstrip implementation. The operating frequency is still f_0 = 1 GHz. The lower/upper bounds for the reference coupler characteristic impedances are 34 and 150 Ω. The optimized design solution for the reference coupler, obtained by (7.1) with β = 10^4, is given by $\boldsymbol{x}_{ref}^*$= [34 116.19]^T, which corresponds to BW_{ref} = 32% and dS = 0. The physical realization of the reference circuit consumes a large real estate area of 91.7 mm × 51.0 mm. We select the slow-wave cell of Figure 7.6(a) for the subsequent construction of the recurrent slow-wave structure. The parameterized cell is described by the vector of six designable parameters, $\boldsymbol{x}_{cell}$ = [l_1 l_2 w_1 w_2 w_3 g]^T. The model of Figure 7.6(b) is exploited in iterated process (7.2) to determine the smallest n, for which the n-element cascade offers the BW of at least 32% and the phase difference $\Delta\varphi$ below 0.5°. As previously, n = 5 is the smallest repetition factor, for which the above design criteria are satisfied. Cascades composed of n parts (n ranging from 1 to 5) are compared in Figure 7.6(c). The subsequent design stages can be summarized as follows: $\boldsymbol{x}_{cell}^*$ = [0.1 0.7 2.0 0.5 6 0.1]^T is obtained with (7.2) using $\boldsymbol{R}_{f.cell}$, β = 10^4, and ϕ_c= –18°; $\boldsymbol{x}_{cas}^*$ = [0.1 0.7 2.0 0.5 6.4 0.1 3.15]^T (where the vector of cascade parameters is $\boldsymbol{x}_{cas}$ = [$\boldsymbol{x}_{cell}$ l_{TL}]^T).

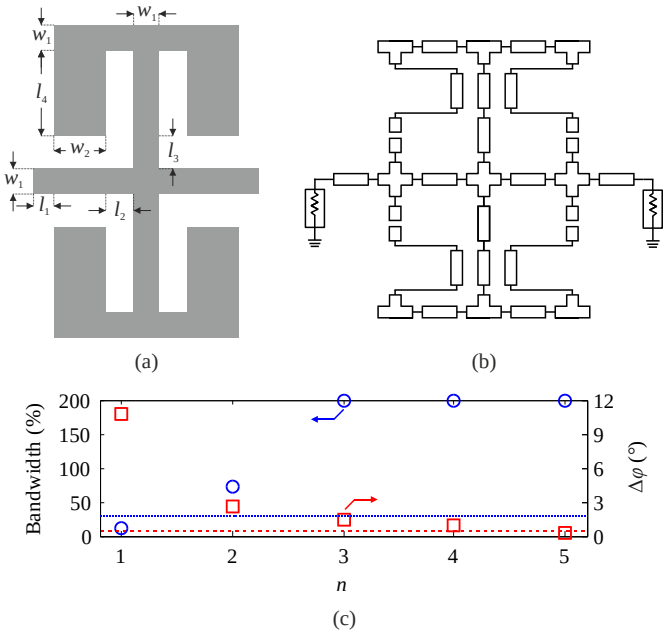

Figure 7.4: (a) Parameterized layout of a T-shaped slow-wave cell, and (b) its equivalent circuit model implemented in ADS [25]; (c) Comparison of n-element cascades (n = 1, 2, …, 5) of slow-wave cell circuit models: BW (circle) and absolute phase difference between a conventional TL of Z_1 impedance and the given n-element cascade at f_h (square). Dotted and dashed lines represent BW_{ref} and ε thresholds, respectively.

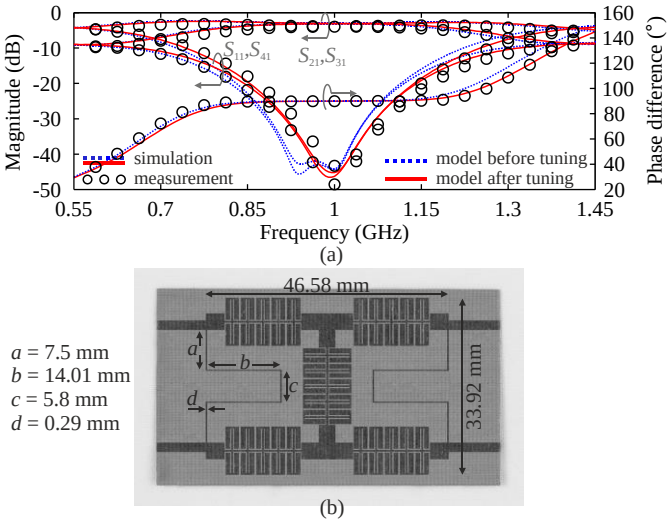

Figure 7.5: (a) S-parameters of compact BLCs based on T-shaped slow-wave structures; (b) Layout of the fabricated BLC.

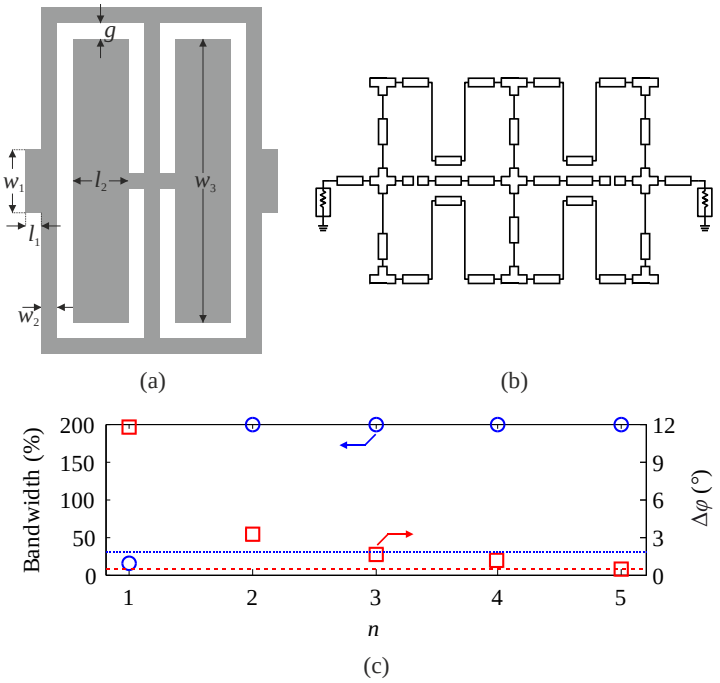

Figure 7.6: (a) Parameterized layout of a dumbbell-shaped slow-wave cell, and (b) its ADS equivalent circuit model; (c) Comparison of n-element cascades (n = 1, 2, …, 5) of slow-wave cell circuit models: BW (circle) and absolute phase difference between a conventional TL of Z_1 impedance and the given n-element cascade at f_h (square). Dotted and dashed lines represent BW_{ref} and ε thresholds, respectively.

The high-impedance line (Z_2 = 116.19 Ω) is folded and optimized using the fine EM model and (7.2), assuming ϕ_c= –90°. The performance and geometry of the compact BLC composed of optimized low-impedance cascade and high-impedance branch design solutions is shown in Figure 7.7. Due to possible interactions between adjacent slow-wave structures, as well as additional T-junctions whose effect has been omitted during the design process, a small 13-MHz frequency shift of $|S_{11}|$ and $|S_{41}|$ curves can be observed. The final design has been adjusted by applying minor corrections given by $\Delta\boldsymbol{x}_{cas}$ = [0 0 0 0 –0.02 0.01 0]^T. As a result, the fine-tuned coupler illustrates a 32% bandwidth and dS = 0 ($|S_{21}|$ = $|S_{31}|$ = –3.16 dB at f_0). The simulated phase difference between the output ports is approximately 90° at f_0. The final compact coupler occupies about 38% of the reference circuit area. The overall cost of the design procedure is less than three EM simulations of the final compact BLC.

The superiority of the designed couplers is evident in the view of comparison with state-of-the-art designs (Table 7.1). Not only they offer an ideal power split (dS = 0), but also provide the highest bandwidth-to-size ratio, η.

7.4 Conclusions

A methodology for expedited and reliable decomposition-based design of compact wideband BLCs has been presented. Our approach combines the merits of theory-based and simulation-driven design strategies. The former exploit equivalent circuit models, and are useful for obtaining an improved reference circuit as well as for establishing important features of compact circuit topology. The latter involve EM modeling and RSA of a single slow-wave cell, together with the application of SM for cascaded model correction. The principal design stage is an SBO, developed specifically for the design purpose of wideband couplers with complex topologies. The proposed BLCs offer superior figures of merit in comparison to competitive designs available in the literature.

TABLE 7.1: COMPARISON WITH STATE-OF-THE-ART WIDEBAND BLCS

Ref.	$BW^{\$}$ (%)	dS (dB)	Size ($\lambda_g \times \lambda_g$)	$\eta^{\#}$
[4]	22.2*	0	0.75 × 0.25	118
[5]	47.8	0.64	0.87 × 0.51	108
[6]	12.4	0	0.75 × 0.75	22
[14]	46.9	1.38	0.39 × 0.37	325
[15]	23.9	1.22	0.29 × 0.38	217
[29]	45.2	0.38	0.83 × 1.26	43
This work (design case 1)	31	0	0.26 × 0.19	628
This work (design case 2)	32	0	0.28 × 0.19	602

$^{\$}$ Bandwidth is defined as a symmetrical intersection of $|S_{11}|$ and $|S_{41}| \leq -20$ dB around f_0
$^{\#}$ η stands for the bandwidth-to-size ratio
* Design solution with the widest bandwidth based on the theory of [4]

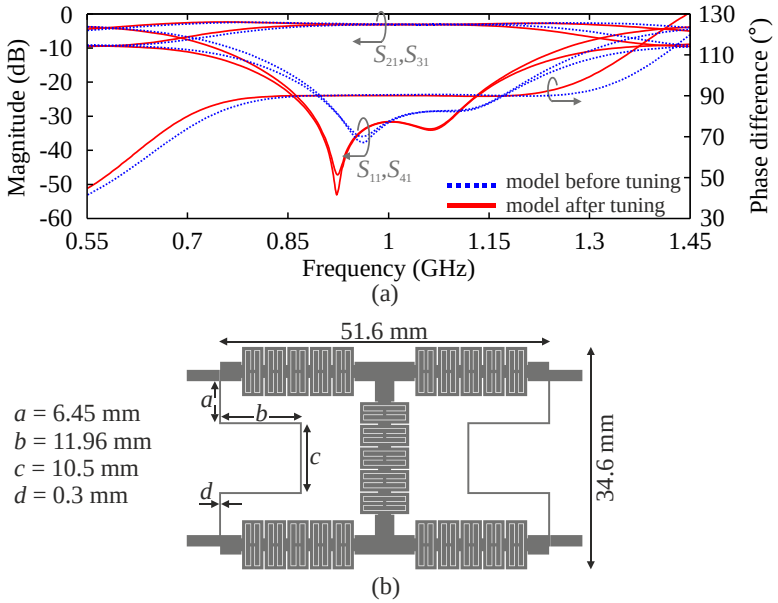

Figure 7.7: (a) S-parameters of compact BLCs based on dumbbell-shaped slow-wave structures; (b) Layout of the designed BLC.

References

[1] D. Pozar, *Microwave Engineering*, John Wiley & Sons, New York, 1998.

[2] M. Muraguchi, T. Yukitake, and T. Naito, "Optimum Design of 3-dB Branch-Line Couplers Using Microstrip Lines," *IEEE Trans. Microw. Theory Tech.*, vol. 31, no. 8, pp. 674–678, 1983.

[3] R. Mongia, I. Bahl, and P. Bhartia, *RF and Microwave Coupled-Line Circuits*, Artech House, 1999.

[4] S. Lee and Y. Lee, "Wideband branch-line couplers with single-section quarter-wave transformers for arbitrary coupling levels," *IEEE Microw. Wire. Comp. Lett.*, vol. 22, no. 1, pp. 19–21, 2012.

[5] W.A. Arriola, J.Y. Lee, and I.S. Kim, "Wideband 3 dB branch line coupler based on λ/4 open circuited coupled lines," *IEEE Microw. Wire. Comp. Lett.*, vol. 21, no. 9, pp. 486–488, 2011.

[6] Y. Wang, M. Ke, and M.J. Lancaster, "Micromachined millimeter-wave rectangular-coaxial branch-line coupler with enhanced bandwidth," *IEEE Trans. Microw. Theory Tech.*, vol. 57, no. 7, pp. 1655–1660, 2009.

[7] R. Levy and L. Lind, "Synthesis of symmetrical branch-guide directional couplers," *IEEE Trans. Microw. Theory Tech.*, vol. 16, no. 2, pp. 80–89, 1968.

[8] P. Kurgan, J. Filipcewicz, and M. Kitlinski, "Development of a compact microstrip resonant cell aimed at efficient microwave component size reduction," *IET Microw. Ant. Propag.*, vol. 6, no. 12, pp. 1291–1298, 2012.

[9] A. Bekasiewicz, P. Kurgan, and M. Kitlinski, "New approach to a fast and accurate design of microwave circuits with complex topologies", *IET Microw. Ant. Propag*., vol. 6, no. 14, pp. 1616–1622, 2012.

[10] C.-H. Tseng and C.-H. Wu, "Design of compact branch-line couplers using π-equivalent artificial transmission lines," *IET Microw. Ant. Propag*., vol. 6, no. 9, pp. 969–974, 2012.

[11] S. Koziel and P. Kurgan, "Rapid design of miniaturized branch-line couplers through concurrent cell optimization and surrogate-assisted fine-tuning," *IET Microw. Ant. Propag*., vol. 9, no. 9, pp. 957–963, 2015.

[12] S. Koziel, A. Bekasiewicz, and P. Kurgan, "Rapid multi-objective simulation-driven design of compact microwave circuits," *IEEE Microw. Wireless Comp. Lett.*, vol. 25, no. 5, pp. 277–279, 2015.

[13] S. Koziel, P. Kurgan, and B. Pankiewicz, "Cost-efficient design methodology for compact rat-race couplers," *Int. J. RF Microw. Comp. Aid. Eng.*, vol. 25, no. 3, pp. 236–242, 2015.

[14] Y.-H. Chun and J.-S. Hong, "Compact wide-band branch-line hybrids," *IEEE Trans. Microw. Theory Tech.*, vol. 54, no. 2, pp. 704–709, 2006.

[15] Y.-H. Chun, and J.-S. Hong, "Design of a compact broadband branch-line hybrid," *IEEE MTT-S Int. Microw. Symp.*, pp. 997–1000, 2005.

[16] S. Koziel, L. Leifsson, and Q.J. Zhang (Eds.), "Surrogate-based optimization", S. Koziel, X.S. Yang, Q.J. Zhang (Eds.), *Simulation-driven design optimization and modeling for microwave engineering*, Imperial College Press, pp. 41–80, 2012.

[17] S. Koziel and X.-S. Yang (Eds.), *Computational optimization, methods and algorithms*, Series: Studies in Computational Intelligence, vol. 356, Springer, 2011.

[18] N.V. Queipo, R.T. Haftka, W. Shyy, T. Goel, R. Vaidynathan, and P.K. Tucker, "Surrogate based analysis and optimization," *Prog. Aerosp. Sci.*, vol. 41, no. 1, pp. 1–28, 2005.

[19] M.B. Yelten, T. Zhu, S. Koziel, P.D. Franzon, and M.B. Steer, "Demystifying surrogate modeling for circuits and systems," *IEEE Circ. Syst. Mag.*, vol. 12, no. 1, pp. 45–63, 2012.

[20] S. Koziel, "Efficient optimization of microwave circuits using shape-preserving response prediction," *IEEE MTT-S Int. Microw. Symp. Dig*, Boston, MA, pp. 1569–1572, 2009.

[21] J.W. Bandler, Q.S. Cheng, S.A. Dakroury, A.S. Mohamed, M.H. Bakr, K. Madsen, and J. Søndergaard, "Space mapping: the state of the art," *IEEE Trans. Microw. Theory Tech*., vol. 52, no. 1, pp. 337–361, 2004.

[22] C. Zhou and H.Y.D. Yang, "Design considerations of miniaturized least dispersive periodic slow-wave structures," *IEEE Trans. Microw. Theory Tech*., vol. 56, no. 2, pp. 467–474, 2008.

[23] S. Seki and H. Hasegawa, "Cross-tie slow-wave coplanar waveguide on semi-insulating GaAs substrates," *Electron. Lett.*, vol. 17, no. 17, pp. 940–941, 1981.

[24] A. Bekasiewicz and P. Kurgan, "A compact microstrip rat-race coupler constituted by nonuniform transmission lines," *Microw. Opt. Techn. Lett.*, vol. 56, no. 4, pp. 970–974, 2014.

[25] ADS, ver. 2011.10, Agilent Technologies, 1400 Fountaingrove Parkway, Santa Rosa, CA 95403-1799, 2011.

[26] T.G. Kolda, R.M. Lewis, and V. Torczon, "Optimization by direct search: new perspectives on some classical and modern methods," *SIAM Rev.*, vol. 45, no. 3, pp. 385–482, 2003.

[27] Sonnet, version 14.54. Sonnet Software, North Syracuse, NY, US, 2013.

[28] J.C. Rautio, B.J. Rautio, S. Arvas, A.F. Horn, III, and J.W. Reynolds, "The effect of dielectric anisotropy and metal surface roughness," *Proc. Asia-Pacific Microw. Conf.*, pp. 1777–1780, 2010.

[29] J.J. Yao, "Nonstandard hybrid design with branch-line structures," *IEEE Trans. Microw. Theory Tech.*, vol. 58, no. 12, pp. 3801–3808, 2010.

8 EXPLICIT SIZE REDUCTION TECHNIQUE

***

S. Koziel, A. Bekasiewicz, and P. Kurgan

Rapid Design and Size Reduction of Microwave Couplers Using Variable-Fidelity EM-Driven Optimization

Published in: *International Journal of RF and Microwave Computer-Aided Engineering*, vol. 26, no. 1, pp. 27–35, 2015.

DOI: 10.1002/mmce.20925

***

Abstract: In this article, fast electromagnetic (EM) simulation-driven design optimization of compact microwave couplers is addressed. The main focus is on explicit reduction of the circuit footprint. Our methodology relies on the penalty function approach, which allows us to minimize the circuit area while ensuring equal power split between the output ports and providing a sufficient bandwidth with respect to the return loss and isolation around the operating frequency. Computational efficiency of the design process is achieved by exploiting variable-fidelity EM simulations, local response surface approximation models, as well as suitable response correction techniques for design tuning. The technique described in this work is demonstrated using two examples of compact rat-race couplers. The size-reduction-oriented designs are compared with performance-oriented ones to illustrate available design trade-offs. Final design solutions of the former case illustrate ~92% of miniaturization for both coupler examples (with corresponding fractional bandwidths of 16%). Alternative design solutions pertaining to the latter case show a lesser size reduction (~90% for both examples), but present a much wider bandwidths (~25% for both couplers). The overall computational cost of the design procedure corresponds to about 20 and 10 high-fidelity coupler simulations for the first and second design example, respectively. Numerical results are also validated experimentally.

8.1 Introduction

Design closure using electromagnetic (EM) simulation tools is a necessary step of the microwave design process, in which geometry parameters of the structure at hand are adjusted to meet the prescribed performance requirements [1], [2]. The use of EM analysis is indispensable to account for complex phenomena such as cross-coupling effects (especially for compact circuits that feature highly compressed layouts) that normally cannot be accurately accounted for by theoretical means (e.g., equivalent circuits). Design closure can be realized automatically by numerical optimization [3], [4]. This is preferable when experience-driven approaches based on repetitive parameter sweeps fail or lead to inferior results, which is particularly true for complex design problems of compact structures, for example, rat-race couplers (RRCs) [5], [6] or branch-line couplers [7], [8]. In such instances, the objective is to accurately identify a design that satisfies given performance criteria, using limited computational resources. The fundamental obstacle here is the computational cost of high-fidelity EM analysis, which is excessive in case of complex structures featuring compact layouts (e.g., based on slow-wave resonant lines [5]). Consequently, direct optimization of high-fidelity EM models using gradient-based algorithms with numerical derivatives [3] or population-based metaheuristics [9], [10] is virtually prohibitive. The reason being a large number of objective function evaluations necessary to accomplish the optimization process (from dozens to thousands depending on the problem complexity).

Challenges of reliable simulation-driven design can be addressed using surrogate-based optimization (SBO) techniques [11], [12] such as space mapping (SM) [13], [14]. These, however, often rely on cheap and fairly accurate circuit models, which are usually not available for geometrically complex small-size structures [15], [16].

Another issue is a simultaneous control of the size of the structure (which might be of primary concern) and its electrical performance. This requires handling of multiple, non-commensurable objectives such as size, bandwidth, power division ratio, and so forth. Approaches such as weighted sum method are not suitable for solving this particular problem because they only allow for trading off some of the objectives for others, with no precise control over either of them. In state-of-the-art works on compact microwave components, circuit miniaturization is dealt with indirectly (as a result of initial compact circuit topology) [17], [18]. At the same time, solving this problem using evolutionary multi-objective optimization algorithms requires tens of thousands of objective function calls and is infeasible for any EM-simulation models used in the process [9], [10], [19].

In this article, we introduce an explicit miniaturization-oriented formulation of the compact circuit design using an expanded penalty function approach. The latter allows us to enforce satisfaction of the prescribed design specifications concerning electrical performance of the circuit, while formulating the entire problem as a single-objective task with the scalar objective function. The cost of EM-based design optimization is kept at practically acceptable levels by exploiting a design strategy that involves multiple EM models of variable fidelity as well as local response surface approximation surrogates [20]. Our approach is demonstrated using two examples of compact RRCs and compared with the alternative results obtained by reformulating the objective into electrical-performance-driven design as well as state-of-the-art methods. Experimental validation of the designs is also provided.

8.2 Design Optimization Using Multi-Fidelity Electromagnetic Models

In this section, we formulate the optimization problem, define the objective function for size-reduction-oriented design, as well as outline the optimization procedure exploiting multi-fidelity EM-simulation models. Design case studies as well as experimental validation are presented in Section 8.3.

8.2.1 Problem Formulation and Objective Function

We will use the symbol $\boldsymbol{S}_f(\boldsymbol{x}) = [S_{11.f}(\boldsymbol{x})\ S_{21.f}(\boldsymbol{x})\ S_{31.f}(\boldsymbol{x})\ S_{41.f}(\boldsymbol{x})]$ to denote the high-fidelity EM-simulated model of the compact coupler of interest, specifically, its essential *S*-parameters versus frequency as functions of geometry parameters represented by a vector $\boldsymbol{x}$. Let $A(\boldsymbol{x})$ denote the coupler footprint area. The goal is to solve the following optimization problem

$$\boldsymbol{x}_f^* = \arg\min_{\boldsymbol{x}} U\left(A(\boldsymbol{x}), \boldsymbol{S}_f(\boldsymbol{x})\right) \tag{8.1}$$

where U is a given objective function.

Although our primary objective is to minimize $A(\boldsymbol{x})$, the process is subject to ensuring sufficient electrical performance of the coupler. The following requirements are considered here:

- $d_S = |S_{21.f}(\boldsymbol{x}) - S_{31.f}(\boldsymbol{x})| \le \varepsilon$ at the operating frequency (the threshold value for the examples considered in Section 8.3 is set to be $\varepsilon = 0.2$ dB);
- $S_{\max} = \max(\min\{S_{11.f}(\boldsymbol{x}), S_{41.f}(\boldsymbol{x})\}) \le S_m$ (we assume $S_m = -25$ dB);
- $f_{S11.f}(\boldsymbol{x})$ and $f_{S41.f}(\boldsymbol{x})$, i.e., the frequencies realizing minimum of $S_{11.f}(\boldsymbol{x})$ and $S_{41.f}(\boldsymbol{x})$, respectively, are as close to the operating frequency f_0 as possible.

The above requirements are supposed to ensure (with certain tolerance) an equal power split as well as sufficient return loss and isolation in the vicinity of the operational frequency. In order to take these specifications into account, the objective function has been defined as follows:

$$\begin{aligned} U\left(A(\boldsymbol{x}), \boldsymbol{S}_f(\boldsymbol{x})\right) &= A(\boldsymbol{x}) + \beta_1\left(\max\left\{\left(d_S - \varepsilon\right)/\varepsilon, 0\right\}\right)^2 + \\ &+ \beta_2\left(\max\left\{\left(S_{\max} - S_m\right)/|S_m|, 0\right\}\right)^2 + \\ &+ \beta_{f1}\left|\left(f_{S_{11.f}}(\boldsymbol{x}) - f_0\right)/f_0\right|^2 + \beta_{f2}\left|\left(f_{S_{41.f}}(\boldsymbol{x}) - f_0\right)/f_0\right|^2 \end{aligned} \tag{8.2}$$

It should be noted that the penalty functions are defined so that they only contribute to the objective function if the aforementioned performance conditions are violated. The coefficients β_1, β_2, β_{f1}, and β_{f2} are chosen so that corresponding functions take noticeable values (when compared to $A(\boldsymbol{x})$) for relative violations larger than a few percent. Here, we use 1000 for all β factors, however, this specific value is not critical. At the same time, the penalty functions are smooth (in particular, continuous and differentiable) with respect to the respective performance figures, which is important from the optimization process standpoint.

It should be emphasized that formulation (8.2) is qualitatively different from, for example, a weighted sum approach. In (8.2), the footprint size is given a full priority, whereas electrical performance parameters only affect U if their assumed thresholds are violated. Owing to this formulation, the optimum design obtained by solving (8.1), (8.2) represents the smallest possible circuit area which still satisfies the remaining conditions concerning the power split and the bandwidth.

8.2.2 Multi-Fidelity Optimization Algorithm

The main optimization engine utilized in this work is a multi-fidelity algorithm [21]. Its most important advantages are as follows:

1. It only relies on EM-simulation models,
2. It allows—because of using variable-fidelity simulations—for considerable savings of the design cost compared with conventional methods solely based on time-consuming high-fidelity simulations.

The first feature is important in the context of compact circuit design because the quality (accuracy) of lumped-element equivalent circuit models as well as their generalization capabilities are normally very poor for such structures. This is because compact components are characterized by intricate topologies, arranged as a composition of high- and low-impedance segments, which

means that they are too complex to be precisely described by simplified theoretical means. The second feature permits computationally feasible EM-driven optimization with the final design obtained in reasonable timeframe.

The multi-fidelity algorithm exploits a family of coarse-discretization EM models of increasing fidelity $\{\boldsymbol{S}_{c.j}\}$, $j = 1, \ldots, K$, where $\boldsymbol{S}_{c.j+1}$ is finer than $\boldsymbol{S}_{c.j}$, which translates into better accuracy, but also longer evaluation time. As opposed to lumped-element equivalent circuits, coarse-discretization models offer relatively good prediction and generalization capabilities [22]. They are also universally available, being implemented and evaluated by the same simulation tool as the one used for the high-fidelity model $\boldsymbol{S}_f$. Coarse-discretization EM models are obtained mainly by applying relaxed mesh requirements to $\boldsymbol{S}_f$ (however, other simplifications are also commonly used, e.g., perfect conductor of infinitesimal thickness instead of thick copper, lossless and/or isotropic dielectric substrate, smaller computational domain, discrete source instead of waveguide ports, etc.). In practice, the discretization density is directly controlled by customized solver-dependent mesh settings, that is, through the number of mesh cells per wavelength pertaining to the highest frequency used during the simulation. Thus, the high-fidelity model $\boldsymbol{S}_f$ is found by increasing the number of circuit mesh cells per wavelength, so that the current distribution at the smallest part of the circuit under analysis changes gradually instead of rapidly. At this point, further increase of the mesh density does not translate into a notable change in the response of the structure of interest. Conversely, the decrease of mesh density leads to a dramatic CPU cost reduction for a given low-fidelity model, however, obtained at the cost of lesser accuracy. In general, it is not obvious how to find an appropriate trade-off between model accuracy and its evaluation time. The rule of thumb is that the evaluation time of $\boldsymbol{S}_c$ should be as small as possible (preferably two orders of magnitude or more in comparison to $\boldsymbol{S}_f$), assuming that the performance of the low-fidelity models preserves key features of its high-fidelity counterpart (e.g., shape of frequency characteristics, the occurrence of a resonance within a given frequency range, etc.), so that the misalignments between the two can be corrected by frequency scaling or similar mapping techniques [23].

The multi-fidelity algorithm works as follows. Starting from the initial design $\boldsymbol{x}^{(0)}$, the coarse-discretization EM model of the lowest fidelity, $\boldsymbol{S}_{c.1}$, is optimized to arrive at $\boldsymbol{x}^{(1)}$, which is the first approximation of the high-fidelity model optimum. The initial design is typically chosen based on experience-guided preliminary studies (e.g., sparse parameter sweeps) done on a very cheap physics-based model (e.g., equivalent circuit). Additionally, the lower and upper bounds for the optimization are determined based on engineering insight and to ensure sufficient flexibility of the structure under design. Having obtained $\boldsymbol{x}^{(1)}$, it is subsequently used as the starting point for the optimization of the second (finer) model, $\boldsymbol{S}_{c.2}$, to produce a more accurate approximation of the high-fidelity model optimum, $\boldsymbol{x}^{(2)}$. The process continues until the optimum $\boldsymbol{x}^{(K)}$ of the finest coarse-discretization model $\boldsymbol{S}_{c.K}$ is found. Typically, only a few $\boldsymbol{S}_c$ models are needed for fast convergence of the discussed algorithm. Here, we use $K = 2$. The models are optimized by conventional means (here, using the pattern search algorithm [24]) [20]. The particular implementation of the pattern search algorithm utilized here follows [25]. It is a stencil-based search using a rectangular grid, equipped with a grid-restricted line search (utilizing gradient estimation obtained from the pattern-based design perturbations).

Having the optimized design $\boldsymbol{x}^{(K)}$ of the finest coarse-discretization model $\boldsymbol{S}_{c.K}$, we evaluate it at perturbed designs around $\boldsymbol{x}^{(K)}$, that is, at $\boldsymbol{x}_k^{(K)} = [x_1^{(K)} \ldots x_k^{(K)} + \text{sign}(k)\cdot d_k \ldots x_n^{(K)}]^T$, $k = -n, -n + 1, \ldots, n - 1, n$. We use the notation $\boldsymbol{S}^{(k)} = \boldsymbol{S}_{c.K}(\boldsymbol{x}_k^{(K)})$. This data is used to refine the final design without directly optimizing $\boldsymbol{S}_f$. Instead, we set up an approximation model based on $\boldsymbol{S}^{(k)}$, and optimize it in the neighborhood of $\boldsymbol{x}^{(K)}$ defined as $[\boldsymbol{x}^{(K)} - \boldsymbol{d}, \boldsymbol{x}^{(K)} + \boldsymbol{d}]$, where $\boldsymbol{d} = [d_1\ d_2 \ldots d_n]^T$.

The approximation is performed using a reduced quadratic model $\boldsymbol{q}(\boldsymbol{x}) = [q_1\ q_2 \ldots q_m]^T$, defined as [20], [26]

$$q_j(\boldsymbol{x}) = q_j\left(\left[x_1 \ldots x_n\right]^T\right) = \lambda_{j.0} + \sum_{k=1}^{n} \lambda_{j.k} x_k + \sum_{k=1}^{n} \lambda_{j.n+k} x_k^2 \tag{8.3}$$

Coefficients $\lambda_{j.r}$ can be found analytically [21] by solving a system of linear regression problems of the form $q_j(\boldsymbol{x}_k^{(K)}) = \boldsymbol{S}_{c.K}(\boldsymbol{x}_k^{(K)})$ for $k = -n, \ldots, 0, \ldots, n$.

In the final step, the refined design is found as

$$\boldsymbol{x}^* = \arg\min_{\boldsymbol{x}^{(K)}-\boldsymbol{d}\le\boldsymbol{x}\le\boldsymbol{x}^{(K)}+\boldsymbol{d}} U\left(\boldsymbol{q}(\boldsymbol{x}) + \Delta\boldsymbol{q}\left(\boldsymbol{x}^{(K)}\right)\right) \tag{8.4}$$

where the output SM term $\Delta\boldsymbol{q}(\boldsymbol{x}^{(K)}) = \boldsymbol{S}_f(\boldsymbol{x}^{(K)}) - \boldsymbol{S}_{c.K}(\boldsymbol{x}^{(K)})$ [13] accounts for misalignment between $\boldsymbol{S}_{c.K}$ and $\boldsymbol{S}_f$. The optional frequency scaling of $\boldsymbol{q}$ [13] is also possible to account for frequency shift between $\boldsymbol{S}_{c.K}$ and $\boldsymbol{S}_f$. If necessary, step (8.4) can be repeated starting from a refined design, that is, $\boldsymbol{x}^* = \text{argmin}\{\boldsymbol{x}^{(K)} - \boldsymbol{d} \le \boldsymbol{x} \le \boldsymbol{x}^{(K)} + \boldsymbol{d} : U(\boldsymbol{q}(\boldsymbol{x}) + \Delta\boldsymbol{q}(\boldsymbol{x}^*)$ (each iteration requires only one evaluation of $\boldsymbol{S}_f$). Figure 8.1 shows the flow diagram of the multi-fidelity optimization algorithm.

8.3 Design Case Studies

In this section, we demonstrate the design optimization approach of Section 8.2 using two examples of compact microstrip RRCs with equal power split. The operating frequency is f_0 = 1 GHz. Both designs are implemented on a Taconic RF-35 dielectric substrate (ε_r = 3.5, tanδ = 0.0018, h = 0.762 mm) and fed using 50-Ω transmission lines of width w_0 = 1.7 mm and length l_0 = 15 mm. For the sake of comparison, a reference coupler of a rectangle shape [27] is designed based on the above specifications. The structure footprint is 4536 mm^2 (47.5 mm × 95.5 mm).

8.3.1 Rat-Race Coupler Based on Slow-Wave Resonant Structures

Our first design example is a RRC constructed using slow-wave resonant structures (SWRSs) [28], [29]. The RRC geometry is shown in Figure 8.2. Each SWRS is built using a cascade of two low-impedance stubs connected by high-impedance meander lines. The design variables are $\boldsymbol{x} = [w_1\ l_1\ w_2\ l_2\ w_3]^T$. The parameters $l_3 = 19w_1 + 18w_2 + w_3 - l_1$, $l_4 = 5w_1 + 6w_2 + l_2 + w_3$, $l_5 = 3w_1 + 4w_2$ and $w_4 = 9w_1 + 8w_2$. The unit for all dimensions is mm. The initial design is: $\boldsymbol{x}^{(0)} = [0.35\ 4\ 0.35\ 2\ 0.35]^T$. The lower/upper bounds $\boldsymbol{l}/\boldsymbol{u}$ are: $\boldsymbol{l} = [0.2\ 2\ 0.2\ 1\ 0.15]^T$, and $\boldsymbol{u} = [0.5\ 5\ 0.5\ 3\ 0.5]^T$.

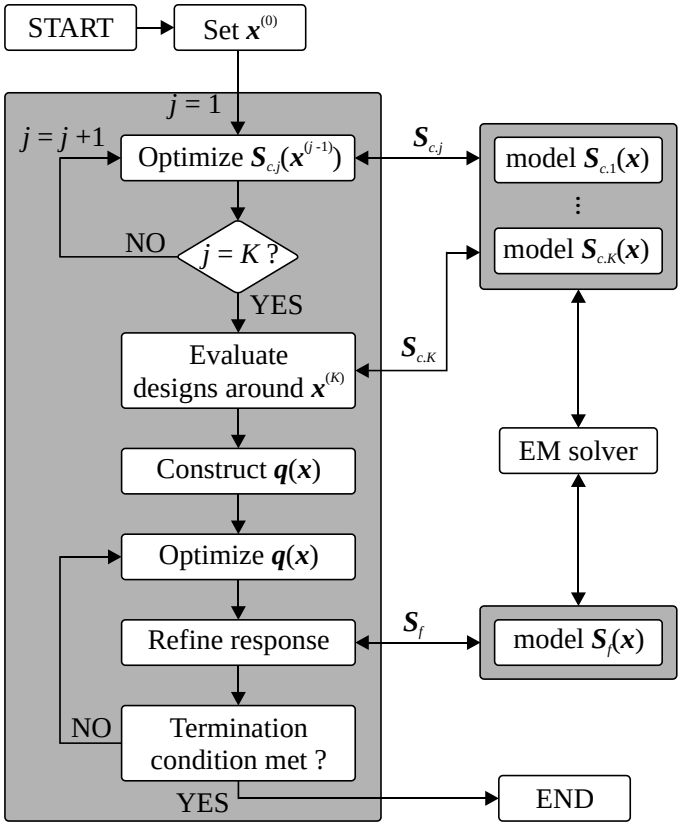

Figure 8.1: Flowchart of the multi-fidelity EM-driven design optimization algorithm.

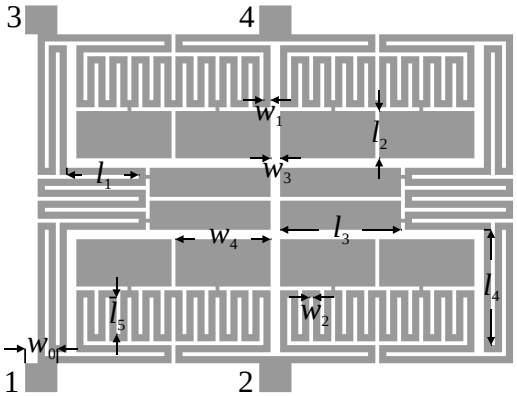

Figure 8.2: Layout of the compact RRC composed of slow-wave resonant structures.

Three models of the RRC, that is, two low- and one high-fidelity, are prepared in CST Microwave Studio and simulated using its frequency domain solver [30]. The $\boldsymbol{S}_{c.1}$ comprises about 44,500 mesh cells and its average simulation time is 100 s. Model $\boldsymbol{S}_{c.2}$ consists of ~120,000 cells and its evaluation time is 312 s. The high-fidelity structure $\boldsymbol{S}_f$ is constructed using ~302,000 mesh cells (simulation time: 30 min). For the sake of comparison, a circuit representation of the RRC is prepared in Agilent ADS [31]. Responses of all models at the selected initial design are shown in Figure 8.3. Note that the poor quality of the network representation makes it virtually useless for anything other than yielding an initial design. This is mostly due to considerable cross-couplings within the structure that can only be accounted for by means of full-wave EM simulations [27], [32].

The main goal of the design process is miniaturization of the coupler, however, we also consider electrical performance to illustrate the trade-offs of compact RRCs. The first objective is maximization of the coupler bandwidth (defined as the frequency range where both return loss $|S_{11}|$ and isolation $|S_{41}|$ are below −20 dB level). The second goal is miniaturization of the coupler footprint using the objective function (8.2) of Section 8.2.1. The area is defined as a rectangle $A \times B$ where $A = 2l_2 + 8w_1 + 7w_2$ and $B = 42w_1 + 3w_3 + 40w_2$.

The circuit is optimized using the algorithm of Section 8.2.2. Dimensions of the structure optimized with respect to bandwidth are $\boldsymbol{x}^* = [0.38\ 4.04\ 0.2\ 2.58\ 0.32]^T$. The structure exhibits over 25% bandwidth for the center frequency and simultaneously offers 90.7% miniaturization ($17.2 \times 24.5 = 422$ mm^2) compared with the conventional RRC. The dimensions of the miniaturized coupler are $\boldsymbol{x}^* = [0.33\ 2.4\ 0.21\ 2.51\ 0.1]^T$. The corresponding operational bandwidth of the structure is 16%, whereas its area reduction rate is 92.4% ($15.7 \times 22.0 = 346$ mm^2). Both optimized RRCs were fabricated and measured. The comparison of their simulated and measured characteristics is shown in Figure 8.4. For the structure optimized with respect to the bandwidth, the obtained insertion loss at the center frequency is 2.93 dB and 3.24 dB for the simulation and measurement, respectively, whereas the coupling values are 3.13 dB and 3.32 dB, respectively. The miniaturized circuit features insertion loss and coupling of 2.94 dB and 3.18 dB for simulation, as well as 3.11 dB and 3.38 dB for measurements, respectively. It should be noted that the measured circuit exhibits about 0.21-dB higher loss in comparison to the simulation results. The reason is probably the lack of SMA connectors in the EM model used here. Overall, the simulation and measurement results are in good agreement.

The total aggregated cost of coupler optimization with respect to bandwidth corresponds to about 19.3 $\boldsymbol{S}_f$ simulations (~9.7 h) and it includes: 60 and 70 simulations of $\boldsymbol{S}_{c.1}$ and $\boldsymbol{S}_{c.2}$ during the first two steps of the optimization process, as well as 11 $\boldsymbol{S}_{c.2}$ required for construction of approximation model $\boldsymbol{q}$. The cost of the refinement stage is 2 $\boldsymbol{S}_f$ evaluations. The miniaturization of RRC required about 22.1 $\boldsymbol{S}_f$ (~11.5 h) including 60 simulations of $\boldsymbol{S}_{c.1}$, a total of 91 $\boldsymbol{S}_{c.2}$ evaluations and 3 $\boldsymbol{S}_f$ simulations for model correction. The detailed cost breakdown is reported in Table 8.1.

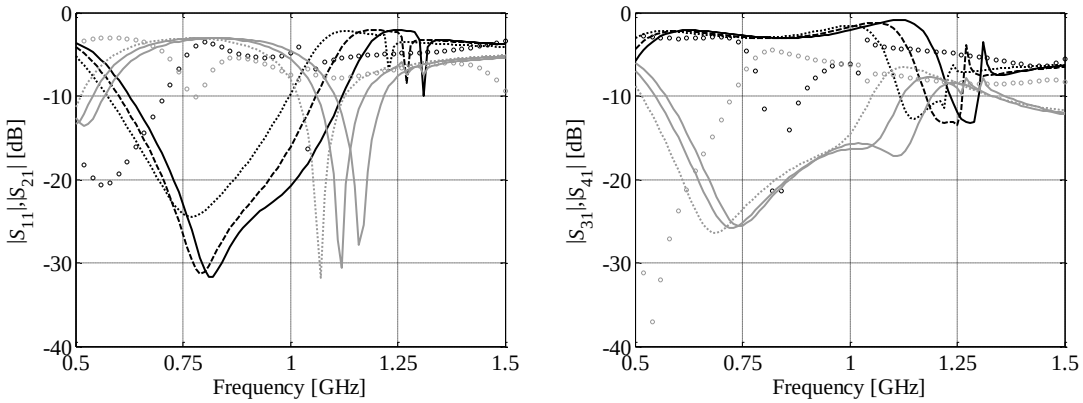

Figure 8.3: Comparison of RRC model responses at a selected design: $\boldsymbol{S}_{c.0}$ (○ ○ ○), $\boldsymbol{S}_{c.1}$ (——), $\boldsymbol{S}_{c.2}$ (– –), $\boldsymbol{S}_f$ (·····). (a) black line – $|S_{11}|$, gray line $|S_{21}|$; (b) black line – $|S_{31}|$, gray line $|S_{41}|$. Poor performance of the equivalent circuit model $\boldsymbol{S}_{c.0}$ limits its utilization as a low-fidelity model for EM-driven optimization.

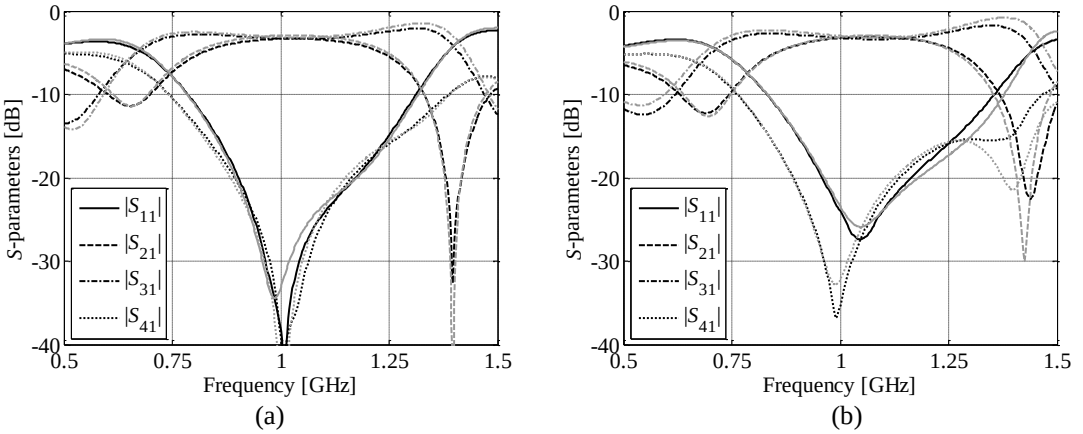

Figure 8.4: Simulated (gray lines) and measured (black lines) frequency characteristics of a compact SWRS-based RRC: (a) design optimized for bandwidth; (b) coupler optimized for size reduction.

Reduction of the CPU time is not the aim of this work; however, it is a highly desirable byproduct of the automated multi-fidelity algorithm utilized in the process. The computational efficiency of the proposed approach—in case of bandwidth-oriented RRC design—is compared with other competitive SBO methods, including implicit space mapping (ISM) and sequential space mapping (SSM), previously utilized for the design of compact structures. Moreover, a conventional direct optimization of the $\boldsymbol{S}_f$ model is performed. The obtained results are gathered in Table 8.2.

While the numerical cost of the variable-fidelity method is comparable to other SBO approaches, the latter are more difficult to implement and require considerable engineering insight. This is because ISM and SSM exploit circuit model representation of the structure which cannot accurately mimic the behavior of complex design. In both approaches, the problem is mitigated by utilization of implicit parameters that are iteratively optimized to fit the surrogate to the response of the high-fidelity model. Unfortunately, ranges of implicit parameters depend on the specific problem and they are to be defined manually based on a number of tests. Additionally, the former of the competitive techniques suffers from convergence issues, so that it cannot always guarantee effective optimization. Even if the results are close to optimum, the algorithm needs to be terminated manually. In contrast, the method discussed in this work is more generic and automated. Consequently, it is attractive in comparison to other SBO approaches. It should be noted that direct optimization of the circuit is virtually impractical.

TABLE 8.1: OPTIMIZATION COST OF THE SWRS-BASED RRC

Design Case	Algorithm Step	Number of Model Evaluations	Evaluation Time	
			Absolute [min]	Relative to $\boldsymbol{S}_f$
Optimization for electrical performance	Optimization of $\boldsymbol{S}_{c.1}$	$60 \times \boldsymbol{S}_{c.1}$	100	3.3
	Optimization of $\boldsymbol{S}_{c.2}$	$70 \times \boldsymbol{S}_{c.2}$	364	12.1
	Setup of model $\boldsymbol{q}$	$11 \times \boldsymbol{S}_{c.2}$	57	1.9
	Evaluation of $\boldsymbol{S}_f$	$2 \times \boldsymbol{S}_f$	60	2.0
	Total time	N/A	**581**	**19.3**
Optimization for reduced size	Optimization of $\boldsymbol{S}_{c.1}$	$60 \times \boldsymbol{S}_{c.1}$	100	3.3
	Optimization of $\boldsymbol{S}_{c.2}$	$80 \times \boldsymbol{S}_{c.2}$	416	13.9
	Setup of model $\boldsymbol{q}$	$11 \times \boldsymbol{S}_{c.2}$	57	1.9
	Evaluation of $\boldsymbol{S}_f$	$3 \times \boldsymbol{S}_f$	90	3.0
	Total time	N/A	**663**	**22.1**

TABLE 8.2: COMPUTATIONAL COST OF RRC OPTIMIZATION USING DIFFERENT ROUTINES

Optimization technique	Cost of low-fidelity evaluations	Number of high-fidelity evaluations	Evaluation time	
			Absolute [min]	Total cost (relative to $\boldsymbol{S}_f$)
This work	$17.3 \times \boldsymbol{S}_f$	$2 \times \boldsymbol{S}_f$	581	19.3
ISM [23]	$7.4 \times \boldsymbol{S}_f$	$15 \times \boldsymbol{S}_f$	702	22.4
SSM [33]	$6.3 \times \boldsymbol{S}_f$	$13 \times \boldsymbol{S}_f$	621	19.3
Direct optimization [24]	N/A	$236 \times \boldsymbol{S}_f$	7080	236

8.3.2 Folded Rat-Race Coupler

Consider a folded RRC illustrated in Figure 8.5 [34]. The structure is composed of four 70.7-Ω sections (the same impedance as in a conventional RRC) that are folded to reduce the structure footprint. The design variables of the circuit are represented by a vector $\boldsymbol{x} = [l_1\ l_2\ l_3\ d\ w]^T$. The high-fidelity model $\boldsymbol{S}_f$ comprises about 210,000 mesh cells and its average simulation time is 20 min. Additionally, two low-fidelity models of the structure are prepared, that is, $\boldsymbol{S}_{c.1}$ (~7,100 mesh cells, 40 s average evaluation time) and $\boldsymbol{S}_{c.2}$ (~21,000 cells, simulation time of 110 s). All models are implemented in CST Microwave Studio.

The lower and upper bounds are: $\boldsymbol{l} = [2\ 10\ 17\ 0.2\ 0.5]^T$, and $\boldsymbol{u} = [12\ 20\ 28\ 1.2\ 2.5]^T$. Initial design parameters are set to $\boldsymbol{x}^{(0)} = [7\ 15\ 22.5\ 0.7\ 1.5]^T$. The design objectives are the same as in Section 8.3.1, that is, (i) maximization of bandwidth, and (ii) minimization of size. The coupler area is defined as a rectangle $A \times B$, where $A = 6w + 7d$ and $B = 8w + 7d + 2w_0 + l_1 + l_2 + l_3$.

The optimal design parameters pertaining to (i) and (ii) are $\boldsymbol{x}^* = [3.67\ 13\ 20.6\ 0.75\ 0.87]^T$ and $\boldsymbol{x}^* = [4.35\ 11.9\ 22.05\ 0.36\ 0.83]^T$, respectively. The former circuit exhibits 26% bandwidth and simultaneously offers 89.4% miniaturization ($8.9 \times 53.7 = 480$ mm^2) comparing to the reference structure. The miniaturization rate of the latter RRC is 92.3% ($6.8 \times 51.7 = 349$ mm^2), whereas the corresponding bandwidth is 16%. Note that a substantial area reduction is obtained at the expense of a shifted center frequency. Nonetheless, the design still satisfies the requirements defined in Section 8.2.1. Both optimized structures have been fabricated and measured (cf. Figure 8.6). The comparison of the simulated and measured characteristics is shown in Figure 8.7. The results are in good agreement. In case of bandwidth-oriented design, the insertion loss at the center frequency is 2.96 dB and 3.21 dB for simulation and measurement, respectively, whereas the coupling values are 3.1 dB and 3.3 dB. At the same time, the simulated response of the coupler optimized for footprint reduction exhibits 2.9 dB and 3.21 dB of insertion loss and cou-

pling, respectively. The corresponding measured values are 3.13 dB and 3.35 dB. Similarly to the previous design example, the EM model lacks SMA connectors, which is a probable reason for additional losses of 0.2 dB.

The total cost of coupler optimization with respect to (i) corresponds to 9.5 $\boldsymbol{S}_f$ evaluations (including a total of 60 × $\boldsymbol{S}_{c.1}$, 71 ×$\boldsymbol{S}_{c.2}$, and 2 × $\boldsymbol{S}_f$ simulations), whereas the cost of (ii) is about 12.4 $\boldsymbol{S}_f$ evaluations (60 × $\boldsymbol{S}_{c.1}$, 81 × $\boldsymbol{S}_{c.2}$, and 3 × $\boldsymbol{S}_f$). The detailed data concerning the optimization cost of both designs are provided in Table **8.3**. The efficiency of the algorithm is compared with ISM technique and a direct search approach (the SSM method is not suitable for the considered coupler). Although the computational efficiency of the compared SBO techniques is similar, the discussed approach is more attractive to design optimization of compact circuits. The reasons have been stated in Section 8.3.1 while discussing the previous example. The cost of direct optimization is two orders higher than SBO, so that it is impractical from the numerical standpoint. The detailed results are listed in Table 8.4.

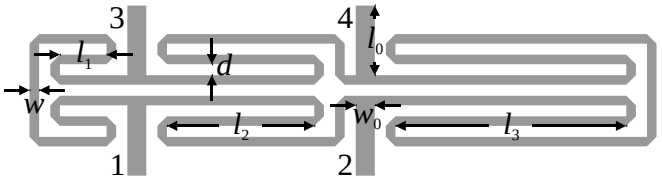

Figure 8.5: Layout of the folded RRC.

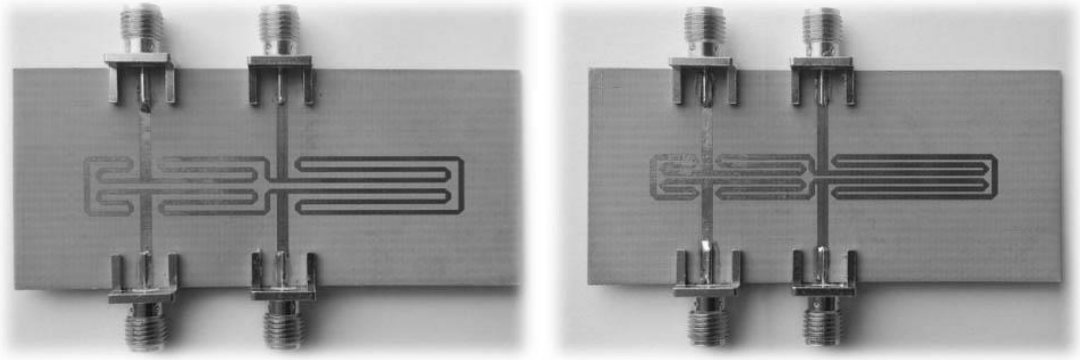

(a) (b)

Figure 8.6: Photograph of the fabricated folded RRCs: (a) bandwidth-oriented and (b) area-reduction-oriented designs.

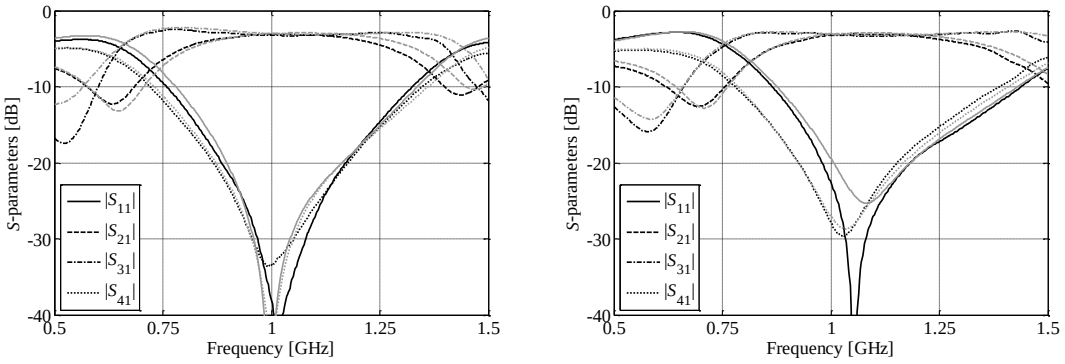

(a) (b)

Figure 8.7: Simulated (gray lines) and measured (black lines) frequency characteristics of two folded RRC designs. Responses of a coupler: (a) optimized for bandwidth; (b) optimized for size reduction.

TABLE 8.3: OPTIMIZATION COST OF THE FOLDED RRC

Design Case	Algorithm Step	Number of Model Evaluations	Evaluation Time	
			Absolute [min]	Relative to $\boldsymbol{S}_f$
Optimization for electrical performance	Optimization of $\boldsymbol{S}_{c.1}$	$60 \times \boldsymbol{S}_{c.1}$	40	2.0
	Optimization of $\boldsymbol{S}_{c.2}$	$60 \times \boldsymbol{S}_{c.2}$	110	5.5
	Setup of model $\boldsymbol{q}$	$11 \times \boldsymbol{S}_{c.2}$	20	1.0
	Evaluation of $\boldsymbol{S}_f$	$2 \times \boldsymbol{S}_f$	40	2.0
	Total time	N/A	**190**	**9.5**
Optimization for reduced size	Optimization of $\boldsymbol{S}_{c.1}$	$60 \times \boldsymbol{S}_{c.1}$	40	2.0
	Optimization of $\boldsymbol{S}_{c.2}$	$70 \times \boldsymbol{S}_{c.2}$	128	6.4
	Setup of model $\boldsymbol{q}$	$11 \times \boldsymbol{S}_{c.2}$	20	1.0
	Evaluation of $\boldsymbol{S}_f$	$3 \times \boldsymbol{S}_f$	60	3.0
	Total time	N/A	**248**	**12.4**

TABLE 8.4: COST OF RRC OPTIMIZATION USING DIFFERENT ROUTINES

Optimization technique	Cost of low-fidelity evaluations	Number of high-fidelity evaluations	Evaluation time	
			Absolute [min]	Total cost (relative to $\boldsymbol{S}_f$)
This work	$7.5 \times \boldsymbol{S}_f$	$2 \times \boldsymbol{S}_f$	190	9.5
ISM [23]	$2.9 \times \boldsymbol{S}_f$	$6 \times \boldsymbol{S}_f$	168	8.9
Direct optimization [24]	N/A	$103 \times \boldsymbol{S}_f$	2060	103

8.4 Conclusion

In this work, we have addressed the issue of optimization-driven size reduction of microwave couplers. We presented a cost function formulation that explicitly aims at circuit area minimization, with penalty components ensuring a required output power division ratio as well as sufficient bandwidth determined for the return loss and isolation. Our approach allows for direct size minimization while controlling electrical performance of the circuit. As demonstrated through examples, low CPU cost of the design process can be maintained by embedding it into the variable-fidelity optimization scheme. The technique described in the article can also be utilized (upon appropriate modification of the objective function) for design optimization of other passive components.

Acknowledgement

The authors thank Computer Simulation Technology AG, Darmstadt, Germany, for making CST Microwave Studio available. This work was supported in part by the Icelandic Centre for Research (RANNIS) Grant 130450051.

References

[1] P. Kurgan and A. Bekasiewicz, "A robust design of a numerically demanding compact rat-race coupler," *Microw. Opt. Techn. Lett.*, vol. 56, pp. 1259–1263, 2014.

[2] A. Bekasiewicz and P. Kurgan, "A compact microstrip rat-race coupler constituted by nonuniform transmission lines," *Microw. Opt. Techn. Lett.*, vol. 56, pp. 970–974, 2014.

[3] J. Nocedal and S.J. Wright, *Numerical Optimization*, 2nd edition, Springer, New York, 2006.

[4] A.R. Conn, K. Scheinberg, and L.N. Vicente, *Introduction to Derivative-Free Optimization*, MPS-SIAM Series on Optimization, MPS-SIAM, 2009.

[5] C.-H. Tseng and H.-J. Chen, "Compact Rat-Race Coupler Using Shunt-Stub-Based Artificial Transmission Lines," *IEEE Microw. Wireless Comp. Lett.*., vol. 18, no. 11, pp. 734–736, 2008.

[6] S. Taravati, "Miniaturized wide-band rat-race coupler," *Int. J. RF Microw. Comp. Aid. Eng.*, vol. 23, no. 6, pp. 675–681, 2013.

[7] M. Nosrati, M. Daneshmand, and B.S. Virdee, "Novel compact dual-narrow/wideband branch-line couplers using T-Shaped stepped-impedance-stub lines," *Int. J. RF Microw. Comp. Aid. Eng.*, vol. 21, no. 6, pp. 642–649, 2011.

[8] G. Monti and L. Tarricone, "Dual-band artificial transmission lines branch-line coupler," *Int. J. RF Microw. Comp. Aid. Eng*., vol. 18, no.1, pp. 53–62, 2008.

[9] Y. Kuwahara, "Multiobjective optimization design of Yagi-Uda antenna," *IEEE Trans. Ant. Prop.*, vol. 53, no. 6, pp. 1984–1992, 2005.

[10] S.H. Yeung and K.F. Man, "Multiobjective Optimization," *IEEE Microw. Mag*., vol. 12, no. 6, pp. 120–133, 2011.

[11] S. Koziel, X.-S. Yang, and Q.-J. Zhang (Eds.), *Simulation-Driven Design Optimization and Modeling for Microwave Engineering*, Imperial College Press, 2013.

[12] N.V. Queipo, R.T. Haftka, W. Shyy, T. Goel, R. Vaidynathan, and P.K. Tucker, "Surrogate based analysis and optimization," *Prog. Aerospace Sci*., vol. 41, no. 1, pp. 1–28, 2005.

[13] J.W. Bandler, Q.S. Cheng, S.A. Dakroury, A.S. Mohamed, M.H. Bakr, K. Madsen, and J. Sondergaard, "Space mapping: the state of the art," *IEEE Trans. Microw. Theory Tech.*, vol. 52, no. 1, pp. 337–361, 2004.

[14] S. Koziel and L. Leifsson (Eds.), *Surrogate-based modeling and optimization: applications in engineering*, Springer, 2013.

[15] S. Koziel, A. Bekasiewicz, and P. Kurgan, "Rapid EM-driven design of compact RF circuits by means of nested space mapping," *IEEE Microw. Wireless Comp. Lett,*, vol. 24, no. 6, pp. 364–366, 2014.

[16] S. Koziel and P. Kurgan, "Low-cost optimization of compact branch-line couplers and its application to miniaturized Butler matrix design," *European Microw. Conf.*, pp. 227–230, 2014.

[17] C.-W. Wang, T.-G. Ma, and C.-F. Yang, "A new planar artificial transmission line and its applications to a miniaturized Butler matrix", *IEEE Trans. Microw. Theory Tech.*, vol. 55, no. 12, pp. 2792–2801, 2007.

[18] C.-H. Tseng and C.-L. Chang, "A rigorous design methodology for compact planar branch-line and rat-race couplers with asymmetrical T-structures", *IEEE Trans. Microw. Theory Tech.*, vol. 60, no. 7, pp. 2085–2092, 2012.

[19] N. Jin and Y. Rahmat-Samii, "Advances in particle swarm optimization for antenna designs: real-number, binary, single-objective and multiobjective implementations," *IEEE Tran. Antennas Propag*., vol. 55, no. 3, pp. 556–567, 2007.

[20] S. Koziel and S. Ogurtsov, "Computational-budget-driven automated microwave design optimization using variable-fidelity electromagnetic simulations," *Int. J. RF Microw. Com. Aid. Eng.*, vol. 23, no. 3, pp. 349–356, 2013.

[21] S. Koziel and S. Ogurtsov, "Robust multi-fidelity simulation-driven design optimization of microwave structures," *IEEE MTT-S Int. Microw. Symp. Dig*., pp. 201–204, 2010.

[22] S. Koziel, J.W. Bandler, and K. Madsen, "Quality assessment of coarse models and surrogates for space mapping optimization," *Opt. Eng.*, vol. 9, no. 4, pp. 375–391, 2008.

[23] S. Koziel, Q.S. Cheng, and J.W. Bandler, "Space mapping," *IEEE Microw. Mag.*, vol. 9, no. 6, pp. 105–122, 2008.

[24] T.G. Kolda, R.M. Lewis, and V. Torczon, "Optimization by direct search: new perspectives on some classical and modern methods," SIAM Review, vol. 45, no. 3, pp. 385–482, 2003.

[25] S. Koziel, "Computationally efficient multi-fidelity multi-grid design optimization of microwave structures," *Appl. Comp. Electromag. Soc. J.*, vol. 25, no. 7, pp. 578–586, 2010.

[26] S. Koziel and S. Ogurtsov, "Microwave design optimization using local response surface approximations and variable-fidelity electromagnetic models," *Int. J. RF Microwave CAE*, vol. 23, no. 3, pp. 349–356, 2013.

[27] S. Koziel, P. Kurgan, and B. Pankiewicz, "Cost-efficient design methodology for compact rat-race couplers," *Int. J. RF Microw. Comp. Aid. Eng.*, vol. 25, no. 3, pp. 236–242, 2015.

[28] P. Kurgan and M. Kitlinski, "Doubly miniaturized rat-race hybrid coupler" *Microw. Opt. Technol. Lett*., vol. 53, pp. 1242–1244, 2011.

[29] P. Kurgan, J. Filipcewicz, and M. Kitlinski, "Development of a compact microstrip resonant cell aimed at efficient microwave component size reduction," *IET Microw. Ant. Propag.*, vol. 6, no. 12, pp. 1291–1298, 2012.

[30] CST Microwave Studio, ver. 2013, CST AG, Bad Nauheimer Str. 19, D-64289 Darmstadt, Germany, 2013.

[31] Agilent ADS, ver. 2011.10, Agilent Technologies, 1400 Fountaingrove Parkway, Santa Rosa, CA 95403-1799, 2011.

[32] S.-Y., Yuan, M.-S. Shiau, S.-S. Liao, P.-T. Sun, and C.-T. Ho, "An extremely compact dual-band branch-line coupler," *Microw. Opt. Technol. Lett*., vol. 49, no. 12, pp. 3011–3014, 2007.

[33] A. Bekasiewicz, P. Kurgan, and M. Kitlinski, "A new approach to a fast and accurate design of microwave circuits with complex topologies," *IET Microw. Ant. Prop.*, vol. 6, no. 14, pp. 1616–1622, 2012.

[34] S. Koziel, A. Bekasiewicz, and P. Kurgan, "Size reduction of microwave couplers by EM-driven optimization," *IEEE MTT-S Int. Microw. Symp.*, pp. 1–3, 2015.

9 Multi-Objective Design Optimization of Compact Hybrid Couplers

***

P. Kurgan and S. Koziel

Surrogate-Assisted Multi-Objective Optimization of Compact Microwave Couplers

Published in: *Journal of Electromagnetic Waves and Applications*, vol. 30, no. 15, pp. 2067–2075, 2016.

DOI: 10.1080/09205071.2016.1230523

***

Abstract: This work presents a rigorous methodology for expedited simulation-driven multi-objective design of microwave couplers with compact footprints. The proposed approach is a viable alternative for computationally expensive population-based metaheuristics and exploits a surrogate-assisted point-by-point Pareto set determination scheme that utilizes—for the sake of computational efficiency—space-mapping-corrected equivalent circuit models. The technique is showcased using a complex design example of a compact rat-race coupler, for which a set of nine alternative design solutions is efficiently identified. The latter design solutions illustrate the best possible trade-offs between conflicting design objectives for the structure at hand, that is, its operational bandwidth and the layout area. The overall design cost corresponds to approximately twenty high-fidelity electromagnetic simulations of the miniaturized coupler. Several selected trade-off designs have been manufactured and measured for the purpose of method validation.

9.1 Introduction

Reliable design of compact microwave circuits for modern wireless communication systems is a challenging task that involves simultaneous adjustment of multiple designable parameters of the structure at hand to satisfy several, often conflicting, objectives such as size, bandwidth, phase response, etc. [1-3]. A common feature of such circuits, e.g., folded or fractal-shaped couplers [4-7], is a high computational cost of their accurate electromagnetic (EM) analysis that results from geometric complexity of miniaturized layouts. This proves to be a fundamental issue for simulation-driven design of compact components, especially when using conventional design strategies, such as repetitive parameter sweeps or direct single-objective optimization, both requiring numerous EM simulations to obtain satisfactory results [8]. On the other hand, alternative means of circuit analysis (e.g., exploiting transmission line theory) are grossly inaccurate and—for the most part—merely capable of providing initial design solutions [9]. This is particularly the case for highly miniaturized microwave circuits with strongly coupled building blocks (e.g., [10]).

To some extent, these shortcomings can be alleviated by surrogate-based optimization (SBO) techniques [11], such as space mapping (SM) [12], which have repeatedly demonstrated their computational superiority over commonly exploited direct optimization algorithms applied to design of conventional microwave circuits. SBO schemes benefit from low-cost surrogates that are well aligned with the high-fidelity EM models through adaptive corrections [13]. Taking advantage of the fact that vast majority of numerical operations are executed at the level of the suitably enhanced low-fidelity models, whereas their high-fidelity counterpart is used exclusively for occasional design verification and the surrogate model update, the overall computational cost of the SBO process might be kept low [14].

As opposed to conventional microwave circuits, compact devices are typically developed using novel topologies (e.g. [15]), for which the relationship between the size of the structure and its electrical parameters cannot be established prior to design itself. This significantly increases the risk of design failure, especially when excessively stringent specifications are applied to the prototype circuit. To formally address this issue, multi-objective optimization is required [3], [5]; the process aims at finding a so-called Pareto set that represents the best possible trade-offs between non-commensurable objectives [16]. The most popular solution approaches to this problem include population-based metaheuristics, such as genetic algorithms [16]. While capable of determining the entire Pareto set in a single algorithm run, these methods are of limited use for design of compact circuits due to a large number of objective function evaluations involved in the process (typically tens of thousands [16]).

In this work, a procedure for rapid multi-objective design optimization of computationally demanding compact microwave couplers is presented. The proposed method is an SBO scheme that exploits an equivalent circuit model of the structure of interest, and SM as the fundamental tool of low-fidelity model correction to identify a discrete representation of the Pareto front which contains the trade-off solutions between the operational bandwidth and the layout area of the structure. The approach is demonstrated by a compact rat-race coupler design example. Experimental verification of several trade-off designs is provided.

9.2 Case Study: Compact Rat-Race Coupler

In this section, we define a complex design problem of a compact rat-race coupler (RRC). It is used to demonstrate the application of the multi-objective optimization methodology presented in Section 9.3. An RRC is a popular microwave coupler that splits an input signal between the output ports with a 0°/180° phase shift or combines two input signals [17]. A conventional RRC is a ring-shaped structure that is composed of six 90°-sections of transmission lines (TLs), which makes it a suitable candidate for circuit miniaturization [18-20].

Let us consider a compact RRC shown in Figure 9.1(a). Size reduction has been achieved here by replacing conventional TL sections with folded shunt-stub-based lines, whose parameterized layouts are given in Figure 9.1(b). The coupler geometry can be described by seven designable parameters denoted as $\boldsymbol{x} = [w\ d_1\ d_2\ l_1\ l_2\ l_3\ l_4]^T$. We choose a Taconic RF-35 dielectric substrate (ε_r = 3.5, h = 0.762 mm, tanδ = 0.0018) for circuit implementation. The operation frequency is set to f_0 = 1 GHz. For the above specifications, the width and the length of the coupler feeding lines are fixed to 1.7 and 15 mm, respectively.

The goal is to find a set of design solutions that represent the best possible trade-offs between the following objectives: F_1 – maximization of the operational bandwidth, where the bandwidth (*BW*) is defined as a symmetrical—with respect to the center frequency f_0—intersection of $|S_{11}|$ and $|S_{41}|$ that remain below the level of –20 dB, and F_2 – minimization of the layout area occupied by the coupler. An equal power division between the output ports at f_0 is not considered here as a separate design objective. Instead, it is ensured by means of a suitably defined penalty function included in F_1.

SBO requires a fast low-fidelity model of a given structure that is also sufficiently aligned with its high-fidelity counterpart [11]. Here, we use an equivalent circuit of Figure 9.2 to serve this purpose. The high-fidelity model is implemented in CST Microwave studio [21] (~350,000 mesh cells, ~25 minute simulation time per design). The solution space is determined by the following lower/upper bounds: $\boldsymbol{l} = [0.2\ 0.1\ 0.1\ 10\ 10\ 0.1\ 0.1]^T$ and $\boldsymbol{u} = [1.5\ 1.2\ 4\ 20\ 20\ 20\ 20]^T$ (all dimensions in mm).

Although the methodology of Section 9.3 is demonstrated here using a compact RRC design example, it is also valid for other types of microwave circuits, provided that a sufficiently fast and accurate equivalent circuit model can be developed.

9.3 Methodology

In this section, we formulate and discuss the methodology for computationally efficient multi-objective design optimization of compact microwave couplers.

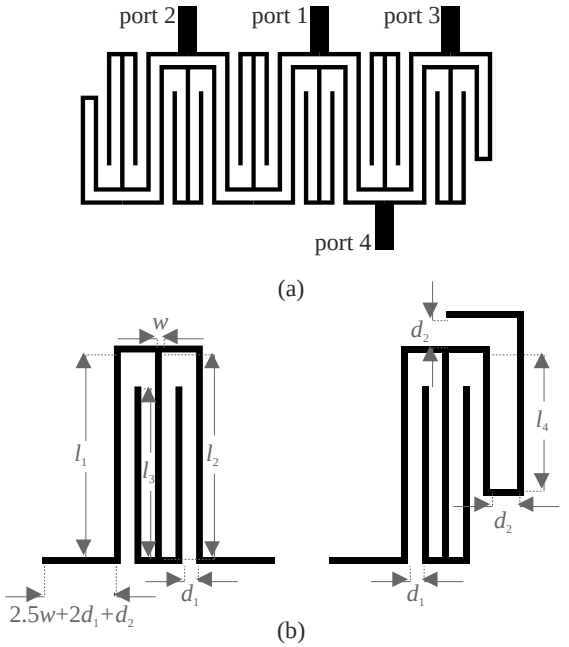

Figure 9.1: (a) Layout of the example compact RRC based on [4]; (b) Parameterized layouts of shunt-stub-based TLs.

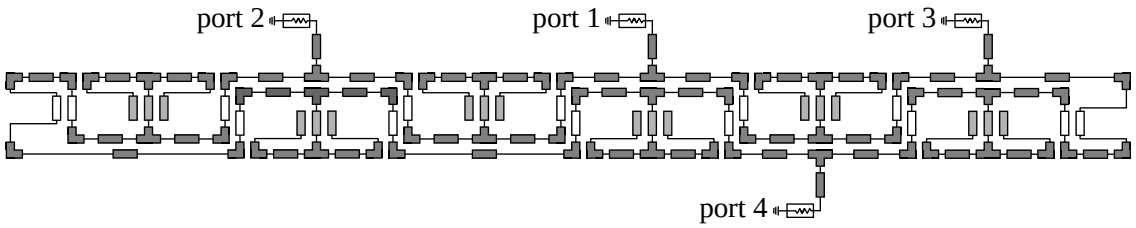

Figure 9.2: Equivalent circuit model of the example compact RRC, implemented in Agilent ADS [22]. Highlighted components have different sets of implicit space mapping parameters $\boldsymbol{p}$ assigned to them (dark grey: ε_1, h_1; grey: ε_2, h_2, white: ε_3, h_3).

9.3.1 Problem Formulation

Let $\boldsymbol{R}_f(\boldsymbol{x})$ denote a response of a fine model of the structure under consideration, where $\boldsymbol{x}$ is a vector of its designable parameters. Typically, $\boldsymbol{R}_f(\boldsymbol{x})$ is obtained by a computationally expensive high-fidelity EM simulation, and represents complex *S*-parameters of the given design solution.

Let $F_k(\boldsymbol{R}_f(\boldsymbol{x}))$, where $k = 1, \ldots, N_{obj}$, be a kth design objective. Considering a class of compact microwave couplers, typical objectives include minimization of the layout area and maximization of the bandwidth, with a specified power division ratio at f_0.

The goal of a multi-objective scheme is to identify a representation of a so-called Pareto-optimal set X_P, which is composed of non-dominated designs such that for any $\boldsymbol{x} \in X_P$, there is no other design $\boldsymbol{y}$ for which the relation $\boldsymbol{y} \prec \boldsymbol{x}$ is satisfied. Design $\boldsymbol{y}$ dominates $\boldsymbol{x}$ ($\boldsymbol{y} \prec \boldsymbol{x}$) if $F_k(\boldsymbol{R}_f(\boldsymbol{y})) \leq F_k(\boldsymbol{R}_f(\boldsymbol{x}))$ for all $k = 1, \ldots, N_{obj}$, and $F_k(\boldsymbol{R}_f(\boldsymbol{y})) < F_k(\boldsymbol{R}_f(\boldsymbol{x}))$ for at least one k) [23].

9.3.2 Surrogate Model

The high-fidelity EM-simulated model of the structure under consideration is too expensive to be directly handled by any population-based metaheuristic algorithm, which typically requires tens of thousands objective function evaluations to converge [16]. Thus, we exploit here a fast auxiliary equivalent circuit of Figure 9.2 as the low-fidelity model $\boldsymbol{R}_c$ of the structure at hand. In order to increase the accuracy of $\boldsymbol{R}_c$, we apply implicit and frequency SM [24] to construct a $\boldsymbol{R}_f$-well-aligned surrogate model $\boldsymbol{R}_s$, to be subsequently utilized in the optimization process. More specifically, the surrogate is defined as

$$\boldsymbol{R}_s(\boldsymbol{x}) = \boldsymbol{R}_{c.F}(\boldsymbol{x}; \boldsymbol{f}, \boldsymbol{p}) \tag{9.1}$$

where $\boldsymbol{R}_{c.F}$ is a frequency-scaled coarse model, whereas $\boldsymbol{f}$ and $\boldsymbol{p}$ denote frequency and implicit SM parameters, respectively. Let $\boldsymbol{R}_c(\boldsymbol{x}) = [R_c(\boldsymbol{x},\omega_1)\ R_c(\boldsymbol{x},\omega_2)\ \ldots\ R_c(\boldsymbol{x},\omega_m)]^T$, where $R_c(\boldsymbol{x},\omega_j)$ is evaluation of the circuit model at a frequency ω_j. Then, $\boldsymbol{R}_{c.F}(\boldsymbol{x};\boldsymbol{f},\boldsymbol{p}) = [R_c(\boldsymbol{x},f_0 + \omega_1 \cdot f_1,\boldsymbol{p})\ \ldots\ R_c(\boldsymbol{x}, f_0 + \omega_m \cdot f_1,\boldsymbol{p})]^T$, with f_0 and f_1 being frequency scaling parameters. Here, the implicit SM parameters are $\boldsymbol{p} = [\varepsilon_1\ \varepsilon_2\ \varepsilon_3\ h_1\ h_2\ h_3]^T$ (substrate permittivity and thickness of equivalent circuit components). They are extracted to minimize misalignment between $\boldsymbol{R}_s$ and $\boldsymbol{R}_f$ as follows:

$$\left[\boldsymbol{f}^*, \boldsymbol{p}^*\right] = \arg\min_{\boldsymbol{f},\boldsymbol{p}} \left\| \boldsymbol{R}_f(\boldsymbol{x}) - \boldsymbol{R}_{c.F}(\boldsymbol{x}; \boldsymbol{f}, \boldsymbol{p}) \right\| \tag{9.2}$$

The improved accuracy of $\boldsymbol{R}_s$ is limited to the vicinity of the design $\boldsymbol{x}$, at which the implicit SM parameters have been extracted. Note that it is not possible to find a single set of SM parameters that would ensure surrogate accuracy across the entire design space. Consequently, in order to lead towards a satisfactory design, the surrogate has to be iteratively refined during the optimization process.

9.3.3 Optimization Procedure

For the sake of computational efficiency, our design approach is based on a point-by-point identification of the Pareto set. First, we execute unconstrained optimization for F_1 objective only

(here, BW maximization). The optimum design $\boldsymbol{x}_p^{(1)}$ obtained this way is used to determine the feature space extreme point of the Pareto set as $(F_1(\boldsymbol{R}_f(\boldsymbol{x}_p^{(1)})); F_2(\boldsymbol{R}_f(\boldsymbol{x}_p^{(1)})))$.

In the subsequent steps, we set the threshold values for the second objective $F_2^{(j)}$, and optimize the structure with respect to the first objective so that the above threshold value is preserved:

$$\boldsymbol{x}_p^{(j)} = \arg\min_{\boldsymbol{x},\, F_2\left(\boldsymbol{R}_f(\boldsymbol{x})\right) \le F_2^{(j)}} F_1\left(\boldsymbol{R}_f\left(\boldsymbol{x}\right)\right) \tag{9.3}$$

Here, $\boldsymbol{x}_p^{(j)}$ is the jth design space element of the Pareto set. The process is continued until $F_1(\boldsymbol{R}_f(\boldsymbol{x}_p^{(j)}))$ is still satisfactory from the point of view of given design specifications.

The problem (9.3) is solved using the SM surrogate model (cf. Section 9.3.2) and it is itself realized as an iterative process

$$\boldsymbol{x}_p^{(j.k)} = \arg\min_{\boldsymbol{x},\, F_2\left(\boldsymbol{R}_s^{(j.k)}(\boldsymbol{x})\right) \le F_2^{(j)}} F_1\left(\boldsymbol{R}_s^{(j.k)}(\boldsymbol{x})\right) \tag{9.4}$$

where

$$\boldsymbol{R}_s^{(j.k)}\left(\boldsymbol{x}\right) = \boldsymbol{R}_{c.F}\left(\boldsymbol{x}; \boldsymbol{f}^{(j.k)}, \boldsymbol{p}^{(j.k)}\right) \tag{9.5}$$

and

$$\left[f^{(j.k)}, p^{(j.k)} \right] = \arg\min_{f,p} \left\| R_f\left(x^{(j.k)}\right) - R_{c.F}\left(x^{(j.k)}; f, p\right) \right\| \tag{9.6}$$

The starting point for the algorithm (9.4) is $\boldsymbol{x}_p^{(j-1)}$. Typically, two iterations of (9.4) are sufficient to obtain $\boldsymbol{x}_p^{(j)}$, which is because the starting point is already a good approximation of the optimum. In practice, the thresholds $F_2^{(j)}$ can be obtained as $F_2^{(j)} = \alpha \cdot F_2^{(j-1)}$ with $\alpha < 1$ (e.g., $\alpha = 0.95$), or $F_2^{(j)} = F_2^{(j-1)} - \beta$ with $\beta > 0$ (e.g., $\beta = 0.05 \cdot F_2^{(1)}$). Central-frequency equal power split between the output ports is secured by adding to F_1 in (9.4) the terms proportional to $(|S_{21}| + 3)^2$ and $(|S_{31}| + 3)^2$ (at f_0), which penalize the designs violating this requirement.

9.4 Numerical and Experimental Results

The methodology of Section 9.3 is showcased here using a compact RRC design example described in detail in Section 9.2. The process (9.4) has been applied to identify nine Pareto-optimal design solutions, illustrating the trade-offs between BW and the layout area of the structure under consideration. The first design, obtained without any area constraints, features BW and the layout area of 258 MHz and 841 mm^2, respectively. Eight consecutive design solutions have been acquired by setting up $F_2^{(j)}$ to 800, 725, 650, 575, 500, 425, 400, and 375 mm^2, respectively. The last two threshold values have been set with higher resolution, after failing to obtain a positive value of BW for the 350 mm^2 layout. Figure 9.3 shows the obtained representation of the Pareto-optimal set. Numerical results are listed in detail in Table 9.1. One can observe that the scale of circuit miniaturization ranges from 86.4% to 94.3%, which corresponds to compact designs that offer broadest and narrowest BWs, respectively. Several trade-off designs have been manufactured and measured to validate the proposed methodology. The simulated and measured characteristics of the selected design solutions are shown in Figure 9.4(a)–(d). One can observe that the experimental data fits the simulated results in a reasonable manner. Minor discrepancies are due to fabrication tolerance as well as the idealized nature of conducted simulations, where SMA connectors or substrate anisotropy have not been included. The measured values of *S*-parameters at the center frequency are collected in Table 9.2. The total cost of the design process corresponds to about twenty fine model evaluations, including the overhead related to multiple evaluations of the coarse model (the latter does not exceed ten percent of the overall EM simulation cost). In comparison with any type of metaheuristic algorithm applied to direct optimization of the compact RRC fine model, the overall cost of the presented method is orders of magnitude lower [1].

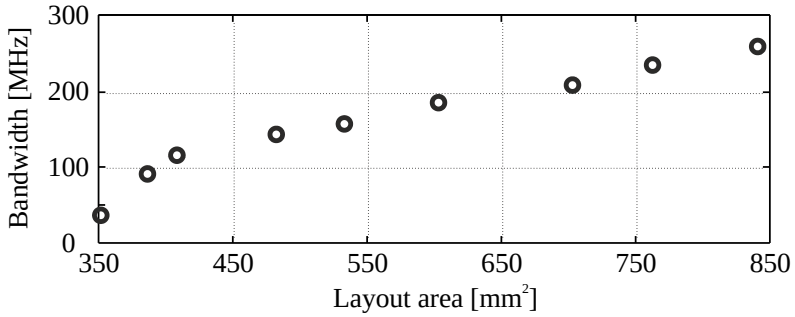

Figure 9.3: Pareto-optimal set representing the best possible trade-offs between bandwidth and layout area of the compact RRC, acquired by means of the presented multi-objective optimization procedure.

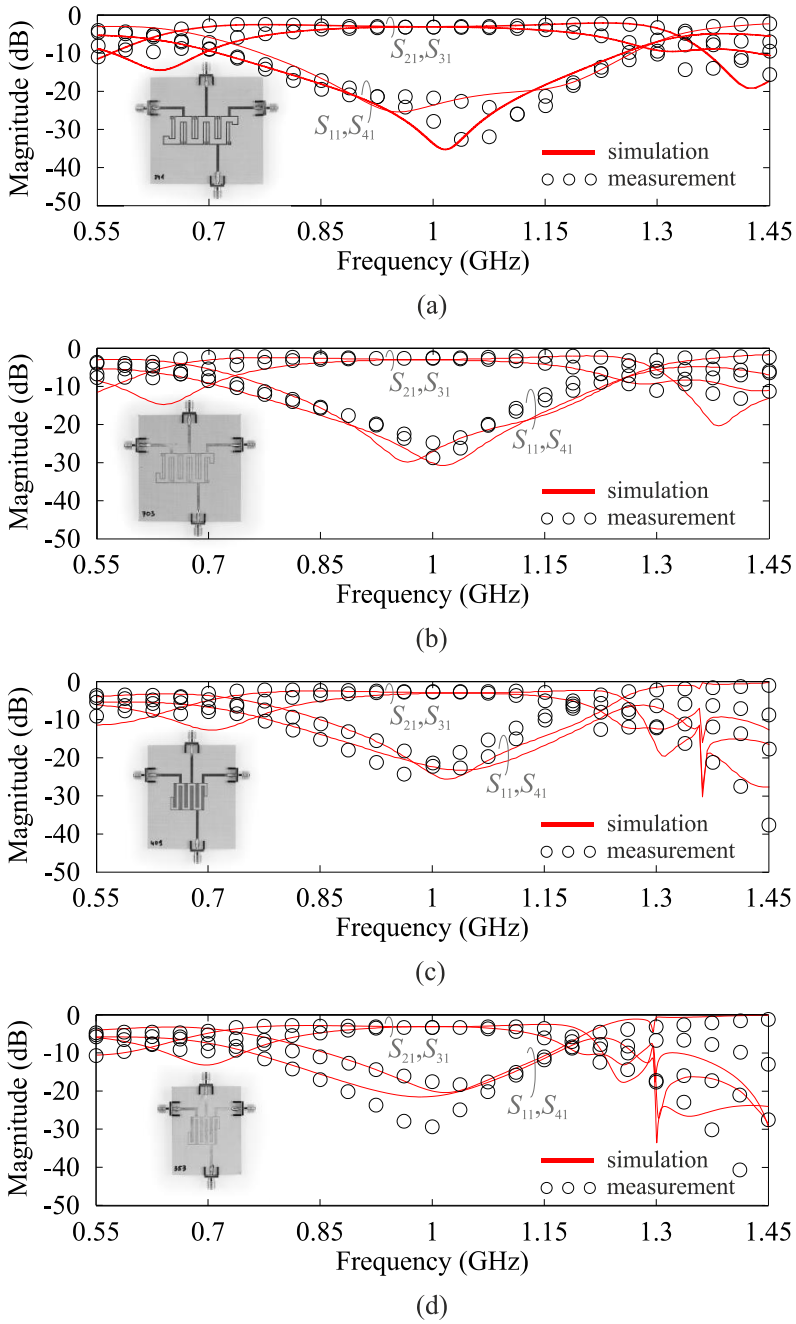

Figure 9.4: Simulated and measured *S*-parameters for selected design solutions with layout areas of: (a) 841 mm^2, (b) 703 mm^2, (c) 409 mm^2, and (c) 353 mm^2.

9.5 Conclusions

This work presents a technique for rapid multi-objective optimization of compact microwave couplers. The main components of the method include an iterative identification of the Pareto-optimal set, using a constrained single-objective SBO scheme with the space-mapping-corrected equivalent circuit model as the underlying surrogate model. Computational efficiency of the presented method is illustrated using a complex design example of a compact RRC. The obtained Pareto set demonstrates trade-offs between conflicting design objective, here, the BW and the layout area. Measurement results of several selected trade-off design solutions confirm the reliability of the proposed design method.

TABLE 9.1: NUMERICAL RESULTS OF MULTI-OBJECTIVE OPTIMIZATION OF COMPACT RRC

Designable parameters [mm]							Design objectives		Miniaturization* [%]
w	d_1	d_2	l_1	l_2	l_3	l_4	BW [MHz]	Area [mm^2]	
0.61	0.3	2.90	13.16	13.16	1.55	0.83	258	841	86.4
0.55	0.3	2.60	13.50	13.50	3.85	1.71	232	763	87.7
0.50	0.27	2.07	15.44	15.44	6.11	3.03	208	703	88.6
0.45	0.2	2.07	14.52	14.52	9.09	2.87	184	604	90.2
0.39	0.2	1.93	14.23	14.23	12.57	3.09	156	534	91.4
0.37	0.17	1.71	14.51	14.51	14.36	8.11	143	483	92.2
0.35	0.15	1.26	15.00	15.00	14.85	6.21	114	409	93.4
0.31	0.15	1.20	15.53	15.53	15.37	5.78	90	387	93.7
0.28	0.15	1.07	15.71	15.71	15.55	6.02	36	353	94.3

* w.r.t. conventional RRC designed for f_0 = 1 GHz and the same substrate: radius = 44.39 mm, size = 6190 mm^2

TABLE 9.2: MEASURED *S*-PARAMETERS OF SELECTED TRADE-OFF DESIGNS

Pareto-optimal solution of:	Measured *S*-parameters at 1 GHz			
	$\|S_{11}\|$ [dB]	$\|S_{21}\|$ [dB]	$\|S_{31}\|$ [dB]	$\|S_{41}\|$ [dB]
Figure 9.4(a)	–21.85	–3.27	–3.19	–27.61
Figure 9.4(b)	–34.17	–3.27	–3.16	–29.72
Figure 9.4(c)	–25.39	–3.37	–3.28	–27.27
Figure 9.4(d)	–17.55	–3.41	–3.45	–29.76

Acknowledgement

The authors thank Computer Simulation Technology AG, Darmstadt, Germany, for making CST Microwave Studio available. This work was supported in part by the Icelandic Centre for Research (RANNIS) under Grant no. 163299051, and National Science Centre of Poland under Grant 2014/15/B/ST7/04683.

References

[1] S. H. Yeung and K. F. Man, "Multiobjective Optimization," *IEEE Microw. Mag.*, vol. 12, no. 6, pp. 120–133, 2011.

[2] S. Koziel, P. Kurgan, and B. Pankiewicz, "Cost-efficient design methodology for compact rat-race couplers," *Int. J. RF Microw. Comp. Aid. Eng.*, vol. 25, no. 3, pp. 236–242, 2015.

[3] S. Koziel, A. Bekasiewicz, and P. Kurgan, "Rapid Multi-Objective Simulation-Driven Design of Compact Microwave Circuits," *IEEE Microw. Wireless Comp. Lett.*, vol. 25, no. 5, pp. 277–279, 2015.

[4] C.-H. Tseng and H.-J. Chen, "Compact Rat-Race Coupler Using Shunt-Stub-Based Artificial Transmission Lines", *IEEE Microw. Wireless Comp. Lett.*, vol. 18, no. 11, pp. 734–736, 2008.

[5] S. Koziel, A. Bekasiewicz, P. Kurgan, and J.W. Bandler, "Rapid multi-objective design optimization of compact microwave couplers by means of physics-based surrogates," *IET Microw. Ant. Propag.*, vol. 10, no. 5, pp. 479–786, 2016.

[6] H. Ghali and T. A. Moselhy, "Miniaturized fractal rat-race, branch-line, and coupled-line hybrids", *IEEE Trans. Microw. Theory Techn.*, vol. 52, no. 10, pp. 2513–2520, 2004.

[7] P. Kurgan and M. Kitlinski, "Doubly miniaturized rat-race hybrid coupler," *Microw. Opt. Techn. Lett.*, vol. 53, no. 6, pp. 1242–1244, 2011.

[8] S. Koziel and X.-S. Yang (Eds.), "*Computational Optimization, Methods and Algorithms*," Springer, 2011.

[9] S. Koziel and P. Kurgan, "Rapid design of miniaturised branch-line couplers through concurrent cell optimisation and surrogate-assisted fine-tuning," *IET Microw. Ant. Propag.*, vol. 9, no. 9, pp. 957–963, 2015.

[10] S.-S. Liao, P.-T. Sun, N.-C. Chin, and J.-T. Peng, "A novel compact-size branch-line coupler," *IEEE Microw. Wireless Comp. Lett.*, vol. 15, no. 9, pp. 588–590, 2005.

[11] S. Koziel and. L. Leifsson (Eds.), *Surrogate-based modeling and optimization: applications in engineering*, Springer, 2013.

[12] J.W. Bandler, Q.S. Cheng, S.A. Dakroury, A.S. Mohamed, M.H. Bakr, K. Madsen, and J. Sondergaard, "Space mapping: the state of the art," *IEEE Trans. Microw. Theory Techn.*, vol. 52, no. 1, pp. 337–361, 2004.

[13] S. Koziel, A. Bekasiewicz, and P. Kurgan, "Rapid EM-driven design of compact RF circuits by means of nested space mapping," *IEEE Microw. Wireless Comp. Lett.*, vol. 24, no. 6, pp. 364–366, 2014.

[14] S. Koziel, L. Leifsson, and X.S. Yang (Eds.), *Solving computationally expensive engineering problems: methods and applications*, Springer, 2014.

[15] P. Kurgan and M. Kitlinski, "Development of a compact microstrip resonant cell aimed at efficient microwave component size reduction," *IET Microw. Ant. Propag.*, vol. 6, no. 12, pp. 1291–1298, 2012.

[16] K. Deb, *Multi-Objective Optimization Using Evolutionary Algorithms*, John Wiley & Sons, 2001.

[17] R. Mongia, I. Bahl, and P. Bhartia, *RF and Microwave Coupled-Line Circuits*, Artech House, 1999.

[18] S. Opozda, P. Kurgan, and M. Kitlinski, "A compact seven-section rat-race hybrid coupler incorporating PBG cells," *Microw. Opt. Techn. Lett.*, vol. 51, no. 12, pp. 2910–2913, 2009.

[19] A. Bekasiewicz and P. Kurgan, "A compact microstrip rat-race coupler constituted by nonuniform transmission lines," *Microw. Opt. Techn. Lett.*, vol. 56, no. 4, pp. 970–974, 2014.

[20] P. Kurgan and A. Bekasiewicz, "A robust design of a numerically demanding compact rat-race coupler," *Microw. Opt. Techn. Lett.*, vol. 56, no. 6, pp. 1259–1263, 2014.

[21] CST Microwave Studio, ver. 2013, CST AG, Bad Nauheimer Str. 19, D-64289 Darmstadt, Germany, 2013.

[22] Agilent ADS, Agilent Technologies, 1400 Fountaingrove Parkway, Santa Rosa, CA 95403-1799, 2011.

[23] S. Koziel and S. Ogurtsov, "Multi-objective design of antennas using variable-fidelity simulations and surrogate models," *IEEE Trans. Ant. Propag.*, vol. 61, no. 12, pp. 5931–5939, 2013.

[24] S. Koziel, Q.S. Cheng, and J.W. Bandler, "Space mapping," *IEEE Microw. Mag.*, vol. 9, no. 6, pp. 105–122, 2008.

10 Conclusions and Future Work

This dissertation presents several original methodologies for reliable and computationally efficient design of miniaturized hybrid couplers. The proposed methods exploit a generic SBO scheme and employ a number of customized techniques for the development of fast surrogates with improved accuracy to be subsequently utilized in the design process. These techniques include circuit decomposition, hierarchical design, EM modeling, equivalent circuits, response surface approximations, and space mapping technology. The discussed methods are equipped with built-in mechanisms that account for internal EM couplings, otherwise resulting in lower model accuracy. Apart from the above, a surrogate-assisted fine-tuning technique that can be used as a stand-alone procedure is also provided. Moreover, some original developments included in this thesis consider circuit size reduction as an explicit design goal with the remaining performance-related goals controlled using a penalty function approach. This new functionality has been implemented both in a single-objective and a multi-objective setting.

The presented methods have been extensively validated on a case-study basis. In total, 25 design solutions have been numerical obtained with 20 of them regarding hybrid couplers. The complementary design examples concern multi-section matching transformers, and have been added to showcase the extended applicability of the developed methodologies. The design complexity expressed as the search space dimensionality ranges from 5 up to 14 for hybrid couplers and from 12 up to 27 for multi-section matching transformers. A suite of novel hybrid couplers have been devised that demonstrate outstanding miniaturization ratios between 82% and 94% for the vast majority of them as well as a high EM-validated performance. These findings have been also confirmed by experimental verification of 12 coupler prototypes. The comparison with state-of-the-art compact couplers reveals that the fabricated structures presented in this thesis offer not only superior frequency characteristics (the assessment based on strictly defined figures of merit), but also one of the best miniaturization coefficients. Furthermore, the proposed methods exhibit a dramatic reduction in the computational cost, offering—on average—25 times speedup in comparison to direct EM optimization. In relative terms, the cost of the design optimization process executed by the original methods presented here is very low and typically does not exceed a few EM simulations of the respective compact coupler.

The most important original contributions of this work include:

1. Development of several methodologies for reliable, automated and computationally efficient design of miniaturized hybrid couplers. These include sequential space mapping technique, nested space mapping technique, and surrogate-assisted EM-driven optimiza-

tion technique (with its extension to wideband coupler applications). Each of the enumerated methods employs a number of general-purpose SBO techniques, specifically adapted here to form a consistent design methodology.

2. Development of a surrogate-based design closure technique for miniaturized hybrid couplers.
3. Development of a new objective function formulation for explicit size reduction of hybrid couplers.
4. Development of a novel multi-objective optimization technique for an expedited identification of design objective trade-offs for miniaturized hybrid couplers.

The presented methods provide comprehensive solutions to most of the pressing issues listed in the introductory section to this work, which—to the best of author's knowledge—have not been addressed in the scientific literature on miniaturization so far. The numerical results presented in this work and validated by experimental investigations indicate that the goals defined in Section 1.2 have been accomplished and the theses put forward herein have been positively verified.

The methodologies presented in this dissertation operate within a commonly accepted framework for microwave circuit miniaturization, which includes (i) selection of a reference design, (ii) decomposition of the circuit into its fundamental building blocks, and (iii) their replacement with compact cells whose role is to duplicate the performance of these original components. The methods included in this thesis cover phase (iii) of the outlined routine. An implicit assumption made here is that a specific compact cell to be used as a substitution for original circuit building blocks is already given at the start of the design process. In practice, a particular cell geometry is chosen completely arbitrary by the designer without the definite knowledge of its applicability or possible outcomes. This appears to be a major weak point of the exploited approach as the underlying cell topology is likely to have a great impact on the obtainable circuit size reduction. However, the unavailability of methodological tools for comparison, assessment, classification and application-specific selection of compact cell geometries leaves no room for alternative. Future work will focus on addressing these issues, although some preliminary studies on the subject are already accepted for presentation at major international conferences this year (see the list below for details).

1. P. Kurgan and S. Koziel, "EM-driven compact cell topology selection for explicit size reduction of hybrid rat-race couplers," accepted for presentation at *European Microwave Conference*, 2017.
2. S. Koziel and P. Kurgan, "On elementary cell selection for miniaturized microstrip rat-race coupler design," accepted for presentation at *International Conference on Electromagnetics in Advanced Applications*, 2017.

APPENDICES

APPENDIX 1 APPLICATION OF NSM TO DESIGN OF MINIATURIZED RAT-RACE COUPLER

***

This appendix showcases an application of the nested space mapping algorithm of Chapter 5 to computationally efficient design of a miniaturized rat-race coupler composed of compact cells. We use here the same notation as in Chapter 5. Numerical data presented below have been originally included in a book chapter on NSM co-authored by P. Kurgan [98].

***

Consider a miniaturized RRC of Figure A1.1. The initial circuit size reduction is obtained by replacing transmission lines of a conventional RRC with compact cells, whose parameterized layouts are shown in Figure A1.2(a). The presented cells are devised according to the engineering approach of Chapter 2 using a T-type network (cf. Figure 2.5). The vectors of designable parameters pertaining to each considered cell are: $\boldsymbol{y}^{(1)} = [w_{11}\ l_{11}\ l_{21}\ l_{31}\ l_{41}]^T$ for the first one, and $\boldsymbol{y}^{(2)} = [w_{12}\ l_{12}\ l_{22}\ l_{32}\ l_{42}]^T$ for the second one. Note that dimensions $w_{10} = 0.75$, $l_{10} = 4.3$, $l_{20} = 0.4$ of Figure A1.1 are established by a designer and fixed to ensure coupler layout consistency (all geometry dimensions are in mm).

The high-fidelity cell models $\boldsymbol{R}_{f.cell}^{(n)}$, $n = 1, 2$, as well as their corresponding low-fidelity models $\boldsymbol{R}_{c.cell}^{(n)}$ [see Figure A1.2(b)] are implemented in CST Microwave Studio and Agilent ADS, respectively. The dielectric substrate used for EM model implementation is RF-35 ($\varepsilon_r = 3.5$, $h = 0.762$ mm, $\tan\delta = 0.0018$).

The goal is to achieve $|S_{11}|$ and $|S_{41}| \leq -20$ dB between 0.9 GHz and 1.1 GHz, as well as $|S_{21}| = |S_{31}|$ at 1 GHz. The search space is defined by the following lower/upper bounds: $\boldsymbol{l}^{(1)} = [0.2\ 0.2\ 0.2\ 0.2\ 0.2]^T$, $\boldsymbol{u}^{(1)} = [0.5\ 0.5\ 4\ 0.5\ 4]^T$, and $\boldsymbol{l}^{(2)} = [0.2\ 0.2\ 0.2\ 0.2\ 0.2]^T$, $\boldsymbol{u}^{(2)} = [0.5\ 1\ 7\ 0.5\ 7]^T$.

To this end, the NSM technique is applied to construct the nested surrogate model $\boldsymbol{R}_s$ of the miniaturized coupler. In the first step, the inner surrogate models $\boldsymbol{R}_{s.cell}^{(1)}$ and $\boldsymbol{R}_{s.cell}^{(2)}$ are developed at the level of individual compact cells. Each $\boldsymbol{R}_{s.cell}^{(n)}$ surrogate is a composition of $\boldsymbol{R}_{c.cell}^{(n)}$ and a combination of SM corrections (here, input, frequency, and implicit SM). The sufficient matching of the inner surrogate models to their high-fidelity counterparts is ensured by a multi-point parameter extraction (PE) procedure based on a star-distributed training set covering the entire range of parameters $\boldsymbol{y}^{(n)}$ (see Figure A1.3). The PE process pertaining to each cell involves 18 extractable SM parameters. In the second step, the surrogate model $\boldsymbol{R}_s$ of the entire coupler is developed by cascading four $\boldsymbol{R}_{s.cell}^{(1)}$ and two $\boldsymbol{R}_{s.cell}^{(2)}$ inner-level surrogates (cf. Figure A1.1) and applying outer SM correction with a limited number of global parameters to compensate for EM cross-couplings between the cells. The designable parameters of the assembled coupler are the following: $\boldsymbol{x} = [w_{11}\ l_{11}\ l_{21}\ l_{31}\ l_{41}\ w_{12}\ l_{12}\ l_{22}\ l_{32}\ l_{42}]^T$. Relative parameters are defined as: $w_{21} = 18l_{11} + 21w_{11}$ and $w_{22} = 6l_{12} + 7w_{12}$. A schematic diagram of the generic surrogate model $\boldsymbol{R}_{s.g}$ of the entire coupler is shown in Figure A1.4.

The obtained $\boldsymbol{R}_s^{(i)}$ surrogate model of the RRC is subsequently utilized in a typical SBO process. The initial design is $\boldsymbol{x}^{(0)} = [0.2\ 0.2\ 2.5\ 0.2\ 2.5\ 0.2\ 0.2\ 5.0\ 0.2\ 5.0]^T$. The final design $\boldsymbol{x} = [0.24\ 0.26\ 3.35\ 0.28\ 2.04\ 0.25\ 0.29\ 6.52\ 0.29\ 5.63]^T$ is obtained after four iterations of the algorithm. The optimized RRC exhibits $|S_{11}|$ and $|S_{41}| \leq -20$ dB between 0.915 GHz and 1.115 GHz as well as an equal power division at 1 GHz with approximation to the user-defined termination condition of the SBO process. The EM-validated performance of the obtained coupler is shown in Figure A1.5. The footprint of the miniaturized structure is 17 mm by 27.3 mm (464 mm^2),

which is about 10% of the real estate designated for the conventional RRC implemented for comparison purposes (47.5 mm × 95.5 mm ≈ 4536 mm^2).

A total cost of the miniaturized RRC design optimization process corresponds to 6.5 evaluations of the its high-fidelity EM model $\boldsymbol{R}_f$ implemented in CST Microwave Studio (~800,000 mesh cells, simulation time: 75 min). The computational efficiency of NSM is compared with ISM (a standard SBO methodology), SSM (cf. Chapter 3), and a direct EM-driven approach based on pattern search (a conventional design approach). For the considered case study, NSM involves the smallest CPU cost to yield an optimized design (for details see Table A1.1).

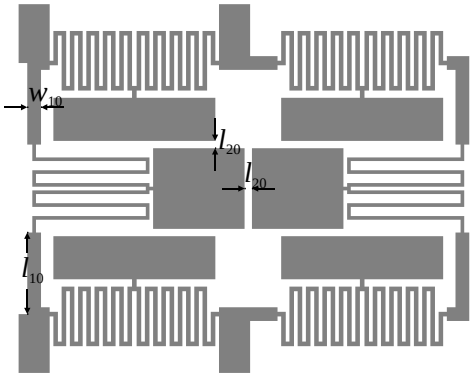

Figure A1.1: Initial layout of miniaturized RRC including designer-dependent geometry parameters.

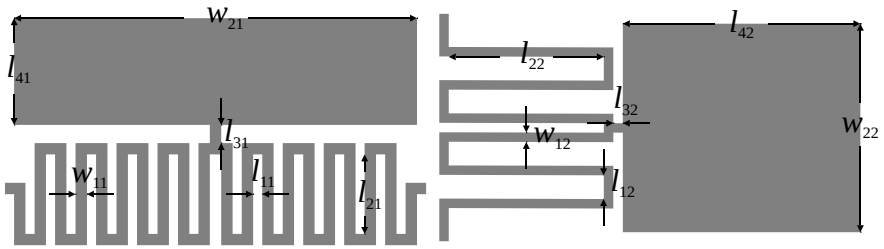

(a)

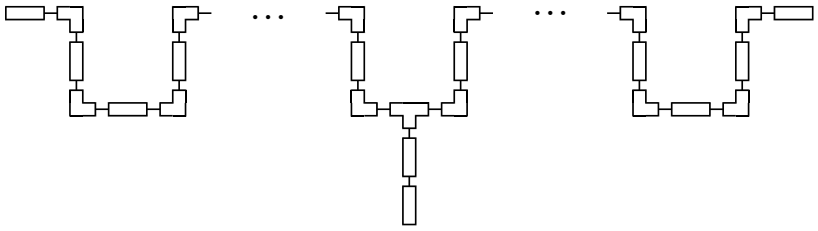

(b)

Figure A1.2: (a) Parameterized layouts of compact cells (on the left – first cell, on the right – second one); (b) generic equivalent circuit cell model.

TABLE A1.1: MINIATURIZED RRC: DESIGN OPTIMIZATION COST

Model Evaluations	Optimization algorithm			
	NSM	ISM	SSM	Direct Search
$\boldsymbol{R}_{s.cell}$	0.9 × $\boldsymbol{R}_f$	N/A	N/A	N/A
$\boldsymbol{R}_{f.cell}$	1.3 × $\boldsymbol{R}_f$	N/A	N/A	N/A
$\boldsymbol{R}_s$	0.3 × $\boldsymbol{R}_f$	3.9 × $\boldsymbol{R}_f$	3.2 × $\boldsymbol{R}_f$	N/A
$\boldsymbol{R}_f$	4 × $\boldsymbol{R}_f$	16 × $\boldsymbol{R}_f$	12 × $\boldsymbol{R}_f$	286 × $\boldsymbol{R}_f$
Total cost	6.5 × $\boldsymbol{R}_f$	18.9 × $\boldsymbol{R}_f$	15.2 × $\boldsymbol{R}_f$	286 × $\boldsymbol{R}_f$
Total cost [hours]	8.6	26.5	18.7	363.6

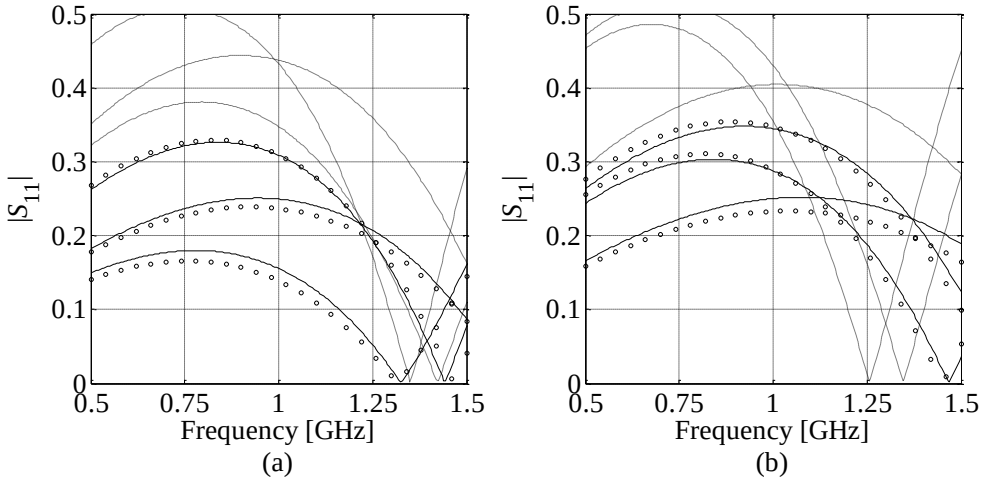

Figure A1.3: Nested SM modeling of compact cells. Responses of coarse model (····), fine model (—), and inner SM model (◦◦◦) at several selected test designs: (a) the first cell; (b) the second cell.

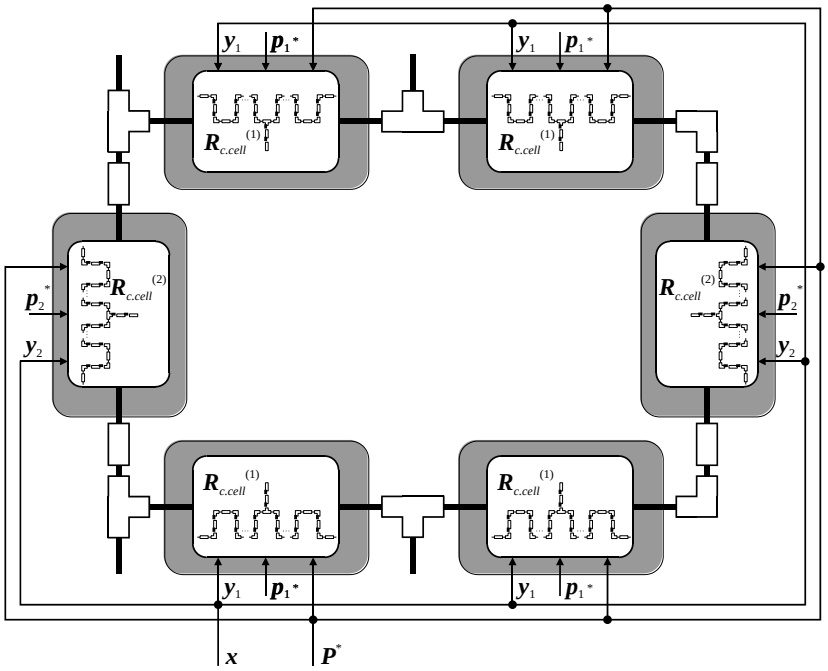

Figure A1.4: Schematic diagram of compact RRC global model $\boldsymbol{R}_{s.g}(\boldsymbol{x},\boldsymbol{P})$ composed of four $\boldsymbol{R}_{s.cell}^{(1)}$ and two $\boldsymbol{R}_{s.cell}^{(2)}$ inner-level surrogates.

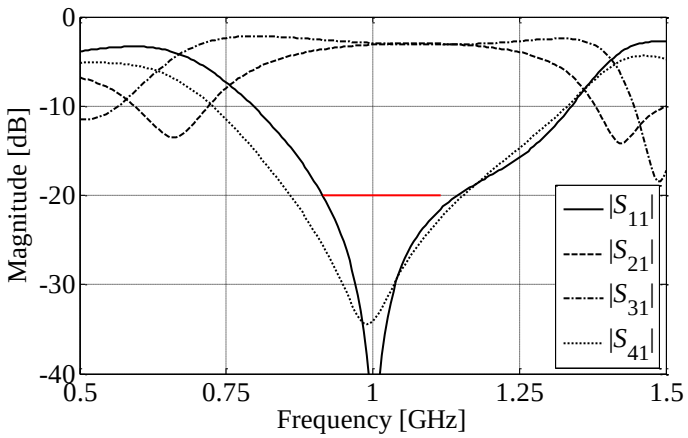

Figure A1.5: EM-validated performance of the optimized compact RRC.

ABOUT THE AUTHOR

Piotr Kurgan was born in Gdansk on April 8, 1983. He received his M.Sc. degree in electronics from Gdansk University of Technology, Poland, in September 2008. From October 2008 to October 2013 he was with the Department of Microwave and Antenna Engineering, Gdansk University of Technology, where he developed prototypes of compact microwave components as a PhD candidate supervised by Dr. Marek Kitliński. In January 2014 he joined the Engineering Optimization & Modeling Center, Reykjavik University, Iceland, to continue his work on microwave circuit miniaturization under the guidance of Prof. Sławomir Kozieł. Since July 2014 he has also been collaborating with the Department of Microelectronic Systems, Gdansk University of Technology.

For the past few years Piotr Kurgan has been involved in active research on surrogate-based modeling and optimization in application to microwave and antenna engineering, radio frequency integrated circuits as well as aerospace or ocean engineering. He has participated in five national research grants (in one as a principal investigator) and two foreign research projects. His research track includes over fifty peer-reviewed articles, half of which appeared in ISI journals. He has also co-authored five book chapters and six papers published in domestic magazines. According to WoS database, his works have been cited over one hundred times by other researchers, whereas his *h*-index is ten by May 2017. The academic activity of Mr. Kurgan also involves serving as a reviewer for several ISI journals, consulting M.Sc. theses (four Master's students) as well as supporting the International Conference on Computer Science as a program committee member (since 2015).

Piotr Kurgan has been recognized for his achievements by the Foundation for Polish Science in 2010 and granted a Young Scientist Scholarship. Throughout his research career, he has also been awarded ten times with competitive scholarships by authorities of Gdansk University of Technology as well as Pomeranian Voivodeship Office.